Investigation of the usage of SHCC as a closure pour to reduce the construction time of widening a prestressed concrete bridge

MSc Thesis

Laura Dieterich Murr

Delft University of Technology

TUDelft

NOBLEO bouw & infra

Investigation of the usage of SHCC as a closure pour to reduce the construction time of widening a prestressed concrete bridge

by

Laura Dieterich Murr

Student Name	Student Number
Laura Dieterich Murr	5386039

Thesis submitted to Delft University of Technology for the degree of
Master of Science
in Civil Engineering
to be publicly defended on 01/November/2023

Thesis committee:	Prof.dr.ir. M.A.N. (Max) Hendriks	TU Delft, Chair
	Dr. ir. Yuguang Yang	TU Delft
	Dr. Branko Šavija	TU Delft
	Ir. Matthijs de Hertog RC	Nobleo Bouw & Infra
Project Duration:	September, 2022 - September, 2023	
Faculty:	Faculty of Civil Engineering and Geosciences, Delft	

Acknowledgements

This thesis was developed to fulfill the graduation requirements for the Delft University of Technology's Master's program in Structural Engineering with a specialization in Concrete Structures. The idea was brought to me by Nobleo Bouw & Infra and made my eyes sparkle. Thank you, Nobleo. I have always been interested in bridges. Thus, when the idea came, I fell in love with the project. The process of my thesis was just like my Master's was lengthy and slow, but it made me thrive as a person and as a structural engineer and learn a great deal.

I am immensely grateful to my thesis committee for their invaluable guidance, knowledge, and inspiration. I extend my heartfelt appreciation to Max Hendriks, the chair of my committee, for his unwavering support, constructive feedback, and honest encouragement throughout this process. He always tried to make time to help me whenever I needed it. I would also like to express my gratitude to Yuguang Yang for posing thought-provoking questions, which undoubtedly enhanced the quality of my work by enabling me to see things from a different perspective, even though it was a rather complicated view. I would also like to thank Branko Šavija for opening up the materials opportunity that could be explored in this thesis and for agreeing that SHCC and ECC are quite the same thing. Besides, observing the level of Dutch that foreigners can achieve was remarkable. Last but definitely not least, I would like to express my deepest gratitude to Matthijs de Hertog, who was extremely patient with me. He shared a wealth of practical knowledge and experience in engineering not only during my thesis but also throughout my internship at Nobleo Bouw & Infra.

I would like to thank my friends, without whom this experience would have been far more problematic. I appreciate all your support and friendship. I appreciate all the support that you gave me during this tough period, just as all the gatherings and trips that we have been to. Sometimes, just being there was enough to keep me moving. I would also like to say my many thanks to my friends from Brazil, who always asked me when I was coming back and expressed their *saudades*.

Finally, I would like to thank the three most important women in my life: my grandma, my mom, and my sister. Without you three, my life would be inconceivable. *Muito obrigada.* I would also like to thank the rest of my extended family. Wherever you may be in this world, I can always count on your support.

I am sad to see this significant chapter of my life end, but I am proud to have made it this far, and I am excited to see what the future has to offer me.

Laura Dieterich Murr
Delft, October 2023

Abstract

The Netherlands is currently facing a significant challenge regarding its highway system due to the rise in traffic, especially in densely populated areas like The Randstad. However, constructing new infrastructure or replacing old bridges is not a practical solution due to environmental concerns. Most of the country's prestressed concrete bridges were built in the 1960s and 1970s with a lifespan of 100 years, and they are deemed incapable of handling the current traffic volume. As the existing bridges are still in good condition, recent projects have focused on widening them. Widening a bridge involves careful consideration of the behavior of all the elements in relation to each other, given the existing deck's relative stability and the inevitable shrinkage and creep of new components. To ensure a monolithic connection between the new and existing sections of the bridge, current projects aim to widen the bridges using a closure pour between the main slabs.

The Schipholbrug, situated close to the Schiphol Airport, is a prime example of a prestressed bridge that needs to be widened, and it is the focus of this thesis. In the Netherlands, reinforced concrete is the preferred material for a closure pour due to its durability, cost-effectiveness, and established properties. However, to maintain the integration between new and old concrete, a 6-9 month delay after constructing the new bridge is necessary to build this closure pour. To minimize significant delays, it is crucial to maintain a strong connection between the original and new materials, including the closure pour. The main challenge is managing the differences in creep and shrinkage between the existing structures, fresh deck, and closure pour. These inconsistencies can cause significant tensile stresses in the closure pour, especially when delays are kept to a minimum. Therefore, identifying a cementitious material that could effortlessly create reliable bonds with the primary decks' prestressed concrete and possess a high tensile strain range property was necessary to reduce this delay.

Strain-Hardening Cementitious Composite, also known as *SHCC*, is a modern material that possesses an impressive tensile strain range and a comparatively lower elastic modulus. Nevertheless, what sets it apart is its strain-hardening quality, which improves its toughness even after experiencing cracks. This exceptional characteristic of *SHCC* allows it to offer an extended tensile strain range, making it a choice for a closure pour.

The thorough literature review investigated crucial subjects, such as the intricacies of closure pour when expanding current bridges. Moreover, it covered the fundamental attributes of concrete that are pertinent to this thesis, such as shrinkage and creep, as well as its post-crack behavior. Another segment focused on the primary material employed in this thesis, *SHCC*, emphasizing its fundamental characteristics, including shrinkage and crack. Lastly, the research included a section on imposed deformation that was custom-made to the specific case of this thesis.

The methodology chapter utilized analytical calculations to gain a better understanding of the deformation issues caused by shrinkage and creep and their effect on the closure pour. These calculations explored composite structure mechanics and imposed deformation to determine the longitudinal stresses present in the mid-span of the decks. To further verify the accuracy of the findings, a linear model was also developed using DIANA FEA.

The results chapter presented the outcomes of the methodology discussed in the previous chapter, taking into account the calculations provided in the Appendix. The results revealed longitudinal stresses in various cases, including scenarios without a closure pour and only the shrinkage of the new deck. Then, the methods with a closure pour were examined, where only the new deck could shrink. The shrinkage of the closure pour and the new bridge were also considered. Additionally, a model with creep, shrinkage, and crack was studied. Creep was investigated for the main decks, shrinkage for the new bridge and closure pour, and crack for the closure pour. The calculations were conducted using both *C40/50* concrete and a specific *SHCC* material. The linear model only considered the previous case, which included all the obstacles, shrinkage, creep, and crack, with both materials for the closure pour, concrete, and *SHCC*. The numerical model presented both the normal and shear stresses and strains.

Throughout the discussion, three primary topics were addressed. The first topic revolved around a comparison between analytical and numerical models. It was noted that the concrete results obtained

from the numerical model were in close agreement with the main span of the Finite Element Analysis (*FEA*) model, which was quite significant. On the other hand, the *SHCC* had results that were more similar to the maximum value of the numerical model, which was attributed to the calibration of the cracked *SHCC* with the maximum value of the plate model rather than the mid-span. The *FEA* linear model also displayed higher values compared to the analytical calculations, implying that numerical models are indispensable for more extensive analyses. Nevertheless, it was noted that analytical models would suffice for more initial and more straightforward estimates.

The second point of discussion involves comparing the normal strains and shear stresses and strain between the two linear models to address the deformation problem. It was demonstrated that the shear strain *SHCC*, due to its high deformation, is able to counterbalance the strains of the new bridge and the old bridge and keep compatibility among the three elements. However, concrete is a stiffer material, which meant that keep compatibility between the old bridge and the closure pour was an issue.

The third discussion topic was the possibility of using *SHCC* as a closure pour. It was observed that despite rigorous calculations, the material was in its early strain-hardening phase rather than approaching its ultimate tensile strength. This meant that the material was able to bear considerable loads and had a high strain tolerance, even under increased loads. Impressively, *SHCC* demonstrated the ability to sustain a 37% increase in strain without failing. The issue of crack width was also raised, which is a crucial consideration when it comes to closure pour. However, *SHCC* boasts a lower crack width of $0.1mm$, which is half of the $0.2mm$ allowed by current norms, as confirmed by the literature review. Moreover, it has been noted that raising the *SHCC* strain up to 35 times would not pose any problem for the material. Additionally, a model was created based on the initial three Schipholbrug spans, demonstrating that the computations remained reliable regardless of whether one or three spans were employed to address shrinkage, creep, and cracking concerns.

During the latter portion of the discussion, the suitability of *SHCC* and concrete as potential closure pour options was evaluated. Upon examination of the second option, it was discovered that the reinforcements required to prevent exceeding the crack width of $0.2mm$ were quite substantial, which could result in increased labor costs and implementation time. As a result, it was concluded that concrete may not be a suitable match for the *SHCC* closure pour, as the latter option does not necessitate such reinforcements. Consequently, the decision was made to reject concrete as a viable solution for the closure pour in order to reduce the construction time of a prestressed concrete bridge widening project. Based on the analyses conducted, it was found that the *SHCC* material also experienced some cracking. Nevertheless, the cracking was still well within the limits of its ultimate tensile strength. The calculations have indicated that utilizing *SHCC* may be a viable choice for closure pour applications.

Upon concluding this thesis, it was determined that although calculations indicated a likelihood of *SHCC* cracking, this concern is not significant thanks to its crack-bridging fibers, strain-hardening properties, and the fact that its crack width remains below $0.20mm$. With an extended tensile strain range and stress and strain values far from ultimate tensile strength and strain, *SHCC* may even experience increased strength and strain. Therefore, it is a reliable closure pour option that effectively mitigates shrinkage and creep stresses on both old and new bridges, as well as self-shrinkage. Moreover, investigating the impact of repetitive freeze-thaw cycles on the tension-strain behavior of *SHCC* is advised, along with additional research to determine its ability to withstand being used as a closure pour for a century.

Contents

List of Figures

List of Tables

Nomenclature

Abbreviations

Abbreviation	Definition
Caltrans	California Department of Transportation
CP	Closure Pour
ECC	Engineered Cementitious Composites
FEA	Finite Element Analysis
FEM	Finite Element Method
HDPE	High-Density Polyethylene
HFC	High Performance Fibre Reinforced Cementitious Composites
JSCE	Japan Society of Civil Engineers
New	New Bridge
Old	Old Bridge
ODE	Ordinary Differential Equation
ODEs	Ordinary Differential Equations
PVA	Polyvinyl Alcohol
RILEM	International Union of Laboratories and Experts in Construction Materials, Systems and Structures
SAA	Schiphol-Amsterdam-Almere
SHCC	Strain-Hardening Cementitious Composite
SP	Superplasticizer
TC	Technical Committee

Symbols

Symbol	Definition	Unit
A	Area	[m^2]
$A_{c,eff}$	Effective Area of Concrete	[m^2]
A'_p	Area of post-tensioned tendons	[m^2]
A_s	Area of steel reinforcement	[m^2]
E	Young's Modulus	[kg/ms^2]
E_s	Reinforced Steel Young's Modulus	[kg/ms^2]
EA	Axial Stiffness	[kgm/s^2]]
EI	Bending Stiffness	[kgm^3/s^2]
$\exists$	Exists	
$\nexists$	Not Exists	
I	Second Moment Of Area	[m^4]
L	Length	[m]
N	Force	[kgm/s^2]
M	Moment	[kgm^2/s^2]
RH	Relative Humidity	[%]
S	Elastic Section Modulus	[m^3]
T	Temperature	[$^\circ C$]

Symbol	Definition	Unit
c	Concrete Cover	[mm]
e	Eccentricity	[m]
f_{ck}	Characteristic compressive strength of concrete at 28 days	[kg/ms^2]
f_{ctm}	Mean value of axial tensile strength of concrete	[kg/ms^2]
f_{ctk}	Characteristic axial tensile strength of concrete	[kg/ms^2]
$f_{ct,eff}$	Mean value of tensile strength of concrete effective	[kg/ms^2]
$h_{c,ef}$	Depth Of Effective Area of Concrete	[mm]
k_1	Bond Properties Coefficient	
k_2	Distribution of Strain Coefficient	
k_3	Coefficient	
k_4	Coefficient	
k_t	Load Duration Factor	
$s_{r,max}$	Maximum Crack Spacing	[mm]
t	Thickness	[m]
u	Perimeter	[m]
w	Width	[m]
w_{k}	Crack Width	[mm]
z	Lever arm of internal forces	[m]
α_e	ratio E_s/E_c	
ε	Strain	[m/m]
ε_{cm}	Concrete Mean Strain Between Cracks	[m/m]
ε_{sm}	Reinforcement Mean Strain	[m/m]
ν	Poisson's ratio	
ξ_1	Adjusted Ratio of Bond Strength	
σ	Stress	[kg/ms^2]
σ_s	Steel Stress	[kg/ms^2]
ϕ	Reinforcement Diameter	[mm]
φ	Creep coefficient	

1
Introduction

1.1 Background

The Netherlands currently faces a significant challenge with its highway system, particularly in densely populated areas like The Randstad, due to the rise in traffic. However, constructing new infrastructure or replacing old bridges is not a practical solution due to environmental concerns. Most of the country's prestressed concrete bridges, with a lifespan of 100 years, were built in the 1960s and 1970s and are deemed incapable of handling the current traffic volume[1]. As the existing bridges are still in good condition, recent projects have focused on widening them. Widening a bridge requires careful consideration of all the elements in relation to each other, taking into account the existing deck's relative stability and the inevitable shrinkage and creep of new components. Many ongoing projects are focused on widening these bridges by employing a closure pour between the main slabs to address this issue. The Schipholbrug is a prime example of a bridge that requires widening to meet current traffic demands.

1.2 Specific case: Schipholbrug

The Schipholbrug plays a crucial role in the Rijswaterstaat mega project, which aims to improve road infrastructure and advance technology in the Schiphol, Amsterdam, and Almere regions. With a focus on enhancing accessibility, improving road safety, augmenting traffic flow, and reducing travel time north of the Randstad region[2], this project is a significant undertaking. The Schipholbrug is part of Project 5 of the *SAA* project, and it is a state-of-the-art bridge that is situated between Badhoevedorp and Holendrecht, near Schiphol Airport and Amsterdam Zuid. Spanning the Ringvaart van de Haarlemmermeerpolder, the bridge links the villages of Nieuwe Meer and Schiphol-Oost, as demonstrated in figs. 1.2 and 1.3.

Figure 1.1: Overview of the entire SAA route.

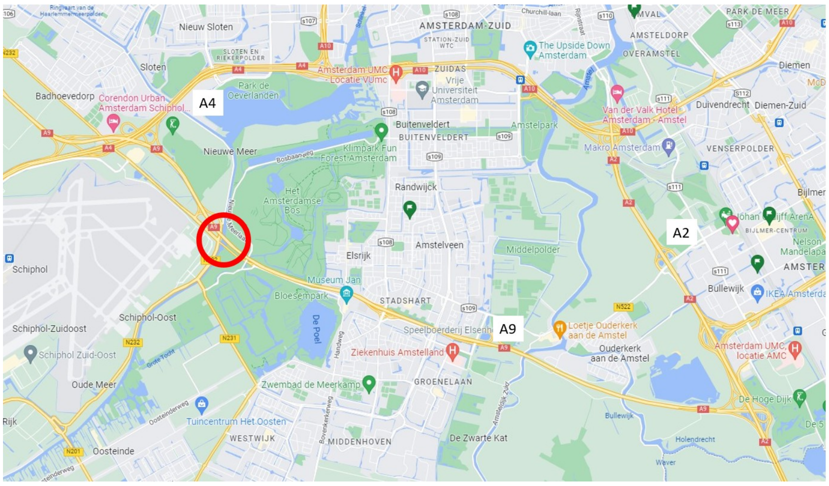

Figure 1.2: Top view of the area from Google Maps, including A9, A4 and A2.

Figure 1.3: Top view from Google Maps of the Schiphol bridge.

Nobleo Bouw & Infra received the necessary drawings for this thesis from Rijkswaterstaat, including Figure 1.4, Figure 1.7, Figure 1.9, Figure 1.10, as well as Figure 1.13, Figure 1.14.

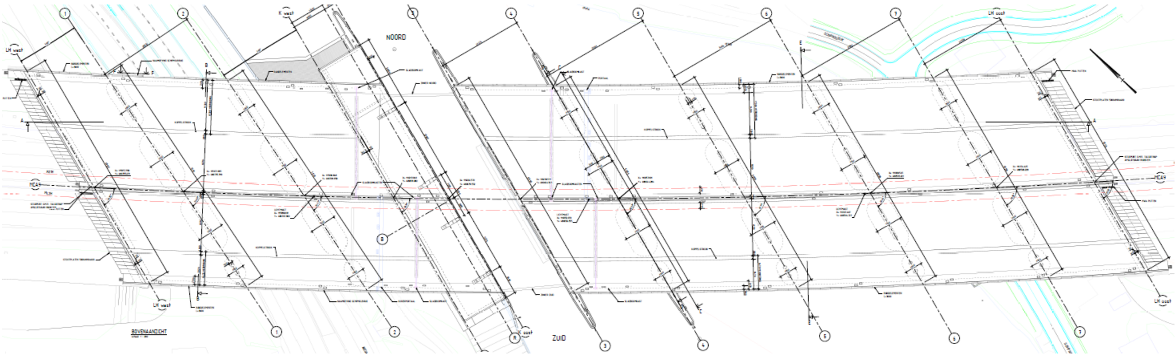

Figure 1.4: Top view drawing of the future widened Schipholbrug given by Rijkswaterstaat (not available for the public).

The Schipholbrug comprises three unique elements, two constructed from concrete and one from steel, as illustrated in Figure 1.5. The steel portion of the bridge is the central component and can be moved to accommodate passing sailing vessels. This feature is especially significant as the canal is integral to the Staande Mastroute, a vital route for cargo transportation and sailing boats. The completed bridge can be seen in Figure 1.6.

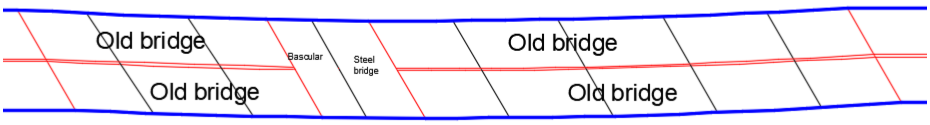

Figure 1.5: Scheme of the original Schipholbrug (top view).

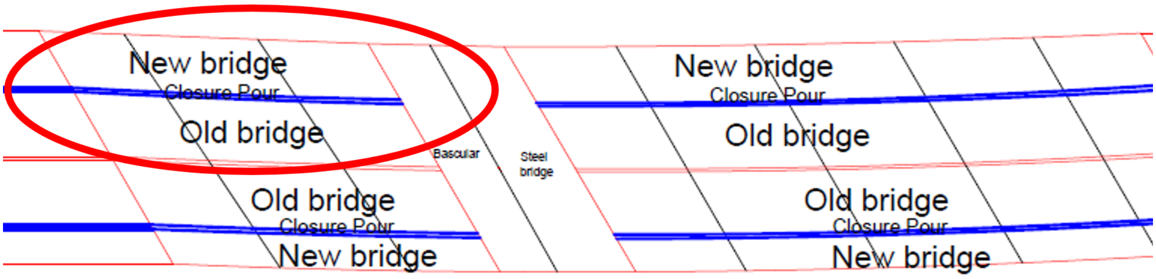

Figure 1.6: Scheme of the future Schipholbrug (top view).

This thesis's primary area of focus was the western (left) section of the concrete bridge, as depicted in figs. 1.6 and 1.8. Specifically, the study centered on a three-span prestressed cast-in-situ deck. Of particular importance was the upper portion of figs. 1.6 and 1.8, which represents this western section's most significant new deck constructed. This section is displayed without skewing in Figure 1.11. The analytical calculations and numerical model were conducted using only one span to simplify calculations, as illustrated in Figure 1.12.

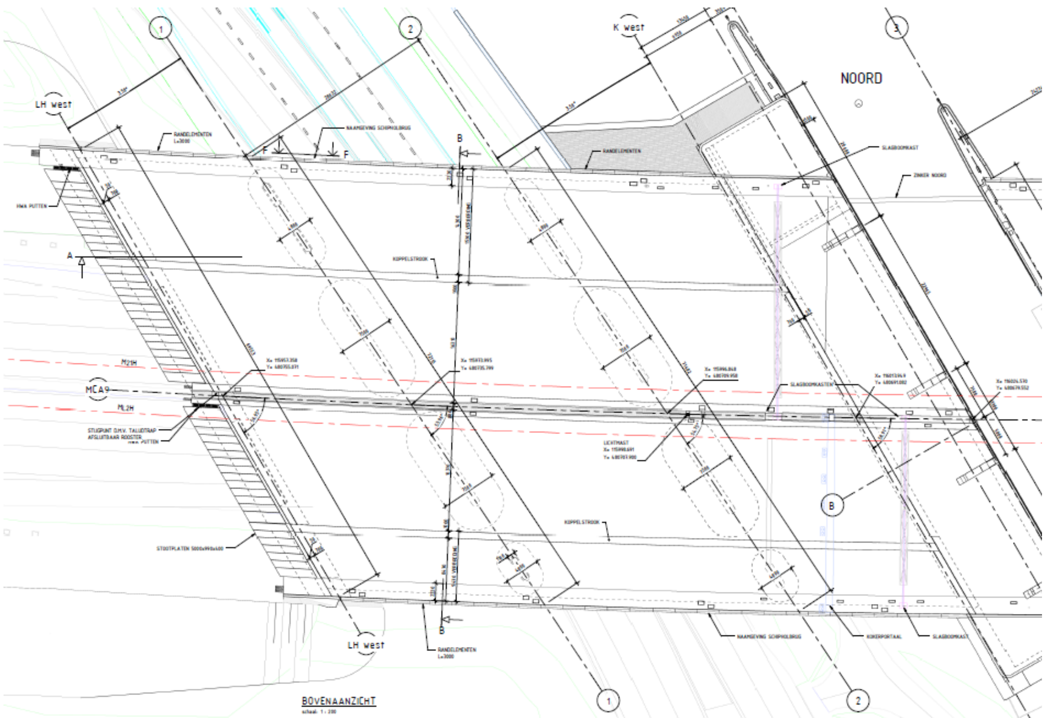

Figure 1.7: West top view drawing of the future widened Schipholbrug given by Rijkswaterstaat (not available for the public).

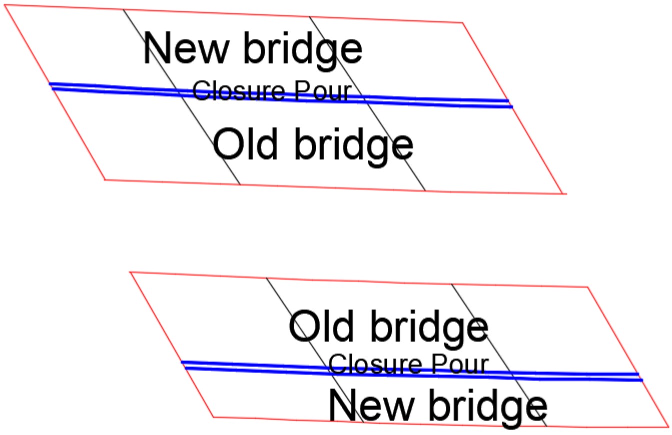

Figure 1.8: West part scheme of Schipholbrug (top view).

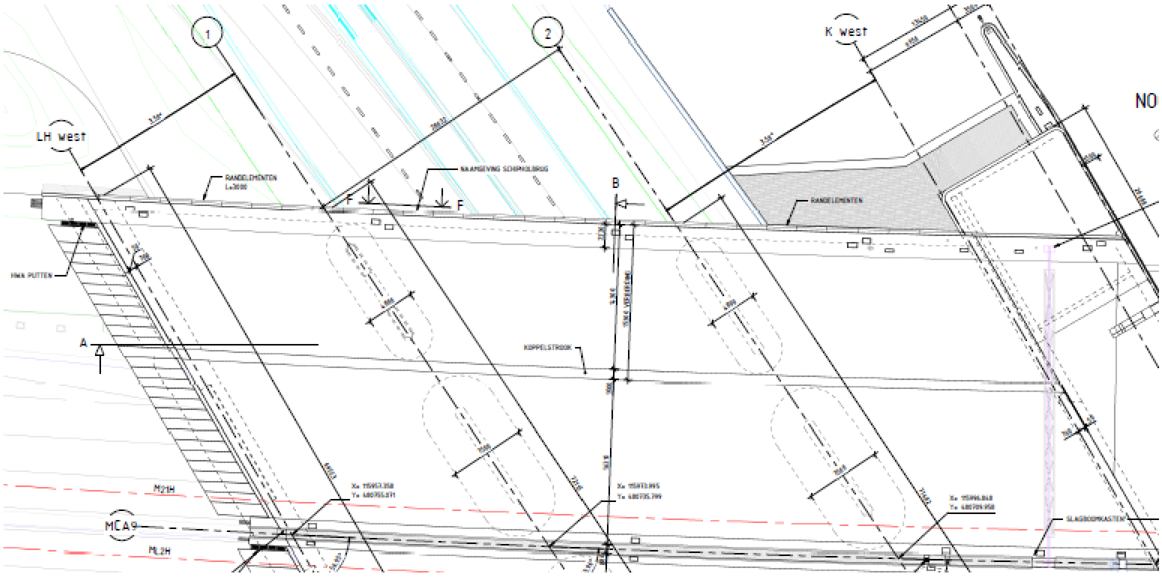

Figure 1.9: Northwest top view drawing of the future widen Schipholbrug given by Rijkswaterstaat (not available for the public).

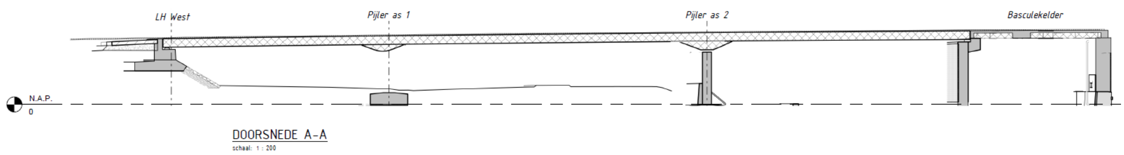

Figure 1.10: Cross-section drawing of the west spans of the future widen Schipholbrug given by Rijkswaterstaat (not available for the public).

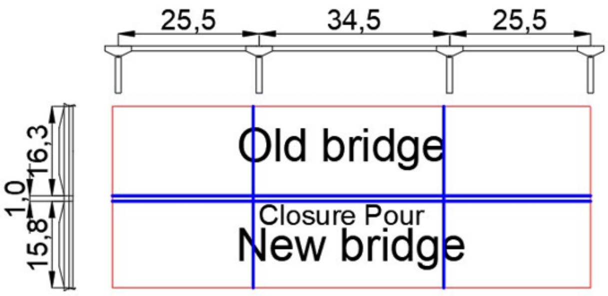

Figure 1.11: Scheme of three spans of the future Schipholbrug (distances are in meters) (top view).

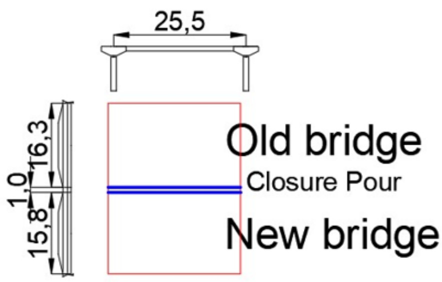

Figure 1.12: Scheme of one span of the future Schipholbrug (distances are in meters) (top view).

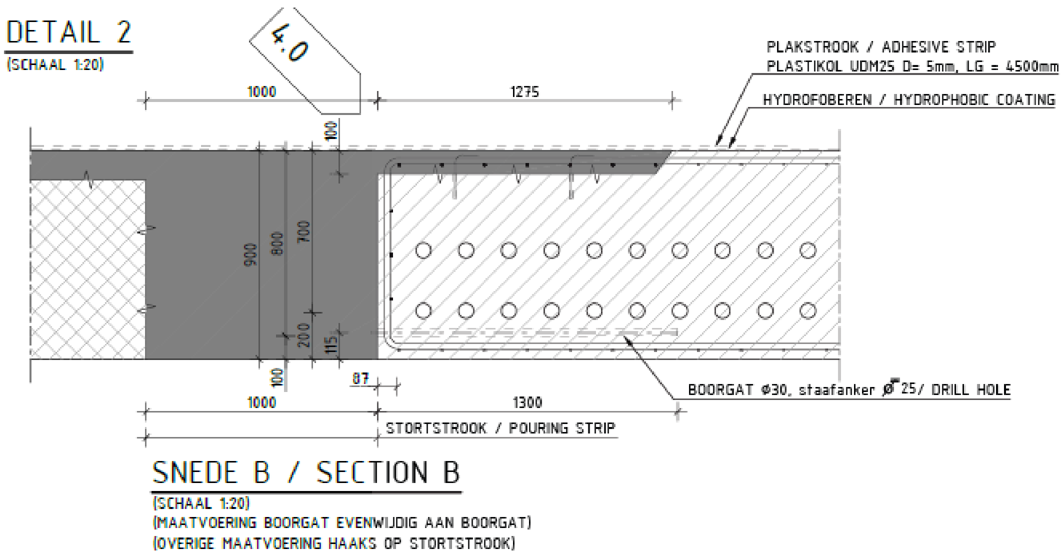

Figure 1.13: Section drawing of the closure pour of the future widen Schipholbrug given by Rijkswaterstaat (not available for the public and distances are in millimeters).

Please consult Figure 1.15 for the cross-sectional view of the span. It is of utmost significance to acknowledge that, for the purpose of this thesis, the bridge's thickness of $0.9m$ will be estimated constant, notwithstanding an increase to $1.8m$ in areas adjacent to the supports. In addition, all computations in this research work will rely on Figure 1.16 as the principal top view.

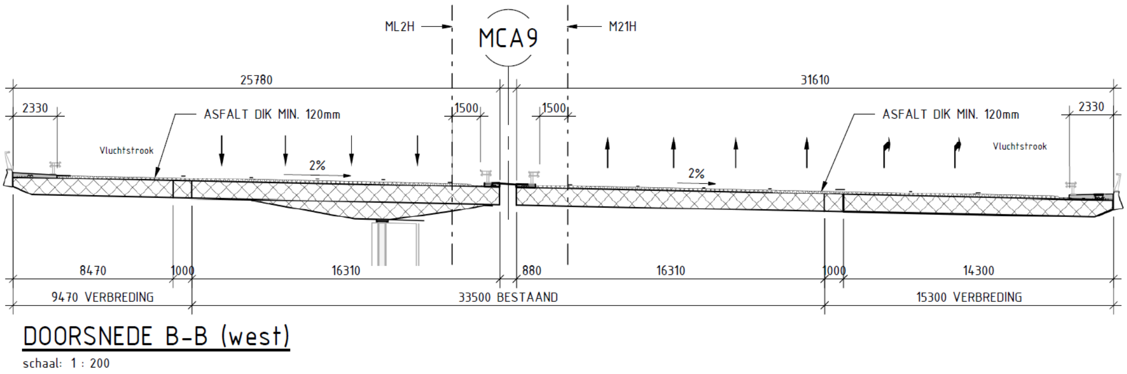

Figure 1.14: Cross-section drawing in the transversal direction of the west spans of the future widen Schipholbrug given by Rijkswaterstaat (not available for the public and distances are in millimeters).

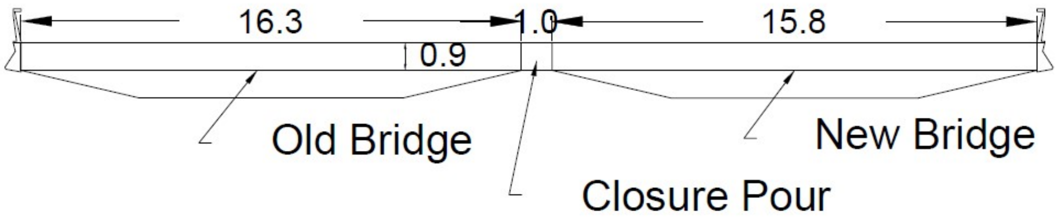

Figure 1.15: Northwest bridge scheme in transversal direction(distances are in meters).

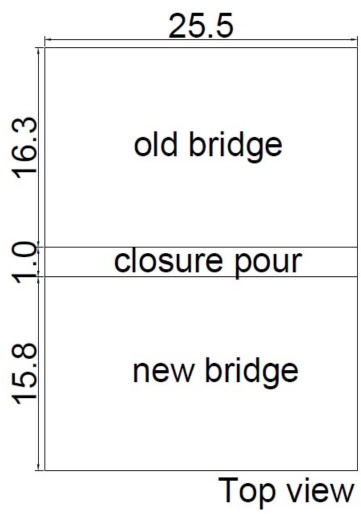

Figure 1.16: Top view scheme of one span of the entire bridge(distances are in meters).

This thesis focuses on the Schipholbrug and its relevance as a case study for bridge expansion. The Schipholbrug is representative of the many bridges constructed in the 1960s and 1970s that now require increased capacity due to growing traffic. As discussed in Section 1.1, replacing the bridge with a new structure is not a feasible option in a country committed to sustainability. Consequently, Rijswaterstaat has decided to widen the bridge by implementing a closure pour while simultaneously minimizing the time needed for casting. Nonetheless, reducing the casting time of the closure pour undergoes an even more significant difference in the deformation of the new and old bridges.

Reducing the casting time of the closure pour presents several challenges that this thesis aims to explore. Specifically, this thesis will examine the difficulties that arise when attempting to reduce casting time while still using reinforced concrete for the closure pour. Furthermore, the proposed solution to overcome these challenges is to integrate an innovative material known as Strain-Hardening Cementitious Composite, or *SHCC*.

1.3 Problem statement

The current method for expanding the width of prestressed concrete bridges involves constructing a new bridge one meter away from the existing structure using standard methods. Prestressing all cables up to 30% allows the concrete to begin deforming before the remaining stress is applied, which is completed within two months. However, it takes six to nine months [3] to create a reinforced concrete closure pour that connects the two bridges, resulting in a lengthy process for widening the bridge. Exploring alternative methods that could have been scientifically proven faster may be worthwhile.

The waiting period serves a crucial purpose in merging old and new concrete, as the two materials present various challenges when constricted to each other[4]. Of primary concern is the persistent gap in creep and shrinkage between the existing bridge (the "old" one) and the newly constructed bridge (the "new" one), as both of these properties develop exponentially. Consequently, the waiting period serves to minimize the need for both bridges to creep and the new bridge, as well as the closure pour, to shrink. It is essential to discover a solution that requires less time, given the critical nature of this issue. Moreover, the optimal method of joining two bridges could be applied to any prestressed concrete slab bridge requiring widening.

The closure pour, an essential component in bridge widening, typically utilizes reinforced concrete due to its advantageous properties, such as durability, cost-effectiveness, and greater rigidity than other materials. However, shortening the construction process when widening a bridge with reinforced concrete can lead to tension stresses within the closure pour that may surpass the material's mean axial tensile strength (f_{ctm}). Subsequently, this could result in the formation of cracks larger than $0.2mm$, which, according to Table 7.1N of the Dutch National Annex EN 1992-1-1[5], is not acceptable. It is important to note that avoiding the formation of such cracks is crucial in ensuring a safe and robust bridge construction project.

Cracks that surpass the Eurocode's limit[5] may impact the maintenance of the bridge. Additionally, the concrete's potential for creep and shrinkage, in combination with the bridge's statically indeterminate structure, could create hazardous conditions by altering moment distribution. This concern is particularly relevant due to the frequent use of deicing salts in the Netherlands to prevent multiple freeze-thaw cycles in the winter. These salts may infiltrate the cracks and corrode the reinforced concrete, ultimately compromising the bridge's ability to withstand the mandated 100-year lifespan for construction in the Netherlands.

In order to reduce the waiting period, the goal was to find a cementitious material that could seamlessly integrate with the primary decks' prestressed concrete, endure continuous traffic while retaining flexibility, and exhibit a high tensile strain range without the risk of cracks exceeding $0.2mm$. The ideal solution turned out to be Strain-Hardening Cementitious Composite, or *SHCC*. This innovative material possesses an impressive tensile strain range and a relatively lower elastic modulus. What truly sets it apart, however, is its strain-hardening capacity, which enhances its toughness in the face of cracks. This remarkable feature gives *SHCC* an extended tensile strain range, making it an option for a closure pour.

1.4 Research Question

Can the construction time needed for widening a prestressed concrete bridge be reduced by applying *SHCC* as a closure pour?

- What is the analytical calculation method for determining the stresses that arise from bridge widening based on the imposed deformation, and can this method be validated using numerical models?
- Is it possible to determine if SHCC would be a suitable and durable replacement for concrete in terms of handling the stresses caused by imposed deformation?

1.5 Outline

This Master's thesis examines the Schipholbrug as a prime example of a prestressed cast-in-situ concrete bridge, addressing the critical need to expand concrete bridges. The forces and stresses triggered by shrinkage and creep were analyzed through analytical calculations, which were validated through a numerical method using a Finite Element Analysis(*FEA*) linear model. To present the findings, the thesis was divided into six chapters: Introduction, Literature Review, Methodology, Results, Discussion, and Conclusion & Recommendations.

The Literature Review covers the main topics discussed in the thesis, including widening existing bridges, closure pour, shrinkage, creep, and crack of concrete, as well as *SHCC* and its composition, crack bridging, crack width, shrinkage, and crack and imposed deformation.

The Methodology chapter provides a clear explanation of the analytical and *FEA* linear model procedures, with data and calculations for both methods included in the appendix.

The Results chapter displays the main findings of the analytical and numerical calculations and highlights the essential data that changed throughout the different methods of each analysis.

In the Discussion chapter, a comparison is made between analytical and numerical calculations. The feasibility of using *SHCC* as a closure pour option is also addressed, followed by the presentation of insightful findings that assist in selecting the most suitable method - either concrete or *SHCC* - based on the obtained results.

The Conclusion & Recommendations chapter presented a conclusion of the entire thesis, answering the research question as well as recommendations for future studies.

2

Literature Review

2.1 Widening Existing Bridge

2.1.1 Problems

Throughout history, bridges were often built with narrow widths to fit within limited budgets and conservative traffic volume predictions. Unfortunately, the rapid traffic growth has made many of these bridges insufficient for their intended purpose. Thankfully, bridge widening has become a cost-effective and efficient solution to meet the rising demand for traffic volume and improve the capability of existing highway bridges[6].

Frequently, freeway bridges may experience a lack of sufficient width before their structural integrity becomes compromised, rendering them functionally obsolete. In such instances, it is typically more economically feasible to widen the bridge rather than completely replace it[7]. However, incorporating post-tensioned concrete bridge deck technology in expanding an existing bridge is a complex undertaking that requires careful consideration of various challenges. The success of this widening project depends on a comprehensive analysis of the factors that influence the relative movement of both the new and existing structures. These factors include dead and live load deflections, temperature fluctuations, prestress deflection, shortening, settlement, seismic activity, structural continuity, and stability. This thorough examination ensures that the expansion aligns with the structural integrity of the existing bridge. Another challenge that may arise is that the new deck's time-dependent deformations may surpass the existing deck's cracking threshold, resulting in elevated stress levels. Conventional methods to address this issue may cause significant construction delays[8, 9].

Additionally, it is crucial to note that bridges, particularly those composed of reinforced and prestressed concrete, experience a gradual reduction in structural capacity over time due to natural factors. Among these factors, the corrosion of reinforcement steel is the primary contributor to progressive deterioration. Ensuring the durability and reliability of infrastructure is of utmost importance, especially when faced with intricate challenges. Thus, it is essential to utilize innovative techniques to expand existing bridges [6].

When undertaking the expansion of a bridge, a thorough analysis of the interaction between the new and existing structures is essential. While it may appear more straightforward to analyze the structures separately, differences and inconsistencies in factors such as live-load distribution, reinforcement corrosion, and concrete shrinkage and creep can complicate the analysis when considering them together. Tu et al.[6] conducted a study on a widened prestressed concrete T-girder bridge that accounted for these differences and inconsistencies. However, according to Wen[10], it is essential to note that the old bridge's shrinkage and creep have already peaked when expanding an existing bridge with a new one, while the new bridge's shrinkage and creep are starting. This can cause significant stress redistribution due to the limitations of concrete stresses caused by the widened new bridge's shrinkage and creep. Therefore, a comprehensive evaluation of the long-term impacts is critical to prevent any potential issues.

2.1.2 Guides

The process of widening a bridge is highly intricate and involves several factors to be considered. To aid in this process, various organizations have created detailed guides. These include the California Department of Transportation[8], the American Concrete Institute[7], and the State of Queensland in Australia[11]. These guides offer valuable insights and recommendations to ensure that the bridge-widening process is carried out efficiently and effectively.

The Guide for Widening Highway Bridges, published by the American Concrete Institute[7], suggests leaving a gap between new and existing bridge deck sections when creating structural connections. This gap should be of an appropriate width for the selected reinforcing bar splice method and subsequently filled with concrete. To ensure the stability of this closure placement, the top and bottom mats of reinforcing bars must extend from both the new and existing bridge deck slabs, with all reinforcement securely tied together to minimize differential movements and the resulting damage to the closure concrete caused by traffic vibrations. It is crucial to note that reinforcing steel ties should only be made just before the concrete closure is placed. Additionally, the connection of diaphragms between the existing bridge and the widening, as well as the installation of forms for the closure placement, should also be made just before the closure is placed. The closure placement serves two critical purposes: firstly, it isolates the widening from live-load deflections and vibrations caused by traffic on the existing bridge; secondly, it allows for dead-load deflection and prestressing shortening of the widening, ensuring that the portion of the new bridge deck that connects to the old will not be overstressed due to differential movements between the old and new structures[7].

The California Department of Transportation (Caltrans) has released a Memo To Designers regarding the widening of existing bridges[8]. The memo highlights the significance of longitudinal expansion joints as a primary cause of maintenance issues in connecting a widening and an existing bridge. As a result, it is recommended that widenings be attached to the existing structure without longitudinal expansion joints. It is essential to emphasize the need for utmost attention to detail when it comes to attaching widenings to existing bridges. This general rule should be followed consistently to avoid any potential maintenance-related issues. The memo serves to provide guidance to designers and professionals involved in the widening of existing bridges and aims to ensure safety and efficiency in these projects[8].

2.1.3 Closure Pour

The closure pour, referred to by various names such as closure placement, closure slab, or "coupling strip", from the Dutch "koppelstrook", is a crucial component in bridge expansion projects. It serves to connect the new primary deck with the existing bridge while accounting for shrinkage and creep. By completing the deck connection, a closure pour ensures that the individual units function as a cohesive whole, mimicking the behavior of a monolithic structure. Specifically for the Schipholbrug, the two primary decks consist of the original bridge, constructed in 1969, and the new bridge, which is currently being built with a newly constructed deck scheduled for completion in 2024.

Closure slabs are a popular choice in bridge construction as they are known to be durable and have a low failure rate. However, research in this area has been limited due to the rarity of such incidents, as highlighted by Chai et al.[12]. Longitudinal joints, which function similarly to closure pours in expanding concrete bridges, were used to connect structural elements. Unfortunately, a failed longitudinal joint incident revealed that water infiltration through the construction joint caused severe corrosion of the epoxy-coated reinforcement. It is important to note that this reinforcement had been implemented during an earlier bridge rehabilitation project, as reported by Sprinkel et al.[13].

According to the Guide for Widening Highway Bridges[7], the process of creating longitudinal joints can pose a significant challenge, as historical data suggests a high likelihood of joint leaks occurring. This is primarily due to concrete shrinkage in the closure pour and the widened section of the bridge deck. Furthermore, the use of reinforced materials, such as epoxy-coated reinforcement, placed across the joint can also be susceptible to issues such as corrosion, section loss, and failure, as highlighted by Sprinkel et al.[13]. Thus, it is no longer common practice to utilize longitudinal joints. Should the existing bridge lack a closure pour or longitudinal joint, it would have to endure all of the deformations caused by the new bridge construction, including creep, shrinkage, and the impact of the new deck's prestressing.

2.1.3.1 Time

It is crucial to consider a waiting period after removing falsework when constructing cast-in-place concrete bridges to achieve the best possible outcomes. This delay allows for early dead-load deflection to occur before connecting the bridge decks. To ensure adequate space for dead-load deflection during closure placement, it is essential to engineer the duration of the delay period and the width of the closure placement with precision [7]. Additionally, delaying the closure pour can yield various benefits, including reducing load transfer to the existing structure, improving deck riding quality, reducing stresses in the closure slab, and allowing for the shortening of prestressed girders. These approaches can result in significant enhancements to the performance and longevity of cast-in-place concrete bridges [8].

2.1.3.2 Freezing-Thawing

Repeated cycles of freezing and thawing can result in more damage to concrete than a single occurrence of frost. The extent of harm caused by these cycles can range from surface scaling to complete disintegration as layers of ice form, starting at the exposed surface of the concrete and progressing through its depth. Highway slabs are especially vulnerable, especially when de-icing salts are used, as they are absorbed by the top surface of the slab, resulting in high osmotic pressures that force water towards the coldest zone where freezing occurs. To prevent damage, it is crucial to ensure that air-entrained concrete is not overvibrated to form laitance and to use a rich mix with a low water/cement ratio. The concrete should also be moist-cured for a sufficient period, followed by a period of drying before exposure[14]. The issue of freezing and thawing is also a concern for *SHCC*, as noted by Yun et al.[15, 16].

2.1.3.3 Crack Width

Another issue of the closure pour is the maximum crack width that the closure pour material could present. Furthermore, since the closure pour is the only element of the bridge deck that could be made of reinforced concrete, it faces potential exposure to chloride spray from de-icing agents, as mentioned at Section 2.1.3.2. According to Eurocode EN 1992-1-1 guidelines[17], the closure pour's exposure class is designated as *XD3*(*XD* stands for "Chloride induced corrosion, not from seawater (**D**e-icing)" and the number *3* refers to a "Humid in combination with de-icing salts") in Table 4.1 of the Eurocode EN 1992-1-1. The *XD3* classification, as per Table 7.1N at the Dutch national annex[5], stipulates that the maximum allowable crack width in reinforced concrete must not exceed $0.20mm$. However, it is essential to note that the calculation for determining the required reinforcement to stay within the limit is beyond the scope of this thesis. Therefore, if the stresses in the closure pour exceed the mean value of axial tensile strength of concrete (f_{ctm}), the concrete closure pour will not be deemed a viable solution to the problem.

2.2 Concrete

Concrete is the primary material employed in the construction of the bridge deck, with both the preexisting and new decks being constructed using prestressed concrete. Additionally, the closure pour can be executed by incorporating reinforced concrete.

When constructing with concrete structures, it is vital to consider the potential impact of volume changes due to shrinkage and external stress. In practical applications, these movements are often restricted, ultimately resulting in stress. Although it may seem as though shrinkage (or swelling) and thermal fluctuations are separate from stress, the reality is more elaborated. The presence of tensile stress, resulting from any type of limitation, poses a significant risk, as concrete is fundamentally brittle in tension and susceptible to cracking. It is essential to prevent or manage cracks, as this ensures the longevity and structural integrity of the structure, as well as its visual appeal[14].

The determination of the material properties of concrete was conducted in accordance with the Eurocode EN 1992-1-1 [17]. The "RTD 1001 Richtlijnen Ontwerp Kunstwerken" [18], which is the primary guideline for infrastructure in The Netherlands, was consistently referred to as well, which ensured that all necessary considerations were studied.

2.2.1 Shrinkage

Walraven et al.[4] made a simple definition of concrete shrinkage: "It is the shortening of the concrete occurring without the influence of any load, which is caused by the drying of the material". This phenomenon's extent is contingent upon four critical factors, namely, the relative humidity, the concrete's strength class, the dimensions of the cross-section, and the age of the concrete, as indicated by Walraven et al.[4]. Based on 3.1.4(6) of Eurocode EN 1992-1-1[17], the shrinkage calculation depends on the drying shrinkage and autogenous shrinkage.

Drying shrinkage is a consequence of water removal from a concrete member, and it can persist for many years, especially in structures with substantial dimensions[4]. To rephrase, this phenomenon occurs when hardened concrete is exposed to unsaturated air, resulting in the removal of moisture. The irreversible aspect of drying shrinkage, which is the focus of this thesis, is associated with forming additional physical and chemical bonds within the cement gel once the absorbed water has been extracted. The typical pattern involves the loss of free water in the capillaries during the drying process. This loss induces variations in the internal relative humidity within the cement paste structure. Over time, water molecules migrate from the extensive surface area of calcium silicate hydrates into vacant capillaries and ultimately out of the concrete. Consequently, the cement paste contracts, but the reduction in volume does not precisely match the volume of removed water. This discrepancy arises because the initial loss of free water does not significantly contract the paste volumetrically, and there are internal constraints on consolidation due to the calcium silicate hydrate structure[14].

Autogenous shrinkage is primarily triggered by the insufficient presence of water during the hydration of concrete. This condition leads to the development of under pressure within the concrete's pore system. It is worth noting that autogenous shrinkage is associated with the development of the hydration process itself, thus reaching its ultimate magnitude within a relatively brief timeframe[4]. It is important to emphasize that autogenous shrinkage persists even when there is no possibility of moisture movement into or out of the cured concrete. This phenomenon arises due to water consumption in the hydration process, leading to a reduction in volume [14]. Autogenous shrinkage exhibits a direct linear correlation with the strength of the concrete. This aspect warrants particular attention, especially in scenarios where fresh concrete is cast against pre-existing hardened concrete[17].

As previously delineated, the evaluation of concrete shrinkage was conducted in accordance with the Eurocode EN 1992-1-1[17] and further referenced the primary infrastructure guidelines of The Netherlands, known as the "RTD 1001 Richtlijnen Ontwerp Kunstwerken" [18]. Appendix A and Appendix B of this report provide a detailed exposition on the determination of shrinkage for both the concrete used in the recent bridge construction and the concrete envisaged for the closure pour, adhering to the guidelines mentioned above.

While it is accepted that concrete shrinkage can persist for a prolonged duration, sometimes surpassing 100 years, it is crucial to recognize that the overwhelming majority (95%) of this shrinkage occurs within the initial 50-year timeframe. Based on this knowledge, it has been reasonably inferred that the shrinkage of the pre-existing bridge was insignificant. Consequently, the current bridge is deemed to possess infinite rigidity.

Shrinkage strains are a crucial consideration in concrete engineering, as they can lead to the development of tensile stresses when restrained. Due to the inherent low tensile strength of concrete, restrained shrinkage often results in the formation of cracks in concrete structures. These cracks can be influenced by factors such as the magnitude of shrinkage strains, the level of restraint, and the effects of drying shrinkage, as discussed in [7].

2.2.2 Creep

In this master thesis, creep was taken into consideration as well, since just as shrinkage, it can cause imposed deformations.

Creep, a phenomenon characterized by the gradual increase in deformation over time under a consistently applied and unvarying load, is intimately linked with relaxation, which entails the maintenance of material deformation at a constant load while the initial stresses progressively diminish with time, as meticulously defined by Walraven et al.[4]. In the context of statically indeterminate structures, creep, in conjunction with relaxation, has the capacity to alleviate stress concentrations stemming from shrinkage-induced effects. Moreover, it is imperative to emphasize that across all concrete structures, the role of creep assumes vital significance in mitigating internal stresses resulting from non-uniform or constrained shrinkage, thereby effecting a significant reduction in the propensity for crack formation, as expounded upon by Neville et al. in "Concrete Technology"[14].

Creep development and its final magnitude are influenced by several critical factors, including relative humidity, concrete age under loading, choice of cement, curing conditions, concrete strength grade, cross-sectional dimensions, and the duration of applied loading[4]. Creep arises from the deformation of its gel structure and the capillary stress of chemically non-bonded water. Consequently, under low relative humidity (*RH*) conditions, there is an increased potential difference between the structure's moisture content and its surroundings, resulting in accelerated drying. Two opposing effects come into play: reduced moisture content within the structure increases creep, while lower moisture content within the structure reduces creep. In practice, the predominant influence stems from the disparity in moisture content between the structure and the environment. A low *RH* coupled with a small size leads to a high φ_{RH}, whereas a high RH with a large size yields a high β_H, consequently reducing $\beta_c(t, t0)$[4].

Regarding concrete strength, two considerations emerge. Firstly, as the strength of the concrete increases, its stiffness also increases, which helps to reduce creep. Secondly, higher-strength concrete is less permeable, leading to a slower drying process, thereby reducing creep deformation. The fineness of the cement and elevated temperatures accelerate the hydration process, resulting in concrete with a high degree of hydration being less prone to creep when subjected to loads. Temperature effects also influence the age at which concrete is loaded, adjusted based on hardening temperature using the concept of adjusted concrete age, as outlined by Walraven et al.[4].

Creep phenomena can manifest when a concrete specimen under load is constrained, leading to a sustained strain over time. In such cases, creep is characterized by a gradual decline in stress as time advances, a phenomenon conventionally denoted as relaxation, as elucidated by Neville et al. in "Concrete Technology" [14].

The calculations were based on Annex B.1(1) of Eurocode EN 1992-1-1[17]. For the sake of simplification, it is commonplace to assume that the sections are fully cracked, and, consequently, stiffness calculations should be predicated upon the utilization of an effective concrete modulus, a practice advocated by 5.8.7.2(4) of the Eurocode EN 1992-1-1 guidelines [17].

Creep in Tension

When subjected to sustained loads, whether in compression or tension, concrete exhibits the development of creep, a mechanism commonly classified as a "delayed" phenomenon in the category of viscoelasticity. This "delayed" characteristic entails a gradual evolution over time following the application of load-induced strain, as documented by Kim et al.[19].

Remarkably, Kim et al.'s experiments[19] highlight a notable disparity between tensile and compressive creep strains. Nonetheless, for this thesis, the consideration of tensile creep effects has been deliberately excluded. This decision is established in the potential complexity introduced when simultaneously factoring in creep and crack-induced modifications to the elastic modulus. Given the greater significance of addressing the issue of cracks, it was deemed prudent to maintain the focus in that direction.

2.2.3 Crack

Cracking has a significant effect on the response of a structure under any type of loading. Cracks may occur under an external load or an imposed deformation. In the case of cracking caused by an imposed deformation, the crack distance is irregular. This case is denoted as a not fully developed crack pattern[20].

According to Mehta et al.[21], concrete has a tendency to develop cracks when the tensile stress level, resulting from the combined effect of elastic modulus and shrinkage strain, reaches its tensile strength. The presence of cracks in unreinforced concrete poses a significant problem as it ultimately results in failure.

In contrast, reinforced concrete structures are also often susceptible to cracking, adversely affecting their durability and appearance. The presence of wide cracks may impede the structure's ability to meet the required standards for durability and serviceability, including liquid tightness. To mitigate these potential issues, a good design and detailing of a structure should be made to limit crack widths [22]. It should be noted that so long as the width of any present cracks adheres to the applicable regulations, their presence should not be deemed a cause for concern.

When evaluating reinforced concrete structures, the occurrence of cracks results in a reduction in stiffness and weaker forces, which can pose a challenge in designing while considering all pertinent variables. In order to account for deformations in structural models, engineers will often opt to lower the uncracked stiffness and reinforce the design. However, the selection of the appropriate reduction factor is a crucial decision. In practical scenarios, it is a common practice to reduce the uncracked concrete Young's modulus to one-third of its initial value when calculating the cracked Young's modulus [22]. It is widely acknowledged that concrete begins to lose its stiffness once it exceeds its tensile strength, and this loss of stiffness continues to develop as cracks form. For the sake of clarity and brevity in this thesis, it was assumed that the elastic modulus is reduced to one-third of its initial value upon cracking.

2.3 *SHCC*

In the field of construction materials, Strain-Hardening Cementitious Composite(*SHCC*) has gained recognition for its remarkable capacity to withstand high tensile forces even after the formation of cracks, covering a wide range of tensile deformation. This ability is attributed to the efficient crack bridging facilitated by the fibers, which extend across multiple micro-scale cracks[23].

2.3.1 Composition

The composition of *SHCC* includes a binder, fine particles, water, and approximately 2% volume of fibers. Typically, Polyvinyl Alcohol(*PVA*) or High-Density Polyethylene(*HDPE*) fibers are utilized for this purpose[24].

Over the course of several years, a diverse collection of composite formulations for Strain-Hardening Cementitious Composites has been developed. The first mixture comprised Ordinary Portland Cement (*OPC*), fly ash, and silica sand. Subsequent modifications proceeded, where binders and aggregates experienced adjustments, specifically the replacement of fly ash with blast furnace slag and the substitution of silicate sand with limestone powder. Simultaneously, adaptations were made to the composition of these mixtures to incorporate elements such as coarse sand, aggregates, and the incorporation of nanomaterial additives. Chemical admixtures were introduced to decrease the curing duration for the restoration of structures[25].

2.3.2 *SHCC* vs *ECC*

Li, V., the original creator, utilized the name Engineered Cementitious Composites (*ECC*) to emphasize the material's construction foundation based on micromechanics [26, 27]. Micromechanics enables a strong connection between materials engineering and structural performance design, making it a powerful tool for directing materials design towards specific composite qualities [28]. The *RILEM TC HFC*, ((International Union of Laboratories and Experts in Construction Materials, Systems and Structures) (Technical Committee) (High-performance fibre reinforced cementitious composites))[29] decided to highlight the material's distinctive tensile strain-hardening response as a constitutive law for structural engineering design in 2006. This class of materials was given the more descriptive name Strain Hardening Cementitious Composites (*SHCC*). The material is also referred to as "Multiple Fine Cracking Fiber Reinforced Cementitious Composites" by the Japan Society of Civil Engineers (*JSCE*) which wishes to emphasize the multiple fine cracks. Fundamentally, all of these materials are meticulously crafted through the utilization of micromechanical instruments, embodying uniform material technology.

Efforts have been made to improve the clarity and accessibility of the information to enhance the comprehensibility of research results. Although some sources refer to Engineered Cementitious Composites (*ECC*), this thesis will mainly use Strain Hardening Cementitious Composite and its abbreviation *SHCC* to make it easier to understand.

2.3.3 Crack-Bridging

According to Figure 2.1, the behavior of the stress-strain diagram is attributed to the emergence of numerous tiny cracks, which are accompanied by several minor stress drops known as pseudo-strain-hardening. When the loading increases, the first micro-crack begins to grow, resulting in the initial decline in the stress-strain diagram. Subsequently, the fibers bridge the crack, leading to slip-hardening, and the load is effectively transferred through the crack, as per Tai et al.'s research on upscaling composites[30]. Compared to regular concrete, Wu et al.[31] have highlighted that *ECC*'s remarkable tensile ductility is due to the crack-bridging effect of fibers[26].

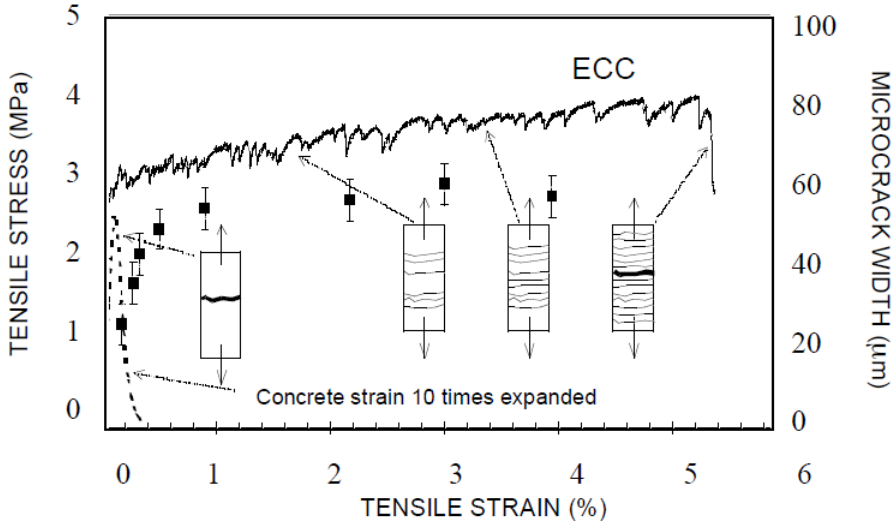

Figure 2.1: Tensile stress-strain curve of an *ECC*[26].

2.3.4 Crack Width

Reinforced concrete is particularly susceptible to issues with crack width due to reinforcement corrosion, but this is not a problem for *SHCC* as it does not require reinforcement. Nevertheless, research has been conducted in this area. According to Wang et al.'s research on beams[32], *SHCC* possesses strain-hardening and multiple cracking properties, as well as exceptional crack resistance and permeability. In fact, *SHCC* features an ultimate tensile strain range of $3-7\%$, surpassing ordinary concrete by $300-700$ times. Notably, even when *SHCC* is subjected to ultimate tensile load, it successfully limits crack width to just $100\mu m$, as reported by Van Zijl et al.[23], Lukovic[25], and Li[26], which is well below the maximum of $0.2mm$ allowed for concrete structures with reinforced members, as stated in table 7.1N of the National Annex EN 1992-1-1[5] and mentioned previously at Section 2.2.3. Martinola et al.[33] mentioned that even if there is a problem with water, *SHCC* could be prepared with water-repellent agents that present very low water absorption coefficient in both the uncracked and cracked state. Besides, after extensively studying Wang's research [32], which serves as the primary reference for the *SHCC* in this thesis, it was discovered that the crack width for *SHCC* is limited to a maximum of $0.05mm$

2.3.5 Shrinkage of the *SHCC*

The presence of fibers and their interface with the fiber matrix may not significantly impact moisture transport. However, it does play a crucial role in driving mechanisms such as drying shrinkage. This phenomenon occurs when moisture moves from a higher to a lower relative humidity environment, causing a decrease in the volume of an unloaded specimen at a constant temperature. It is worth noting that certain fibers, particularly natural fibers, have the ability to absorb moisture and undergo swelling or shrinking based on the relative humidity. This alteration in strain could potentially affect the bond between the fiber and matrix[34].

At *SHCC*, a precisely measured quantity of fine sand is incorporated into the matrix to regulate the material's fracture toughness and attain targeted mechanical characteristics, such as strain-hardening and multiple cracking behaviors. This unique requirement prevents the use of coarse aggregates, resulting in a higher cement content that causes a high drying shrinkage strain during the setting and hardening of the composite. Under normal drying conditions of $20°C$ and 60% relative humidity, regular concrete produces an ultimate drying shrinkage strain of 400×10^{-6} to 600×10^{-6}. In contrast, conventional *SHCC* can produce an ultimate drying shrinkage strain of approximately 1200×10^{-6} to 1800×10^{-6} under similar conditions[35].

When working on construction projects utilizing Strain-Hardening Cementitious Composite (SHCC), it is crucial to consider the drying shrinkage that may occur carefully. Compared to standard concrete, *SHCC* can exhibit shrinkage rates that are twice as significant due to its elevated cement content and inclusion of fine particles, leading to a finer microstructure pore size. The behavior of cementitious composites is influenced by both aggregates and fibers, with coarse aggregates reducing overall shrinkage while facilitating stable crack propagation and fibers primarily controlling crack width, especially in the absence of larger aggregate particles. It is also worth noting that *SHCC* displays impressive strain-hardening behavior[34].

The difference in shrinkage deformation between *SHCC* and concrete can potentially lead to an increased risk of shrinkage-induced cracking in structures that utilize *SHCC*, which could result in durability issues over time and should be considered, as noted by Zhang in their study on engineered shrinkage[35]. While *SHCC* does have some resistance to drying shrinkage, microcracks in harsh conditions can significantly compromise the efficacy and durability of *SHCC* as a repair material, as pointed out by Weimann in their research on drying *SHCC*[36].

In the case of restrained strain, the tensile stress starts to build up in the material. After exceeding the tensile strength of *SHCC*, cracks will appear in the material. No localized cracks in *SHCC* will appear. It will have rather many fine shrinkage cracks[34].

2.3.6 Applied *SHCC* Properties

For this thesis, it was chosen a specific *SHCC* from Wang's article[32] since he had a formula to calculate the shrinkage of his *SHCC* at any moment in time, which is crucial for the calculations of this thesis.

This *SHCC*[32] had a compressive strength of $48.49MPa$ ($100mm \times 100mm \times 100mm$) after 28 days of indoor curing ($T = 25 \pm 3°C$, $RH = 60 \pm 5\%$) was used. The mix proportion of *SHCC*, optimized with local materials, is shown in Figure 2.2. Ordinary Portland cement P O 42.5 and local fly ash with chemical compositions (determined by X-ray Fluorescence) shown in Figure 2.3 were used. Sand with a maximum grain size of $0.3mm$ was also used. Additionally, *PVA* fibers with properties (provided by the manufacturer) shown in Figure 2.4 were added to the fresh mix to enhance *SHCC*'s workability. A small amount of superplasticizer(SP) was added to improve workability further[32].

No.	Cement	Fly Ash	Sand	Water	SP	PVA Fiber
SHCC	555	680	490	420	27.8	26

Figure 2.2: Mix proportion of *SHCC* from [32].

Material	CaO	SiO_2	Al_2O_3	MgO	SO_3	Fe_2O_3	K_2O	TiO_2	MnO	Na_2O	P_2O_5
Cement	57.27	20.60	7.17	4.70	4.43	3.85	0.77	0.40	0.35	0.17	0.13
Fly ash	1.83	58.10	31.79	-	0.51	3.76	1.51	1.57	0.02	0.36	0.20

Figure 2.3: Chemical composition of cement and fly ash from [32].

Length (mm)	Diameter (μm)	Young's Modulus (GPa)	Elongation (%)	Tensile Strength (MPa)	Density, (g/cm^3)
8	39	42	7	1600	1.3

Figure 2.4: Property of *PVA* fiber from [32].

Shrinkage

According to Wang's research[32], a formula was developed to determine the shrinkage of *SHCC* by utilizing a graphical curve displayed in Figure 2.5. The formula earlier mentioned was subsequently applied in the computations presented in this thesis, which are depicted in Equation 2.1, where t is the drying time, counted in days.

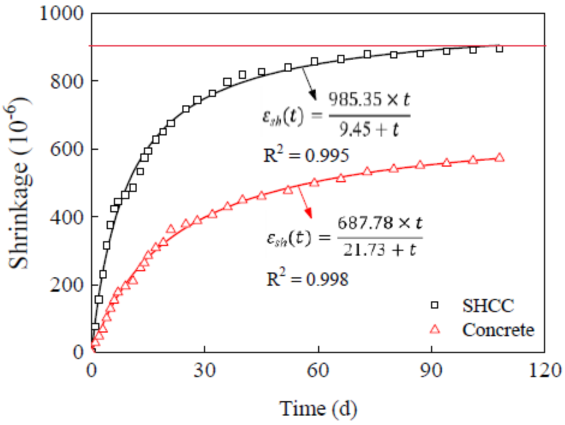

Figure 2.5: Graphic and formula used to calculate the shrinkage of 100 years of the *SHCC* from [32].

$$\varepsilon_{shr}(t) = \frac{985.35 \times t}{9.45 + t} = \frac{985.35 \times 36500}{9.45 + 36500} = 985.09 = 9.85 \times 10^{-4} m/m \quad (2.1)$$

Crack

As shown in Figure 2.1, the tensile stress of *SHCC* increases instead of decreasing like concrete. Therefore, the method for calculating when *SHCC* is cracked differs from concrete.

Utilizing the values at the 28-day mark as highlighted in Figure 2.7, a simplified version of Figure 2.6 was developed and is presented in Figure 2.8.

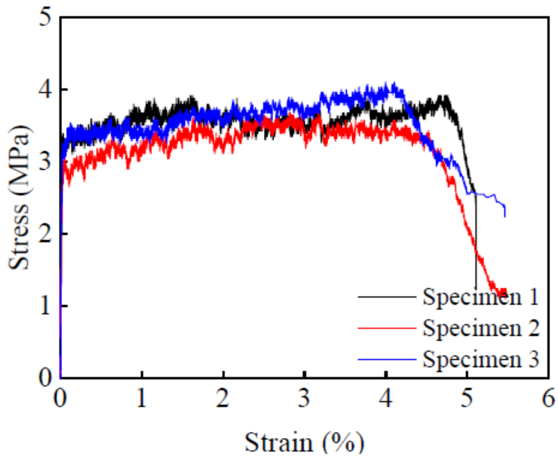

Figure 2.6: Stress-strain curve of the *SHCC* from [32].

Age (day)	F_t (MPa)	ε_t (%)	E_t (GPa)	f_{tu}, (MPa)	ε_{tu} (%)
1	2.050 ± 0.028	0.0237 ± 0.00024	8.645 ± 0.064	2.945 ± 0.143	4.247 ± 0.370
14	2.893 ± 0.125	0.0242 ± 0.00076	11.945 ± 0.489	3.750 ± 0.057	4.336 ± 2.956
28	2.950 ± 0.166	0.0237 ± 0.00055	12.421 ± 0.956	3.824 ± 0.219	4.331 ± 0.306
90	3.073 ± 0.018	0.0223 ± 0.00106	13.795 ± 0.586	3.950 ± 0.291	3.545 ± 0.287

Figure 2.7: Mechanical parameters of *SHCC* from [32].

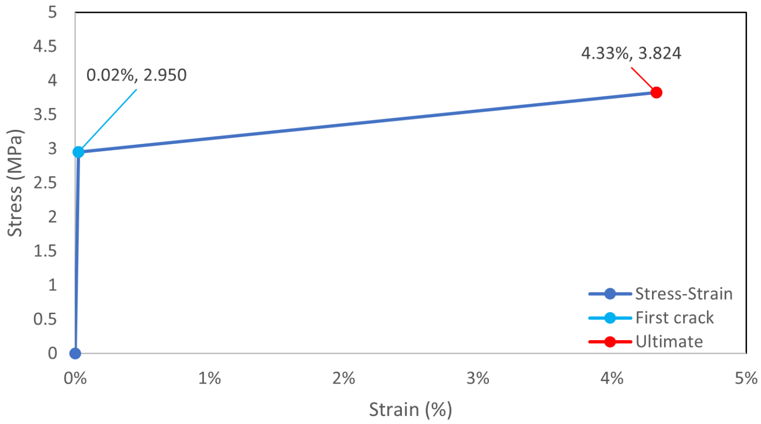

Figure 2.8: Simplified stress-strain curve of the *SHCC*.

Table 2.1 consolidates crucial *SHCC* data required for the calculations presented in this thesis. The shrinkage parameter (ε) was derived from Equation 2.1, while the modulus of elasticity was extracted from the 28-day mark, as depicted in Figure 2.7. Furthermore, a Poisson's ratio of 0.2 was employed, consistent with the methodology, which aligns with the approach taken by numerous other researchers[37, 38, 39, 40].

Material properties	*SHCC*
Shrinkage (ε)	9.85×10^{-4}
Modulus of Elasticity(MPa)	12421
Poisson's Ratio	0.2

Table 2.1: *SHCC* properties.

2.4 Imposed Deformation

2.4.1 Definition

The term "imposed deformation" can be a source of confusion and misunderstanding, according to the "Pink Book"[20]. To avoid such confusion, it is essential to note that a more accurate and appropriate term that conveys the intended meaning is "restrained deformation," as explained in detail in Figure 2.9. This figure illustrates a prismatic bar of length L, fixed at one end and free at the other, Figure 2.9a, which undergoes a temperature drop of ΔT. The length of the bar changes by an increment $\Delta L(\Delta T)$ without any stress, as it can freely shorten[20].

However, in Figure 2.9b, a bar rigidly clamped at both ends undergoes shortening due to a temperature drop, but the boundary conditions do not allow it. This leads to the development of tensile stresses, which may be misleading since there is no visible bar deformation[20].

To clarify this, a fictitious cut is made at one end of the bar, as shown in Figure 2.9a. To restore the original situation, a tensile force P must be introduced, generating an elongation of the bar equal to the imposed deformation ΔL. Therefore, the term "imposed deformation" refers to the situation of free deformation of the bar[20].

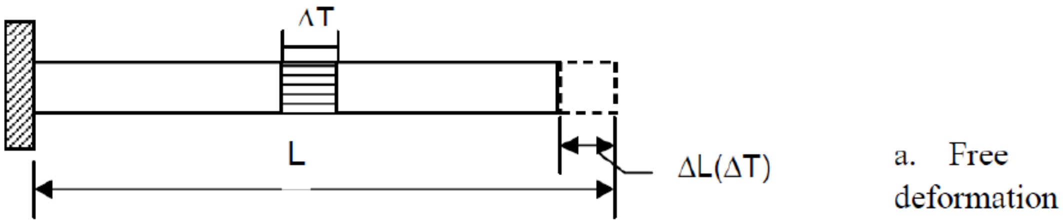

(a) Bar, fixed at one end, shortened by an imposed temperature drop. No stresses.

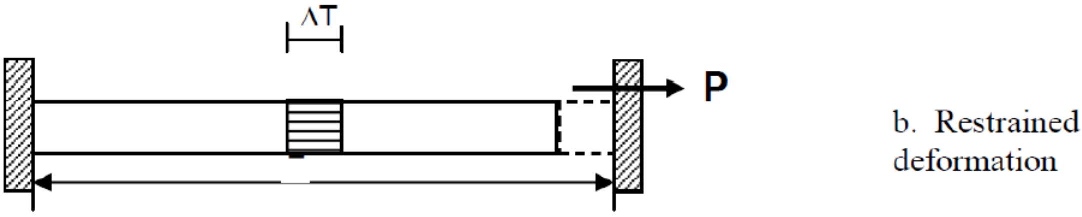

(b) Bar, fixed at both ends, prevented to shorten under temperature drop.

Figure 2.9: Imposed Deformation - Definition[20].

The example in Figure 1 highlights the importance of determining the stresses and forces caused by an imposed deformation. Firstly, it is necessary to determine the free deformation of a structural element due to any changes in temperature, shrinkage, or swelling, among others. Then, the forces required to restore deformational compatibility are calculated, considering the kinematic boundary conditions. This process is critical in the design of structures to ensure optimal performance and safety[20].

2.4.2 Young To Old Concrete

A relevant example of imposed deformation to consider within the context of this thesis is the scenario of a wall being cast onto a rigid foundation.

The concept of "young to old concrete" is a fundamental principle in wall construction, whereby a sturdy foundation is the key to a durable structure. As depicted in Figure 2.10, the portion on the left has already been cast, possessing exceptional strength and rigidity, while the section on the right is cast at a later time. During the process of concrete hardening, heat is released, leading to an increase in the concrete's temperature. Depending on the wall's size and the type of cement utilized, the temperature within the hardening concrete can rise as high as 60-80℃. Once the wall starts to cool, it will contract. If the newly cast portion can deform without constraint in relation to the older concrete, no tension will arise, as shown in Figure 2.10a. However, in practice, the new concrete's shortening is constrained at the joint with the old concrete Figure 2.10b. To restore the deformation compatibility, a shear force (resulting in tension between the "new" and "old" sections) is introduced, which produces tensile stresses. The crucial question is whether the tensile stresses generated σ_{ct} exceed the actual tensile strength f_{ct}. If the tensile stress develops quicker than the tensile strength, cracking will result[20].

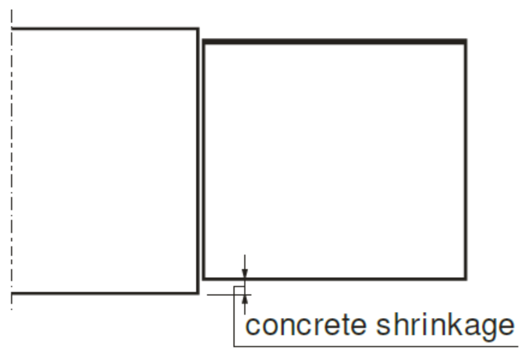

(a) Fictitious case, where young concrete can deform freely relative to the old concrete.

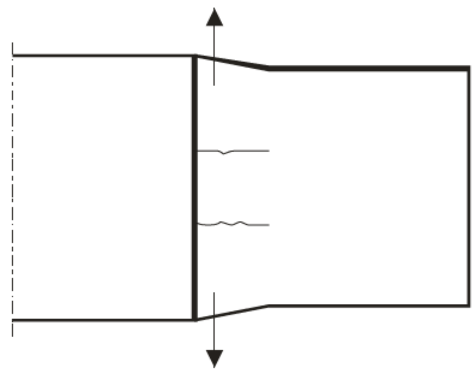

(b) Restrained deformation and cracking caused by imposed deformation.

Figure 2.10: Young concrete cast against old concrete[20].

2.4.3 Schipholbrug

The topic of this thesis explores the phenomenon known as "young-to-old concrete". Although early-age cracking is a common issue, this study primarily examines the long-term shrinkage differences that cause a deformation gap between the original section of a bridge and newly constructed parts, like the closure pour and new bridge, that are added during the widening of a prestressed concrete bridge. For a visual depiction of this phenomenon, please refer to Figure 2.12.

Additionally, due to the differences in materials and casting times, there may also be a discrepancy in shrinkage between the closure pour and the new bridge. As noted by Reinhardt in his work[41], when interconnected concrete components have varying shrinkage histories, they can cause deformations in each other that may lead to tensile forces and, ultimately, cracking. This issue can prove to be particularly challenging to address[41].

The top view of the Schipholbrug without any imposed deformation is depicted in Figure 2.11. Meanwhile, Figure 2.12 showcases the expected behavior of the new bridge and closure pour, taking into account the varying levels of shrinkage among the three structures. Notably, Section 2.2.1 previously established that the old bridge is no longer experiencing any shrinkage.

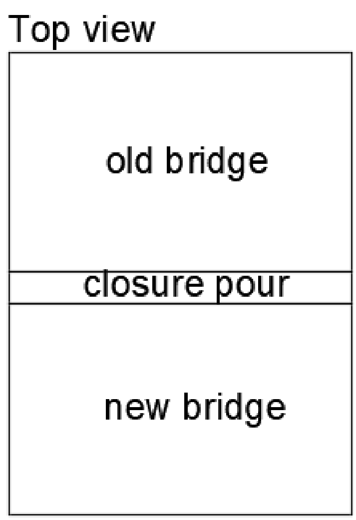

Figure 2.11: Schipholbrug without imposed deformation.

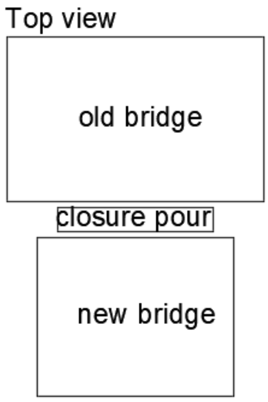

(a) Fictitious case, where closure pour and new bridge can deform freely relative to the old bridge and to each other.

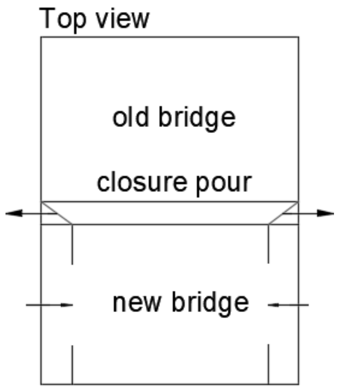

(b) Restrained deformation caused by imposed deformation.

Figure 2.12: Imposed Deformation of Schipholbrug.

3 Methodology

3.1 Introduction

This chapter provides an explanation of the methodology used in this thesis. The analytical and numerical calculations were the two forms of methodologies utilized. The purpose of implementing the latter was to support the former and determine whether *SHCC* is a better material than concrete for expediting the construction of the bridge's closure pour.

The main decks' material was not the central topic of this thesis, so they remained unchanged. The new bridge consists of prestressed concrete $C50/60$, while the old bridge is made of prestressed concrete assumed to be $K450$ with an elastic modulus of $31.5GPa$, as mentioned in Appendix F. It is worth noting that the calculations did not account for the fact that the bridges were prestressed. The thesis focused on the closure pour, which aimed to reduce the construction time for widening a bridge. Two materials were considered for this purpose - reinforced concrete, which is the current preferred material in the Netherlands, and *SHCC*. The reinforced concrete used was a $C40/50$ without taking the reinforcements into account. Additionally, the chosen *SHCC* was a specific type from Wang's article, as it is further explained with the reason behind this choice in Section 2.3.6.

3.1.1 Analytical calculations

In this thesis, the primary methodology utilized involved analytical calculations that solve imposed deformation with composite structure mechanics[1], as explained in Section 2.4 and further elaborated on in Section 2.4.3. This approach was specifically developed to accurately assess the stress generated by temperature fluctuations that occur while pouring fresh concrete into existing structures during different stages of construction, usually in the short term. The calculations were based on the variance in strain between the two materials, meaning that the procedure would function in the same manner even if the difference is in shrinkage between the two materials that spans 100 years. Therefore, the study of shrinkage is examined as an in-plane load.

Then, with this application, three methods were created to determine the longitudinal stresses present in the mid-span of the decks, all of them using just a cross-section of one span of the bridge, disregarding the entire length of the span. The first was tested with a part of just the old and the new bridge, considering only the shrinkage of the new bridge. The second method included a closure pour, but it was assumed that only the new bridge was shrinking. The third method analyzed the old and the new bridges, and the closure pour and examined the shrinkage of the closure pour and the new bridge. Table 3.1 and Table 3.2 provide simplified explanations of these three methods. Table 3.1 outlines the elements present in the widening bridge. In contrast, Table 3.2 illustrates the source of the force. The second and third methods were tested with a concrete closure pour. Since the third method was deemed the most realistic, it was also tested with *SHCC* closure pour.

[1]The designation “Composite structure” pertains to structures constructed of interconnected elements that possess varying properties, often of a concrete nature. The term “composite” is typically applied at the macro level but may also refer to materials composed of multiple constituents at the micro- or meso level[20].

	Method 1	Method 2	Method 3
Old bridge	$\exists$	$\exists$	$\exists$
Closure Pour	$\nexists$	$\exists$	$\exists$
New bridge	$\exists$	$\exists$	$\exists$

Table 3.1: Element of the widening bridge that is presenting which method.

	Method 1	Method 2	Method 3
Old bridge	-	-	-
Closure Pour	-	-	Shrinking
New bridge	Shrinking	Shrinking	Shrinking

Table 3.2: Nature of the acting force per element and method.

3.1.2 Analytical and Numerical calculations

Afterward, it was incorporated creep and crack into the third method, which was analyzed for analytical and numerical calculations. The elastic modulus was adjusted to account for creep in both the new and old bridges, as explained in Section 2.2.2. Additionally, the elastic modulus of the concrete and *SHCC* used in the closure pour was modified to address crack formation as shown in Table 3.3. The high tensile stress of *SHCC* made it necessary to include crack alteration, as it exceeded its first cracking strength. Notably, the concrete closure pour demonstrated a significantly higher axial tensile strength of concrete (f_{ctm}) compared to its mean value of $3.5MPa$, taken from Table F.1. As a result, it was inferred that the closure pour material would likely experience cracking. Therefore, its elastic modulus was reduced to one-third of its original value as explained in Section 2.2.3.

	Shrinkage	Creep	Crack
Old Bridge	-	✓	-
Closure Pour	✓	-	✓
New Bridge	✓	✓	-

Table 3.3: Caracteristics affected by each element.

3.1.3 Failure Criteria

In the event that concrete develops cracks, its elastic modulus is assumed to be substantially reduced to only one-third of its original value, as mentioned on Section 2.2.3. However, it is essential that since concrete is cracked, it must still be able to keep the maximum allowable crack width, which is $0.020mm$, as mentioned on Section 2.1.3.3. Thus, if the concrete is cracked, it will be essential to calculate the amount of reinforcements necessary not to surpass the maximum allowable crack width, which was calculated in Appendix E.

One of the crucial aspects of *SHCC* material is determining its stress-strain position, primarily due to its high tensile strain range. Unlike regular concrete, the cracking in *SHCC* does not necessarily require reinforcements. As mentioned in Section 2.3.4, crack width is typically not a concern for *SHCC* as it measures around $0.10mm$, which is well below the specified limit of $0.20mm$ stated in Section 2.1.3.3. Therefore, the failure of *SHCC* occurs only when both the ultimate tensile stress and strain limits are surpassed simultaneously. Hence, it is crucial to determine the stress-strain position of the *SHCC* material to ensure its strength and durability.

3.1.4 E-modified

The calculation involved an iterative process, which follows the assumption that the elastic modulus of a material is the tangent of its stress-strain graphic.

Initially, the stress of the case was assumed, where the old and new bridge would creep, but the *SHCC* would not crack. The original value of the elastic modulus of the *SHCC* and the calculated stress with the given conditions were used to compute the new strain by applying Equation 3.1. Next, using the *SHCC* values and the rule of three, the new stress was determined, considering the first cracking strength, $2.950MPa$, and first cracking strain, 0.02%, along with ultimate tensile strength, $3.824MPa$, and ultimate tensile strain, 4.33%. Having the stress and strain at a specific point, the modified elastic modulus for that point was calculated. The modified elastic modulus was then applied to the model, and a new stress was established. Equation 3.1 and Equation 3.2 were utilized, where "x" is the trial number, ε is the strain, σ_M is the stress determined by the model, and E_x is the elastic modulus adopted at the model in each trial. The upcoming trial would incorporate the elastic modulus E_{x+1}, calculated at Equation 3.3, as part of its model.

$$\varepsilon_x = \frac{\sigma_M}{E_x} \tag{3.1}$$

$$\sigma_x = \frac{(\varepsilon_x - \varepsilon_t) \times (f_{tu} - F_t)}{(\varepsilon_{tu} - \varepsilon_t)} + F_t \tag{3.2}$$

$$E_{x+1} = \frac{\sigma_x}{\varepsilon_x} \tag{3.3}$$

3.1.5 Assumptions

As detailed in Section 2.1.3.1, selecting the appropriate waiting period for casting the closure pour after building a new bridge is absolutely essential. Currently, a waiting period of 6-9 months is typically recommended. However, for the purposes of this thesis, the aim is to reduce this waiting time. As such, a waiting period of 60 days or two months was tested and chosen based on the findings in Section 1.3. This waiting period allows for the completion of prestressing and the occurrence of prestress deflection, as well as other advantageous deformations outlined in Section 2.1.1 and Section 2.1.3.1.

In order to simplify both calculations, the following assumptions were considered:

- Only one span is being investigated, similar to the one depicted in Figure 1.16, as highlighted in Section 1.2.
- The old bridge's shrinkage is considered negligible, as previously noted in Section 2.2.1.
- Shrinkage is studied as an in-plane axial load, as mentioned in Section 3.2.
- Creep and cracks are accounted for by modifying the elastic modulus of the corresponding material, as mentioned in Section 2.2.2, Section 2.2.3, and Section 3.1.4.

3.2 Deformation problem

Before starting the analytical calculations, an extra step has to be developed.

As mentioned in Section 2.4.2, one of the primary challenges when combining young and old concrete is that the young material continues to experience creep and shrinkage. In contrast, the old has already undergone free deformation due to these factors. This creates a discrepancy in deformation between the two materials, stemming from their differing ages and properties.

As mentioned in Section 2.4.3, the difference in deformation caused by the difference in shrinkage created a problem when widening a prestressed concrete bridge. To understand this problem better and to calculate the stresses caused by it, it was necessary to let the parts of the bridge that actually suffer the shrinkage deform freely, without any interference from the other parts of the widened bridge, as shown in Figure 3.1 and Figure 3.2.

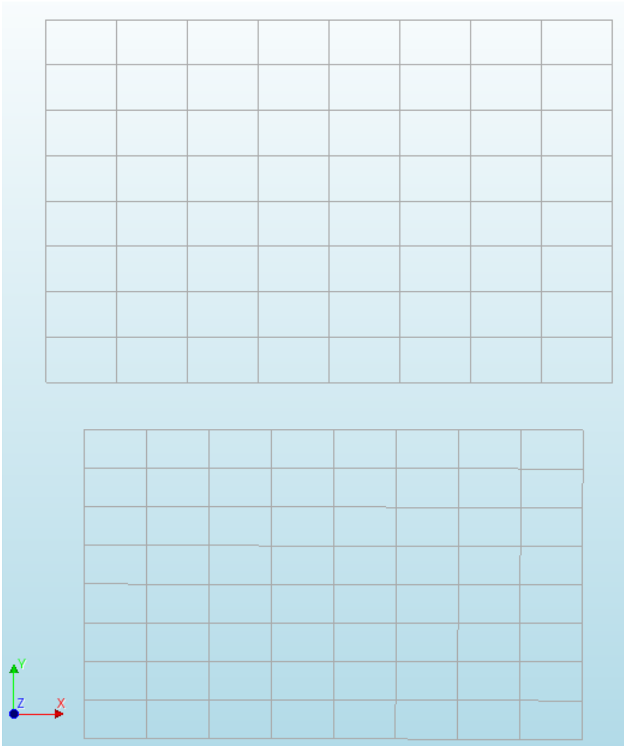

Figure 3.1: Deformation of the old bridge and new bridge with nothing in the middle.

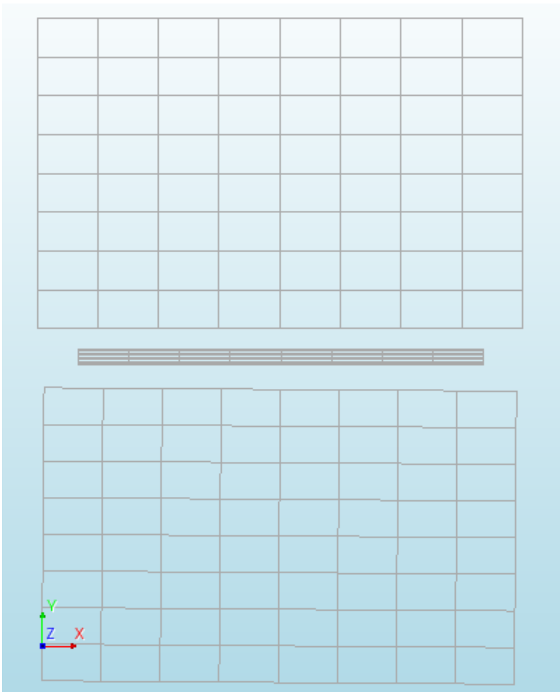

Figure 3.2: Freely deformation of the old bridge, the closure pour, and the new bridge.

As mentioned in Section 3.1.5, the old bridge does not deform. In both figures, the old bridge is only in the picture to illustrate the deformation of the other elements.

Once the shrinkage part of the bridge has deformed, an in-plane axial force, N^*, is then applied to the center of gravity of the element to eliminate the shrinkage-induced deformation and restore compatibility with the other parts. This axial force is calculated through Equation 3.4.

$$N^* = \varepsilon \times E \times A \tag{3.4}$$

Once the force was applied, the other elements were connected to the new bridge. After that, the force N^* was applied to the whole structure with the reverse sign.

Next, the N^* force is shifted to the elastic center of gravity of the entire structure. To compensate for that, a moment M^* is introduced, with the Equation 3.5, where "e" is the distance between the center of gravity of the element that caused the force and the whole structure.

$$M^* = N^* \times e \tag{3.5}$$

When the closure pour, and the new bridge are both shrinking, there will be two forces that will both be moved to the center of gravity of the entire structure to create the moment.

3.3 Analytical Calculations With In-Plane Loads Resulting In Normal Stresses

3.3.1 Introduction

This section (Section 3.3) contains the methodology for the analytical calculations for the normal stresses in the three bridge parts(old bridge, closure pour, and new bridge). The analysis used a single span and is depicted in Figure 1.16 of the Chapter 1. It is crucial to mention that only a cross-section of one span is considered. One span is illustrated in Figure 3.3, and a cross-section can be seen in figs. 3.4 to 3.6.

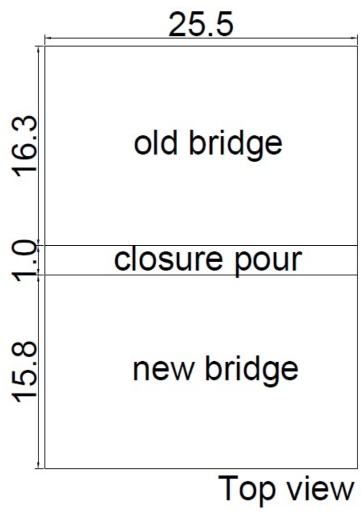

Figure 3.3: Top view of one span of the bridge(distances are in meters).

These calculations are made to analyze the Schipholbrug's behavior after 100 years with regard to shrinkage, creep, and cracks.

In order to improve the understanding of the issue of widening bridges subjected to deformation, three distinct strategies have been developed:

1. No closure pour
2. No shrinking closure pour
3. Shrinking closure pour

The second and the third were calculated with the $C40/50$ reinforced concrete as mentioned in Section 3.1. The third method was also analyzed with a closure pour made with *SHCC*, also mentioned in Section 3.1.

In all these strategies, Section 3.2 was taken into account, especially to let the parts of the bridge freely deform before an axial load and a moment were applied. This load depended on the shrinkage of the specific material used in the elements, new bridge, and closure pour. Once the shrinkage part of the bridge has deformed, an axial force, N^*, is then applied to the center of gravity of the element to eliminate the shrinkage-induced deformation and restore compatibility with the other parts. This axial force is calculated through Equation 3.4.

The calculations of the shrinkage followed the methodology described in Section 2.2.1, and the calculations were made in Appendix A for the new bridge and Appendix B for the concrete closure pour. The shrinkage of the *SHCC* closure pour was taken from Table 2.1 in Section 2.3.6.

Initially, the calculations omitted accounting for the creep and crack in order to simplify the process. However, later on, and only in strategy 3, creep, and crack were included in the following manner:

As stated in Section 3.1.5, the creep was addressed through adjustments to the elastic modulus of the old and new bridge in accordance with the recommendations outlined in Section 2.2.2. The calculations for the creep in both main decks can be found in Appendix C.

The reinforced concrete crack used on the closure pour was also considered by modifying the elastic modulus, as mentioned in Section 3.1.5. This was done by following the methodology described in Section 2.2.3, which suggested that the elastic modulus of cracked concrete could be reduced to one-third of its original value.

The elastic modulus of the *SHCC* used on the closure pour was also modified to account for its crack. However, since this material is relatively new, an iterative process was employed, as explained in Section 3.1.4 of Chapter 3. The calculations for the numerical model can be found in Section D.1 of Appendix D.

The results of these methods were presented in Section 4.1.

Summary

For Method 1, it was assumed a conservative approach, where the new bridge will connect to the old bridge without a closure pour. Therefore, all the shrinkage of the new bridge has to be taken by the old bridge.

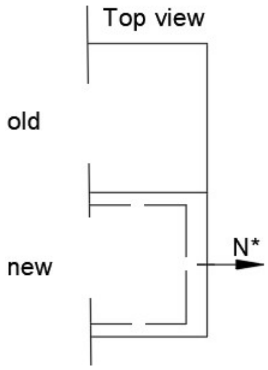

Figure 3.4: 1st case.

In Method 2, the closure pour is cast two months after the new bridge is completed, resulting in some initial free shrinkage. However, only the shrinkage of the new bridge is taken into account.

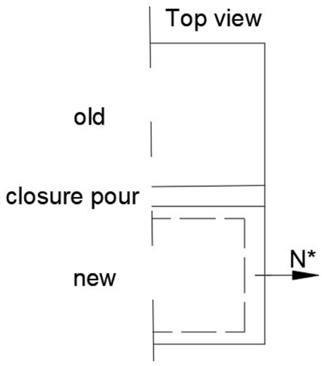

Figure 3.5: 2nd case.

Then, at Method 3, when the new bridge and the closure pour are both shrinking.

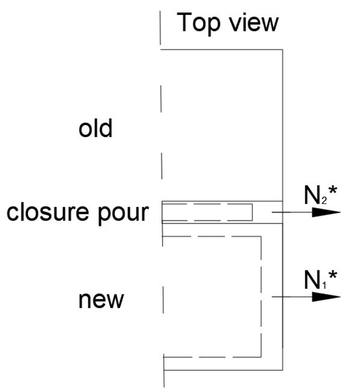

Figure 3.6: 3rd case.

3.3.2 No closure pour

The first stress calculation was made only considering the old and new bridge. Therefore, the procedure between the old bridge and the new bridge is explained in Section 3.3.2, and afterward, the calculation is made in Section G.1.

At first, it was assumed that there was only the old bridge and the new bridge, as shown in Figure 3.7. Also, it was considered that the old bridge no longer shrinks; only the new bridge does shrink.

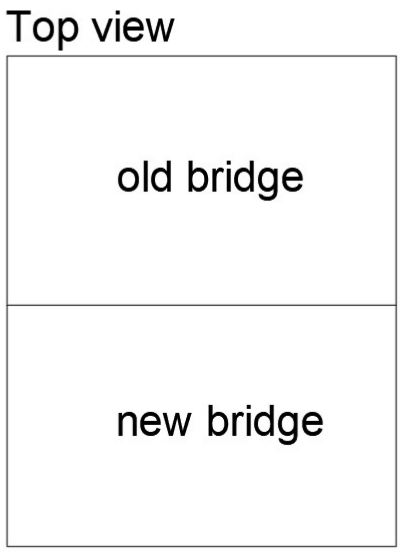

Figure 3.7: Top view of old bridge and new bridge.

Moreover, as shown in Figure 3.8, only a part of the section is used.

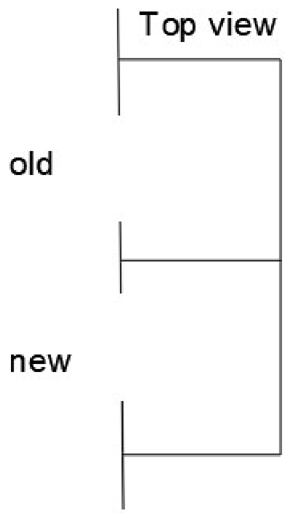

Figure 3.8: Part of the old bridge and new bridge (top view).

Since only the new bridge shrinks, the hatched part (new bridge) will be shortened due to its shrinkage, as shown in Figure 3.9.

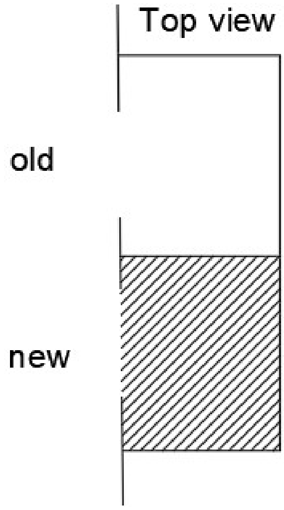

Figure 3.9: Shortened of the new bridge due to its shrinkage.

It is assumed that the layer of the new bridge deforms freely. Furthermore, the shortening due to the shrinkage of the new bridge is ε_{new}. An axial force, N^*, was applied to eliminate the shrinkage-induced deformation on the center of gravity of the new bridge, and this force is defined by Equation 3.6 and shown in Figure 3.10:

$$N^* = \varepsilon_{new} \times E_{new} \times A_{new} \tag{3.6}$$

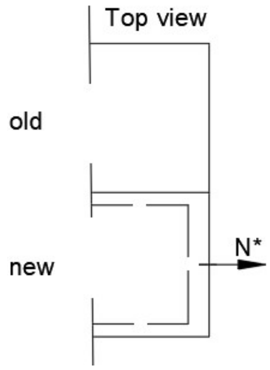

Figure 3.10: N^* to cancel the shrinkage-induced deformation.

Once the force was applied, the old bridge was connected to the new bridge. After that, the force N^* was applied to the whole structure (old and new bridge) with the reverse sign.

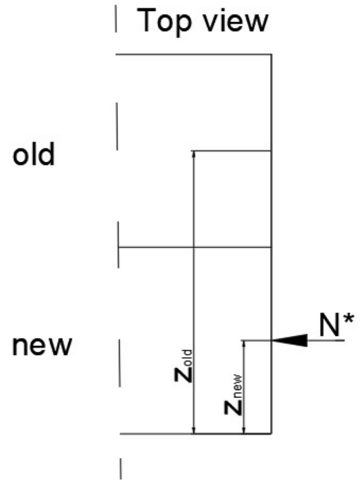

Figure 3.11: N^* applied to the entire structure with the reverse sign.

Next, the N^* force is shifted to the elastic center of gravity of the entire structure. To compensate for that, a moment M^* is introduced, with the Equation 3.7, where "e" is defined here(3.3.2). The compensation is shown in Figure 3.12.

$$M^* = N^* \times e \tag{3.7}$$

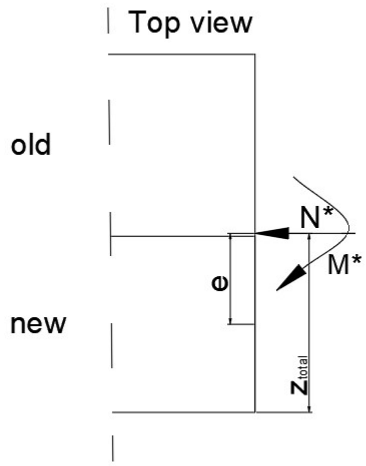

Figure 3.12: N^* is shifted creating a moment M^*.

To calculate "e", a few definitions were necessary:

- z_{new} in Figure 3.11 is the distance between the bottom side of the new bridge and the center of gravity of the new bridge;
- z_{old} in Figure 3.11 is the distance between the bottom side of the new bridge and the center of gravity of the old bridge;
- z_{total} in Figure 3.12 is the distance between the bottom side of the new bridge and the center of gravity of the entire structure;
- "e" in Figure 3.12 is the distance between the center of gravity of the entire structure and the center of gravity of the new bridge.

According to the definitions, z_{new} is half of the height of the new bridge; z_{old} is half of the size of the old bridge plus the height of the new bridge, z_{total} is given in the Equation 3.8 and $e = z_{total} - z_{new}$.

$$z_{total} = \frac{z_{new} \times EA_{new} + z_{old} \times EA_{old}}{EA_{new} + EA_{old}} \tag{3.8}$$

With N^* and M^*, all the other layers' forces and moments can be determined.

There are two formulas for the axial force in any layer, e.g., the old bridge, with the abbreviation "o". "total" is the abbreviation for the entire structure. The first due to the force N^* (Equation 3.9) and the second due to the moment M^* (Equation 3.10).

$$N_{old} = \frac{(EA)_{old}}{(EA)_{total}} \times N^* \tag{3.9}$$

$$N_{old} = \frac{M^*}{(EI)_{total}} \times (EA)_{old} \times a_{old} \tag{3.10}$$

For the bending moment, Equation 3.11 was the:

$$M_{old} = M^* \times \frac{(EI)_{old}}{(EI)_{total}} \tag{3.11}$$

Therefore, to find the final longitudinal stresses in the cross-section, a force or a moment was used, as previously shown.

For the stress, because of the axial tensile force, only the shortened layer was included, in this case, the new bridge. Thus, it followed the Equation 3.12 below.

$$\sigma_{wb} = \sigma_{wo} = \frac{N^*}{A_{new}} \tag{3.12}$$

The N^* on the entire structure caused stresses in the whole system (old and new bridge), and it used Equation 3.9 for the old bridge, and the force of the new bridge was shown in Equation 3.13.

$$N_{new} = N^* - N_{old} \tag{3.13}$$

Moreover, their stresses were calculated through the forces obtained in eqs. (3.9) and (3.13). Thus, the stresses were calculated in the eqs. (3.14) and (3.15):

$$\sigma_{wb} = \sigma_{wo} = -\frac{N_{old}}{A_{old}} \tag{3.14}$$

$$\sigma_{wb} = \sigma_{wo} = -\frac{N_{new}}{A_{new}} \tag{3.15}$$

The stresses originating due to the M^* on the entire structure affected both parts as well (old and new bridge), and it used Equation 3.10 for the old bridge, and the force of the new bridge is shown in Equation 3.16.

$$N_{new} = \frac{M^*}{(EI)_{total}} \times (EA)_{new} \times a_{new} \tag{3.16}$$

Furthermore, their stresses will be calculated through the forces obtained in eqs. (3.10) and (3.16). Thus, the stresses are calculated in the eqs. (3.17) and (3.18):

$$\sigma_{wb} = \sigma_{wo} = +\frac{N_{old}}{A_{old}} \tag{3.17}$$

$$\sigma_{wb} = \sigma_{wo} = -\frac{N_{new}}{A_{new}} \tag{3.18}$$

The moment M^* per layer will create stresses using Equation 3.11 for the old bridge and the Equation 3.19 for the new bridge.

$$M_{new} = M^* \times \frac{(EI)_{new}}{(EI)_{total}} \tag{3.19}$$

Additionally, their corresponding stresses will be Equation 3.20 for the old bridge and the Equation 3.21 for the new bridge, where S_{old} and S_{new} are the associated section modulus of each part of the cross-section.

$$\sigma_{wb} = -\sigma_{wo} = -\frac{M_{old}}{S_{old}} \tag{3.20}$$

$$\sigma_{wb} = -\sigma_{wo} = -\frac{M_{new}}{S_{new}} \tag{3.21}$$

Adding the stresses found for each layer resulted in the final shear stresses in each layer for this part of the structure.

3.3.3 No shrinking closure pour

The second stress calculation considered the bridge's three elements: the old, the new bridge, and the closure pour. The procedure between the old bridge, the closure pour, and the new bridge is explained in Section 3.3.3, and afterward, the calculation is made in Section G.2.

At Method 2, it was assumed that the total structure is present (old, new bridge, and closure pour), as shown in Figure 3.13. Also, it was considered that the old bridge and the closure pour do not shrink; only the new bridge does shrink.

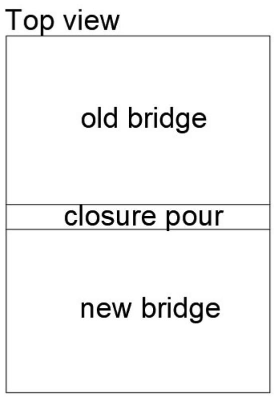

Figure 3.13: Top view of old, new bridge and closure pour.

As shown in Figure 3.14, only a part of the section is used.

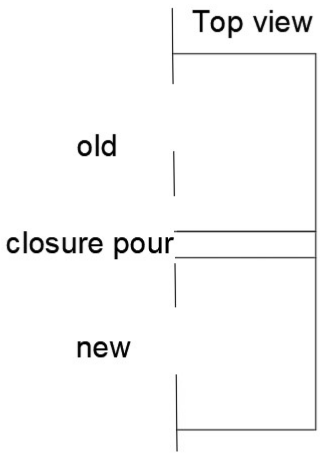

Figure 3.14: Part of the old bridge, closure pour and new bridge (top view).

Since only the new bridge shrinks, the hatched part (new bridge) will be shortened due to its shrinkage, as shown in Figure 3.15.

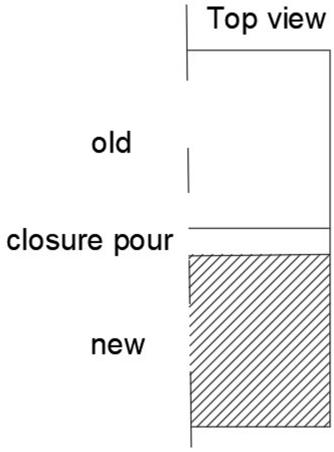

Figure 3.15: Shortened of the new bridge due to its shrinkage.

Assuming that the layer of the new bridge deforms freely. Furthermore, the shortening due to the shrinkage of the new bridge is ε_{new}. An axial force, N^*, was applied to eliminate the shrinkage-induced deformation on the center of gravity of the new bridge, and this force is defined by Equation 3.22 and shown in Figure 3.16:

$$N^* = \varepsilon_{new} \times E_{new} \times A_{new} \tag{3.22}$$

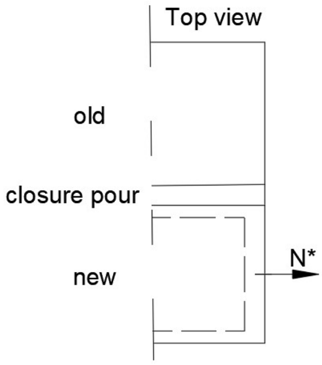

Figure 3.16: N^* to cancel the shrinkage-induced deformation.

Once the force was applied, the old bridge and closure pour were connected to the new bridge. After that, the force N^* was applied to the whole structure (old bridge, closure pour, and new bridge) with the reverse sign.

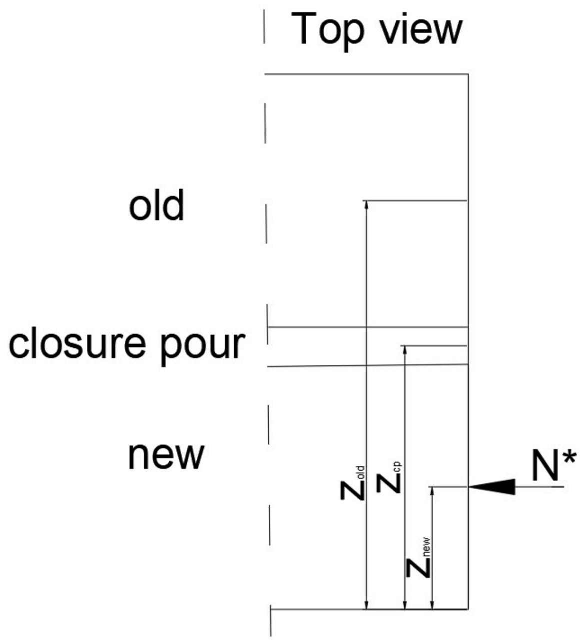

Figure 3.17: N^* applied to the entire structure with the reverse sign.

Next, the N^* force is shifted to the elastic center of gravity of the entire structure. To compensate for that, a moment M^* is introduced, with the Equation 3.23, where "e" is defined here(3.3.3). The compensation is shown in Figure 3.18.

$$M^* = N^* \times e \tag{3.23}$$

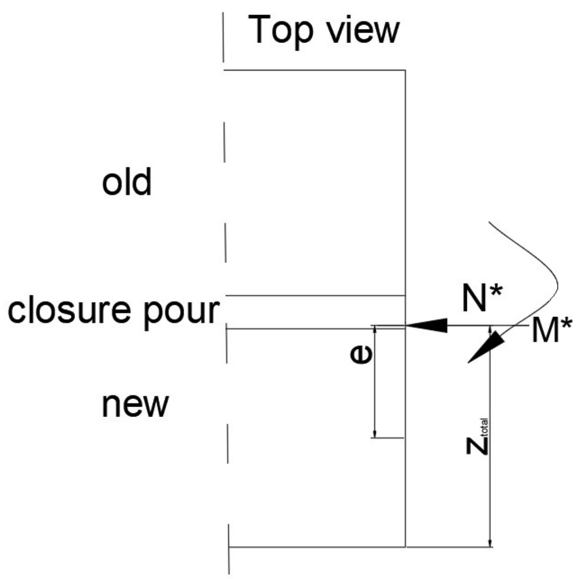

Figure 3.18: N^* is shifted creating a moment M^*.

To calculate "e", a few definitions were necessary:

- z_{new} in Figure 3.17 is the distance between the bottom side of the new bridge and the center of gravity of the new bridge;
- z_{cp} in Figure 3.17 is the distance between the bottom side of the new bridge and the center of gravity of the closure pour;

- z_{old} in Figure 3.17 is the distance between the bottom side of the new bridge and the center of gravity of the old bridge;
- z_{total} in Figure 3.18 is the distance between the bottom side of the new bridge and the center of gravity of the entire structure;
- "e" in Figure 3.18 is the distance between the center of gravity of the entire structure and the center of gravity of the new bridge.

According to the definitions, z_{new} is half of the height of the new bridge; z_{cp} is half of the size of the closure pour plus the height of the new bridge; z_{old} is half of the size of the old bridge plus the height of the closure pour plus new bridge, z_{total} is given in the Equation 3.24 and $e = z_{total} - z_{new}$.

$$z_{total} = \frac{z_{new} \times EA_{new} + z_{cp} \times EA_{cp} + z_{old} \times EA_{old}}{EA_{new} + EA_{cp} + EA_{old}} \tag{3.24}$$

With N^* and M^*, all the other layers' forces and moments can be determined.

There are two formulas for the axial force in any layer, e.g., "total" is the abbreviation for the entire structure. One due to the force N^* (Equation 3.25) and the other due to the moment M^* (Equation 3.26).

$$N_{old} = \frac{(EA)_{old}}{(EA)_{total}} \times N^* \tag{3.25}$$

$$N_{old} = \frac{M^*}{(EI)_{total}} \times (EA)_{old} \times a_{old} \tag{3.26}$$

For the bending moment,Equation 3.27 was applied:

$$M_{old} = M^* \times \frac{(EI)_{old}}{(EI)_{total}} \tag{3.27}$$

Therefore, to find the final longitudinal stresses in the cross-section, a force or a moment was used, as previously shown.

For the stress, because of the axial tensile force, only the shortened layer was included, in this case, the new bridge. Thus, it followed the Equation 3.28.

$$\sigma_{wb} = \sigma_{wo} = \frac{N^*}{A_{new}} \tag{3.28}$$

The N^* on the entire structure caused stresses in the whole system (old, new bridge, and closure pour), and it used Equation 3.25 for the old bridge, the force of the new bridge was shown in Equation 3.29 and Equation 3.30 was used for the closure pour.

$$N_{new} = \frac{(EA)_{new}}{(EA)_{total}} \times N^* \tag{3.29}$$

$$N_{cp} = N^* - N_{old} - N_{new} \tag{3.30}$$

Furthermore, their stresses were calculated through the forces obtained in eqs. (3.25), (3.29) and (3.30). Thus, the stresses were calculated in the eqs. (3.31) to (3.33):

$$\sigma_{wb} = \sigma_{wo} = -\frac{N_{old}}{A_{old}} \tag{3.31}$$

$$\sigma_{wb} = \sigma_{wo} = -\frac{N_{new}}{A_{new}} \tag{3.32}$$

$$\sigma_{wb} = \sigma_{wo} = -\frac{N_{cp}}{A_{cp}} \tag{3.33}$$

The stresses originating due to the M^* on the entire structure affected the three parts as well (old, closure pour, and new bridge), and it used Equation 3.26 for the old bridge; the force of the new bridge is shown in Equation 3.34 and for the closure pour was used Equation 3.35.

$$N_{new} = \frac{M^*}{(EI)_{total}} \times (EA)_{new} \times a_{new} \tag{3.34}$$

$$N_{cp} = \frac{M^*}{(EI)_{total}} \times (EA)_{cp} \times a_{cp} \tag{3.35}$$

Moreover, their stresses will be calculated through the forces obtained in eqs. (3.26), (3.34) and (3.35). Thus, the stresses are calculated in the eqs. (3.36) to (3.38):

$$\sigma_{wb} = \sigma_{wo} = +\frac{N_{old}}{A_{old}} \tag{3.36}$$

$$\sigma_{wb} = \sigma_{wo} = -\frac{N_{new}}{A_{new}} \tag{3.37}$$

$$\sigma_{wb} = \sigma_{wo} = +\frac{N_{cp}}{A_{cp}} \tag{3.38}$$

The moment M^* per layer will create stresses using Equation 3.27 for the old bridge, for the new bridge was used Equation 3.39, and the Equation 3.40 for the closure pour.

$$M_{new} = M^* \times \frac{(EI)_{new}}{(EI)_{total}} \tag{3.39}$$

$$M_{cp} = M^* \times \frac{(EI)_{cp}}{(EI)_{total}} \tag{3.40}$$

Furthermore, their corresponding stresses will be Equation 3.41 for the old bridge, equation Equation 3.42 for the new bridge, and the Equation 3.43 for the closure pour, where S_{old}, S_{cp} and S_{new} are the associated section modulus of each part of the cross-section.

$$\sigma_{wb} = -\sigma_{wo} = -\frac{M_{old}}{S_{old}} \tag{3.41}$$

$$\sigma_{wb} = -\sigma_{wo} = -\frac{M_{new}}{S_{new}} \tag{3.42}$$

$$\sigma_{wb} = -\sigma_{wo} = -\frac{M_{cp}}{S_{cp}} \tag{3.43}$$

Adding the stresses found for each layer resulted in the final shear stresses in each layer for this part of the structure.

3.3.4 Shrinking closure pour

The third stress calculation considered the bridge's three elements: the old, the new bridge, and the closure pour. The procedure between the old bridge, the closure pour, and the new bridge is explained in Section 3.3.4, and afterward, the calculation is made in Section G.3.

In Method 3, it was assumed that the total structure is present (old, new bridge, and closure pour), as shown in Figure 3.19. Also, it was considered that the old bridge no longer shrinks; the new bridge and the closure pour do shrink.

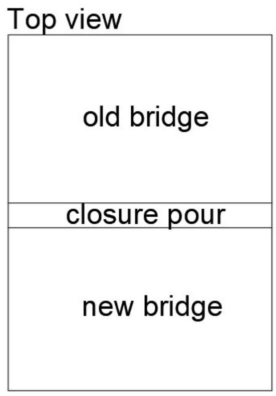

Figure 3.19: Top view of old, new bridge and closure pour.

As shown in Figure 3.20, only a part of the section is used.

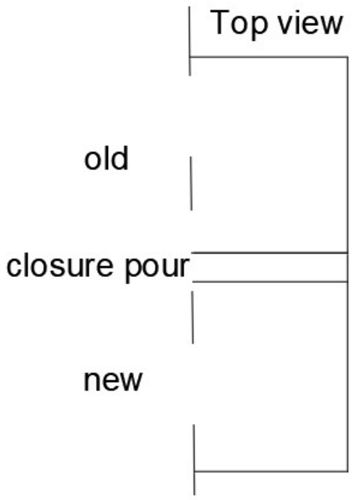

Figure 3.20: Part of the old bridge, closure pour, and new bridge (top view).

The hatched sections (new bridge and closure pour) will both shrink, causing them to become shorter. The amount of shrinkage differs between the two sections, as depicted in figs. 3.21 and 3.22.

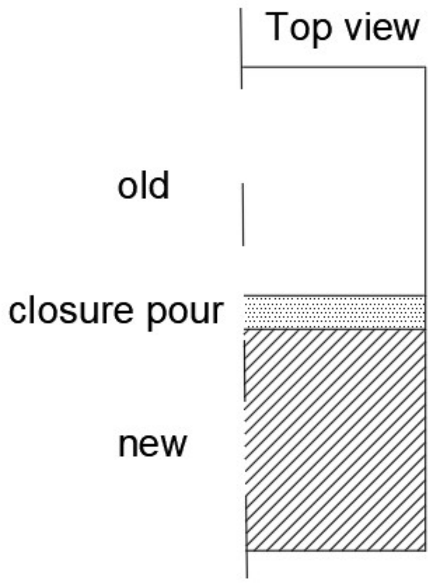

Figure 3.21: Shortened of the new bridge and closure pour due to their shrinkage.

Assuming that the layers of the new bridge and the closure pour deform freely. The shortening due to the shrinkage of the new bridge is ε_{new}, and due to the shrinkage of the closure pour is ε_{cp}. Two axial forces, N_1^* and N_2^*, were applied to eliminate the shrinkage-induced deformations on the center of gravity of each element, and these forces are defined by eqs. (3.44) and (3.45) and, being shown in Figure 3.22:

$$N_1^* = \varepsilon_{new} \times E_{new} \times A_{new} \tag{3.44}$$

$$N_2^* = \varepsilon_{cp} \times E_{cp} \times A_{cp} \tag{3.45}$$

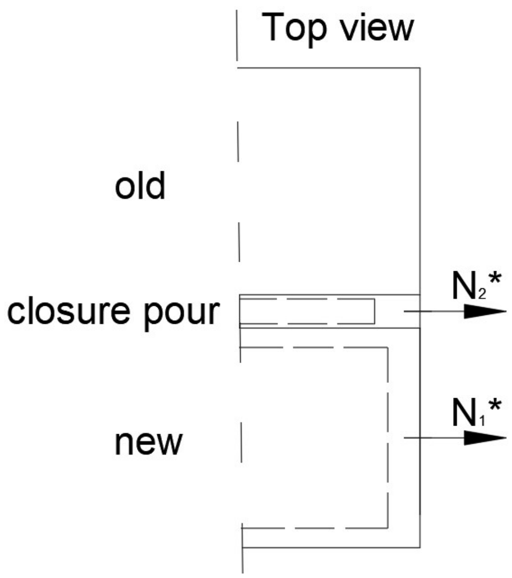

Figure 3.22: N_1^* and N_2^* to cancel the shrinkage-induced deformation.

Once the forces were applied, the old bridge was connected to the closure pour and the new bridge. After that, the forces N_1^* and N_2^* were applied to the whole structure (old bridge, closure pour, and new bridge) with the reverse sign.

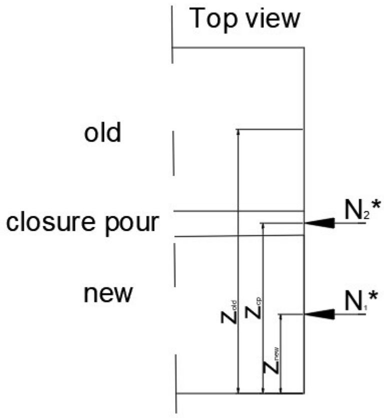

Figure 3.23: N_1^* and N_2^* applied to the entire structure with the reverse sign.

Next, the forces N_1^* and N_2^* were summed, $N^* = N_1^* + N_2^*$, and the force, N^*, was shifted to the elastic center of gravity of the entire structure. To compensate for that, a moment M^* is introduced, with the Equation 3.46, where "e_1" and "e_2" is defined here(3.3.4). The compensation is shown in Figure 3.24

$$M^* = N_1^* \times e_1 + N_2^* \times e_2 \tag{3.46}$$

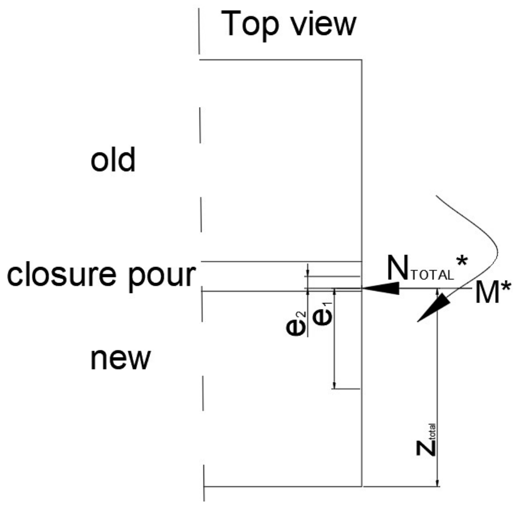

Figure 3.24: N^* is shifted creating a moment M^*.

To calculate "e", a few definitions were necessary:

- z_{new} in Figure 3.23 is the distance between the bottom side of the new bridge and the center of gravity of the new bridge;
- z_{cp} in Figure 3.23 is the distance between the bottom side of the new bridge and the center of gravity of the closure pour;
- z_{old} in Figure 3.23 is the distance between the bottom side of the new bridge and the center of gravity of the old bridge;
- z_{total} in Figure 3.24 is the distance between the bottom side of the new bridge and the center of gravity of the entire structure;
- "e_1" in Figure 3.24 is the distance between the center of gravity of the entire structure and the center of gravity of the new bridge;
- "e_2" in Figure 3.24 is the distance between the center of gravity of the entire structure and the center of gravity of the closure pour;

According to the definitions, z_{new} is half of the height of the new bridge; z_{cp} is half of the size of the closure pour plus the height of the new bridge; z_{old} is half of the size of the old bridge plus the height of the closure pour plus new bridge, z_{total} is given in the Equation 3.47 and $e_1 = z_{total} - z_{new}$ and $e_2 = z_{total} - z_{cp}$.

$$z_{total} = \frac{z_{new} \times EA_{new} + z_{cp} \times EA_{cp} + z_{old} \times EA_{old}}{EA_{new} + EA_{cp} + EA_{old}} \tag{3.47}$$

With N^* and M^*, all the other layers' forces and moments can be determined.

There are two formulas for the axial force in any layer, e.g., "total" is the abbreviation for the entire structure. One due to the force N^* (Equation 3.48) and the other due to the moment M^* (Equation 3.49).

$$N_{old} = \frac{(EA)_{old}}{(EA)_{total}} \times N^* \tag{3.48}$$

$$N_{old} = \frac{M^*}{(EI)_{total}} \times (EA)_{old} \times a_{old} \tag{3.49}$$

For the bending moment, Equation 3.50 was applied:

$$M_{old} = M^* \times \frac{(EI)_{old}}{(EI)_{total}} \tag{3.50}$$

Therefore, to find the final longitudinal stresses in the cross-section, a force or a moment was used, as previously shown.

For the stress, because of the axial tensile force, only the shortened layers were included, in this case, the new bridge and closure pour. Thus, it followed the formulas eqs. (3.51) and (3.52).

$$\sigma_{wb} = \sigma_{wo} = \frac{N_1^*}{A_{new}} \tag{3.51}$$

$$\sigma_{wb} = \sigma_{wo} = \frac{N_2^*}{A_{cp}} \tag{3.52}$$

The N^* on the entire structure caused stresses in the whole system (old, new bridge, and closure pour), and it used Equation 3.48 for the old bridge, the force of the new bridge was shown in Equation 3.53 and Equation 3.54 was used for the closure pour.

$$N_{new} = \frac{(EA)_{new}}{(EA)_{total}} \times N^* \tag{3.53}$$

$$N_{cp} = N^* - N_{old} - N_{new} \tag{3.54}$$

Their stresses were calculated through the forces obtained in eqs. (3.48), (3.53) and (3.54). Thus, the stresses were calculated in the eqs. (3.55) to (3.57):

$$\sigma_{wb} = \sigma_{wo} = -\frac{N_{old}}{A_{old}} \tag{3.55}$$

$$\sigma_{wb} = \sigma_{wo} = -\frac{N_{new}}{A_{new}} \tag{3.56}$$

$$\sigma_{wb} = \sigma_{wo} = -\frac{N_{cp}}{A_{cp}} \tag{3.57}$$

The stresses originating due to the M^* on the entire structure also affected the three parts (old, new bridge, and closure pour). It used Equation 3.49 for the old bridge, the force of the new bridge is shown in Equation 3.58, and for the closure pour was used Equation 3.59.

$$N_{new} = \frac{M^*}{(EI)_{total}} \times (EA)_{new} \times a_{new} \tag{3.58}$$

$$N_{cp} = \frac{M^*}{(EI)_{total}} \times (EA)_{cp} \times a_{cp} \tag{3.59}$$

Their stresses will be calculated through the forces obtained in eqs. (3.49), (3.58) and (3.59). Thus, the stresses are calculated in the eqs. (3.60) to (3.62):

$$\sigma_{wb} = \sigma_{wo} = +\frac{N_{old}}{A_{old}} \tag{3.60}$$

$$\sigma_{wb} = \sigma_{wo} = -\frac{N_{new}}{A_{new}} \tag{3.61}$$

$$\sigma_{wb} = \sigma_{wo} = +\frac{N_{cp}}{A_{cp}} \tag{3.62}$$

The moment M^* per layer will create stresses using Equation 3.50 for the old bridge, and the Equation 3.63 for the new bridge, and the closure was used Equation 3.64.

$$M_{new} = M^* \times \frac{(EI)_{new}}{(EI)_{total}} \tag{3.63}$$

$$M_{cp} = M^* \times \frac{(EI)_{cp}}{(EI)_{total}} \tag{3.64}$$

Furthermore, their corresponding stresses will be Equation 3.65 for the old bridge, Equation 3.66 for the new bridge, and Equation 3.67 for the closure pour, where S_{old}, S_{new}, and S_{cp} are the associated section modulus of each part of the cross-section.

$$\sigma_{wb} = -\sigma_{wo} = -\frac{M_{old}}{S_{old}} \tag{3.65}$$

$$\sigma_{wb} = -\sigma_{wo} = -\frac{M_{new}}{S_{new}} \tag{3.66}$$

$$\sigma_{wb} = -\sigma_{wo} = -\frac{M_{cp}}{S_{cp}} \tag{3.67}$$

Adding the stresses found for each layer resulted in the final shear stresses in each layer for this part of the structure.

3.4 Maximum deformation of *SHCC* analysis

To prove the maximum deformation of *SHCC*, another analysis was developed.

The strain used was the ultimate tensile strain of the material from Figure 2.8, which means that *SHCC* could suffer a deformation of 4.33%, which could caused by shrinkage or any other factor, and the material still would be within its limits.

Based on the analytical steps outlined in both Section 3.2 and Section 3.3, the load applied was calculated using Equation 3.4. For the closure pour, a strain of 4.33×10^{-2} was utilized, which corresponds to the ultimate tensile strain of the *SHCC*. Additionally, the shrinkage of the new bridge was calculated using the methodology outlined in Section 2.2.1 and can be found in Appendix A. The load of the shrinkage of the new bridge was also calculated using Equation 3.4.

Following Equation 3.3, the elastic modulus of the *SHCC* used on the closure pour was also modified through the ultimate tensile stress and strain ($3.824MPa$ and 4.33×10^{-2}) of *SHCC*, which are shown in Figure 2.8.

In accordance with the recommendations outlined in Section 2.2.2, adjustments were made to the elastic modulus of both the old and new bridge to address the issue of creep, as mentioned in Section 3.1.5. The calculations detailing the creep in both main decks can be found in Appendix C.

The results of this example are shown in Section 4.2.

3.5 Finite Element Analysis Linear Model

The Finite Element Analysis (*FEA*) linear model was utilized to perform a numerical analysis of the Schipholbrug's behavior after 100 years with regards to shrinkage, creep, and cracks. The model used a single span and is depicted in Figure 1.16 of the Chapter 1. two models were created. The first one had a closure pour made with a reinforced concrete of $C40/50$, as mentioned in Section 3.1, and the second had a closure pour made with *SHCC*, also mentioned in Section 3.1.

The load was applied as a prescribed strain in the model, and the shrinkage strain of the respective parts of the bridge, closure pour, and new bridge were taken into account. The calculations of the shrinkage followed the methodology described in Section 2.2.1, and the calculations were made in Appendix A for the new bridge and Appendix B for the concrete closure pour. The shrinkage of the *SHCC* closure pour was taken from Table 2.1 in Section 2.3.6. The shrinkage was considered to be the same for all directions since concrete shrinks evenly in all directions.

As stated in Section 3.1.5, the creep was addressed through adjustments to the elastic modulus of the old and new bridge in accordance with the recommendations outlined in Section 2.2.2. The calculations for the creep in both main decks can be found in Appendix C.

The reinforced concrete crack used on the closure pour was also considered by modifying the elastic modulus, as mentioned in Section 3.1.5. This was done by following the methodology described in Section 2.2.3, which suggested that the elastic modulus of cracked concrete could be reduced to one-third of its original value.

The elastic modulus of the *SHCC* used on the closure pour was also modified to account for its crack. However, since this material is relatively new, an iterative process was employed, as explained in Section 3.1.4 of Chapter 3. The calculations for the numerical model can be found in Section D.2 of Appendix D.

The span's geometry used in the model consisted of a single span with a length of 25.5 meters and a thickness of 0.9 meters. The old bridge was 16.31 meters wide, the new bridge was 15.80 meters wide, and the closure pour was 1.0 meter wide, as shown in Figure 3.25.

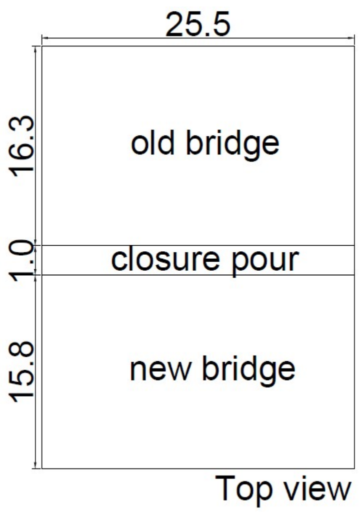

Figure 3.25: Top view of one span of Schipholbrug (distances are in meters).

The numerical model's conclusive outcomes are featured in Section 4.3. These results display both the normal and shear stresses and strains for the two closure pour options: Model 1, which utilized reinforced concrete, and Model 2, which incorporated *SHCC*. By comparing these models, a comprehensive analysis can be conducted to determine whether *SHCC* is a superior material to concrete in terms of shortening the construction time for the bridge's widening section. Furthermore, the normal stresses serve to authenticate the analytical method presented in Section 3.3.

Table 3.4 was made to summarize which part of the bridge is affected by shrinkage, creep, and crack.

	Shrinkage	Creep	Crack
Old Bridge	-	✓	-
Closure Pour	✓	-	✓
New Bridge	✓	✓	-

Table 3.4: Characteristics affected by each element.

As previously mentioned, the results of these models, which are present in Section 4.3, were designed to compare results with those in Section 4.1.3.2. A discussion between these results is in Chapter 5.

The model was created on DIANA FEA, and its manual[42] was followed to create it. In order to simplify the calculations, the assumptions in Section 3.1.5 were also taken into consideration.

4

Results

4.1 Analytical Calculations With In-Plane Loads Resulting In Normal Stresses

The following section provides the results of the findings obtained through the methodology explained in Section 3.3. To enhance clarity and facilitate comprehension, the results have been organized into distinct subsections.

1. Only shrinkage is considered.
   1. Results without a closure pour.
   2. Results of no shrinking concrete closure pour.
   3. Results of shrinking concrete closure pour.
   4. Results of shrinking *SHCC* closure pour.
2. Shrinkage, creep, and crack are considered.
   1. Results of shrinking concrete closure pour.
   2. Results of shrinking *SHCC* closure pour.

4.1.1 Only shrinkage is considered

4.1.1.1 Results without a closure pour

Using Section 3.3.2 methodology, the calculations were made at Section G.1 with the data from Table 4.1, and the results are in Table 4.2 and Figure 4.1.

Dimensions	Old Bridge	New Bridge
Elastic Modulus (MPa)	31500	37000
Shrinkage (ε)	-	2.44×10^{-4}

Table 4.1: Data for without closure pour.

Stresses (MPa)	Old top	Old bottom	New top	New bottom
item 1	0.00	0.00	9.03	9.03
item 2	-4.09	-4.09	-4.81	-4.81
item 3	3.07	3.07	-3.17	-3.17
item 4	2.93	-2.93	3.33	-3.33
Total	1.90	-3.95	4.39	-2.27

Table 4.2: Results without a closure pour.

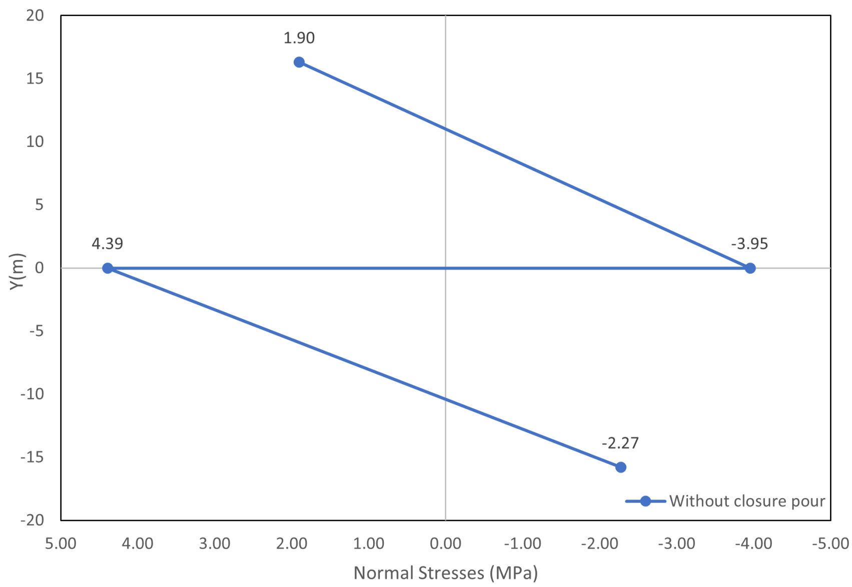

Figure 4.1: Results without a closure pour.

4.1.1.2 Results of no shrinking concrete closure pour

Using Section 3.3.3 methodology, the calculations were made at Section G.2 with the data from Table 4.3, and the results are in Table 4.4 and Figure 4.2.

Dimensions	Old Bridge	Concrete *CP*	New Bridge
Elastic Modulus (MPa)	31500	35000	37000
Shrinkage (ε)	-	-	1.57×10^{-4}

Table 4.3: Data for Concrete closure pour.

Stresses (MPa)	Old top	Old bottom	CP top	CP bottom	New top	New bottom
Item item 1	0.00	0.00	0.00	0.00	5.82	5.82
Item item 2	-2.55	-2.55	-2.84	-2.84	-3.00	-3.00
Item item 3	2.03	2.03	0.10	0.10	-2.11	-2.11
Item item 4	1.83	-1.83	0.12	-0.12	2.08	-2.08
Total	1.31	-2.35	-2.61	-2.86	2.79	-1.37

Table 4.4: Results of no shrinking concrete closure pour.

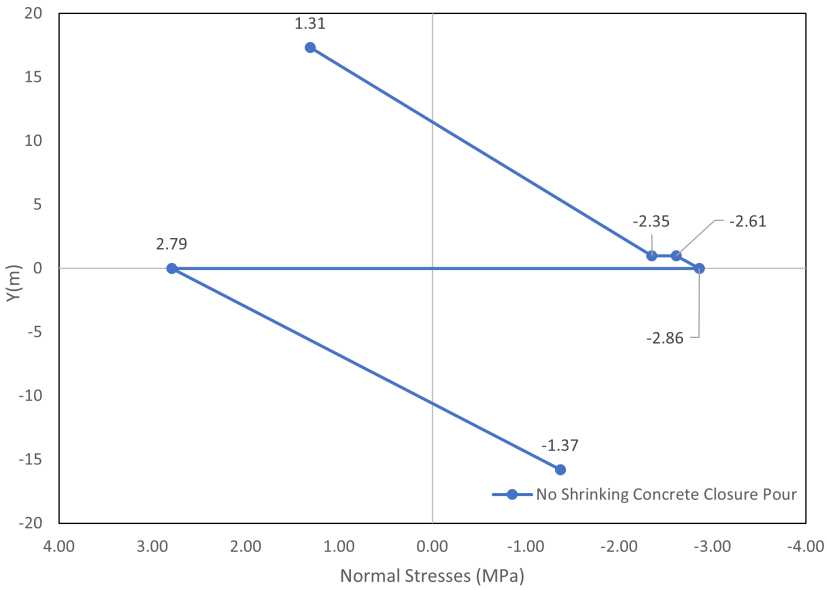

Figure 4.2: Results of no shrinking concrete closure pour.

4.1.1.3 Results of shrinking concrete closure pour

Using Section 3.3.4 methodology, the calculations were made at Section G.3 with the data from Table 4.5, and the results are in Table 4.6 and Figure 4.3.

Dimensions	Old Bridge	Concrete *CP*	New Bridge
Elastic Modulus (MPa)	31500	35000	37000
Shrinkage (ε)	-	2.37×10^{-4}	1.57×10^{-4}

Table 4.5: Data for concrete closure pour.

Stresses (MPa)	Old top	Old bottom	CP top	CP bottom	New top	New bottom
Item item 1	0.00	0.00	8.30	8.30	5.82	5.82
Item item 2	-2.79	-2.79	-3.10	-3.10	-3.27	-3.27
Item item 3	2.02	2.02	-0.10	-0.10	-2.10	-2.10
Item item 4	1.82	-1.82	0.12	-0.12	2.07	-2.07
Total	1.06	-2.58	5.23	4.98	2.52	-1.62

Table 4.6: Results of shrinking concrete closure pour.

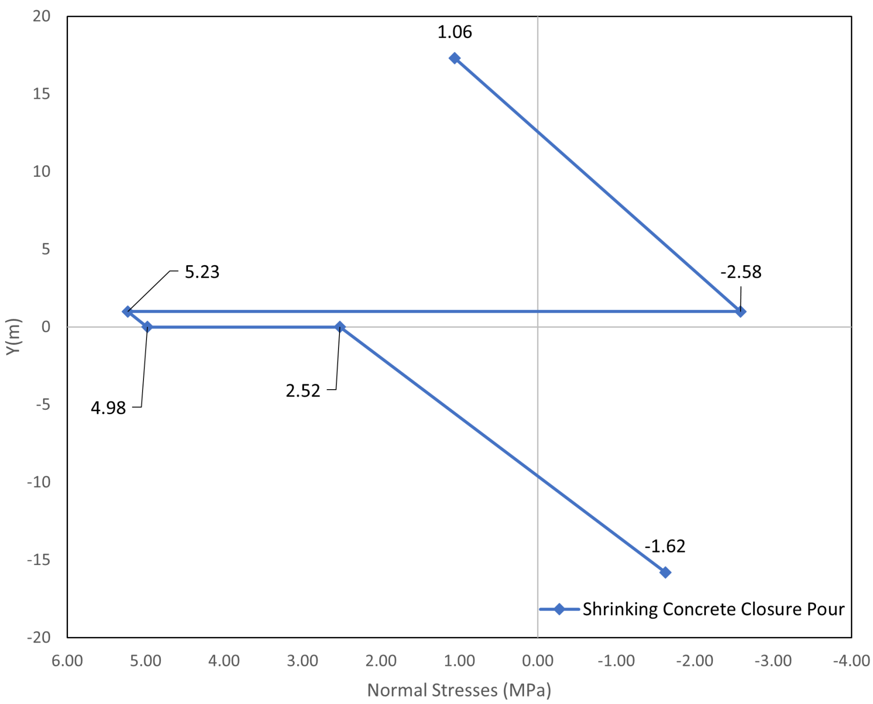

Figure 4.3: Results of shrinking concrete closure pour.

4.1.1.4 Results of shrinking *SHCC* closure pour

Using Section 3.3.4 methodology, the calculations followed the same procedure as at Section G.3. The procedure is better explained at Section G.4 with the data from Table 4.7 and the results are in Table 4.8 and Figure 4.4.

Dimensions	Old Bridge	*SHCC CP*	New Bridge
Elastic Modulus (MPa)	31500	12421	37000
Shrinkage (ε)	-	9.85×10^{-4}	1.57×10^{-4}

Table 4.7: Data for *SHCC* closure pour.

Stresses	Old top	Old bottom	CP top	CP bottom	New top	New bottom
Item	0.00	0.00	12.24	12.24	5.82	5.82
Item	-2.95	-2.95	-1.16	-1.16	-3.47	-3.47
Item	2.05	2.05	0.04	0.04	-2.12	-2.12
Item	1.84	-1.84	0.04	-0.04	2.09	-2.09
Total	0.94	-2.75	11.15	11.06	2.33	-1.86

Table 4.8: Results of shrinking *SHCC* closure pour.

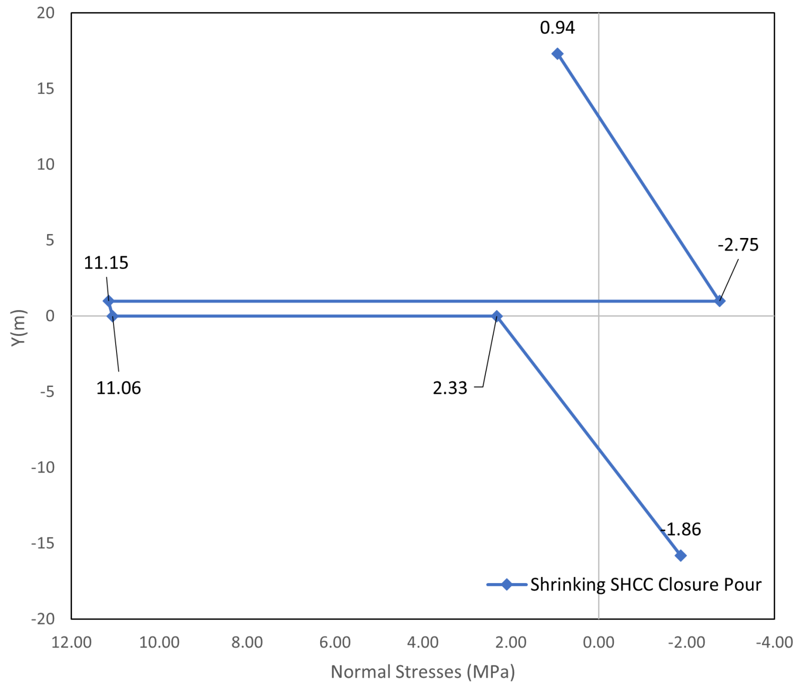

Figure 4.4: Results of shrinking *SHCC* closure pour.

4.1.2 Shrinkage, creep, and crack are considered.

For the addition of the crack and creep, the same procedure as Method 3 was done following the steps of Section G.3. However, the elastic modulus of all elements was changed. The old and new bridges changed due to creep that was calculated at appendices C.1 and C.2, the concrete closure pour, due to crack, was reduced to one-third of the original ($35000/3 = 11667MPa$), and the *SHCC*, also due to crack, was a more complex process showed at Section D.1. And the final input values are in Table 4.9 and Table 4.11.

4.1.2.1 Results of shrinking concrete closure pour

Kindly refer to Section G.5 for a detailed explanation regarding the pre-determined cracking of the concrete closure pour. In order to obtain the results of the shrinking concrete closure pour, the values from the old bridge, concrete closure pour, and new bridge were utilized as shown in Table 4.9. The final outcomes of this analysis are presented in Table 4.10 and Figure 4.5.

Dimensions	Old Bridge	Concrete *CP*	New Bridge
Elastic Modulus (MPa)	30941	11667	18461
Shrinkage (ε)	-	2.37×10^{-4}	1.57×10^{-4}

Table 4.9: Data for concrete closure pour.

Stresses (MPa)	Old top	Old bottom	*CP* top	*CP* bottom	New top	New bottom
item 1	0.00	0.00	2.77	2.77	2.90	2.90
item 2	-1.86	-1.86	-0.70	-0.70	-1.11	-1.11
item 3	1.33	1.33	-0.19	-0.19	-1.36	-1.36
item 4	1.73	-1.73	0.04	-0.04	1.00	-1.00
Total	1.20	-2.26	1.92	1.83	1.43	-0.57

Table 4.10: Results of shrinking cracked concrete closure pour.

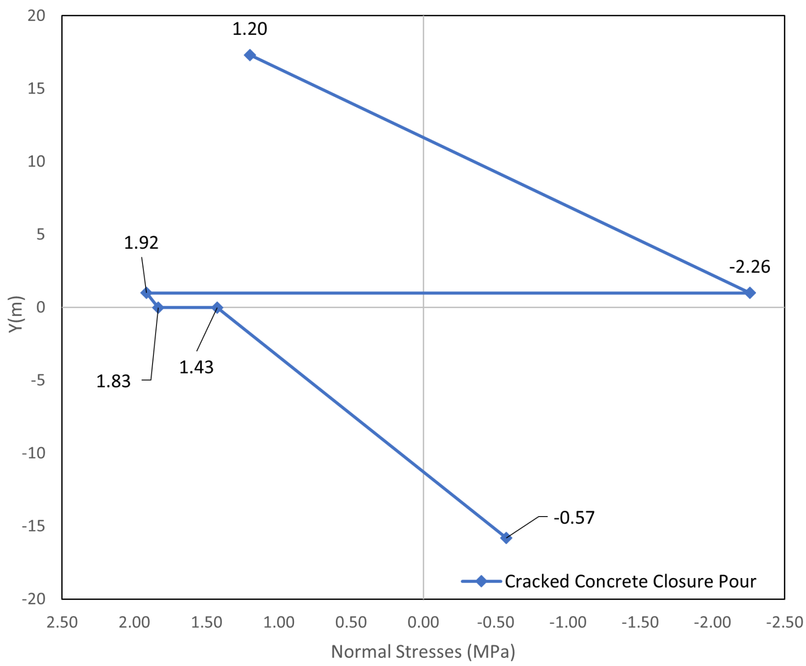

Figure 4.5: Results of shrinking cracked concrete closure pour.

4.1.2.2 Results of shrinking *SHCC* closure pour

Please refer to Section G.6 for the explanation as to why the *SHCC* closure pour was pre-determined to be cracked. As mentioned in Section 4.1.2, the cracked of *SHCC* involved some calculations that were made in Section D.1 and resulted after cracking its elastic modulus being reduced to $3139MPa$ as shown in the last line of Table D.1. Its final maximum stress is $2.964MPa$, shown at Figure 4.6.

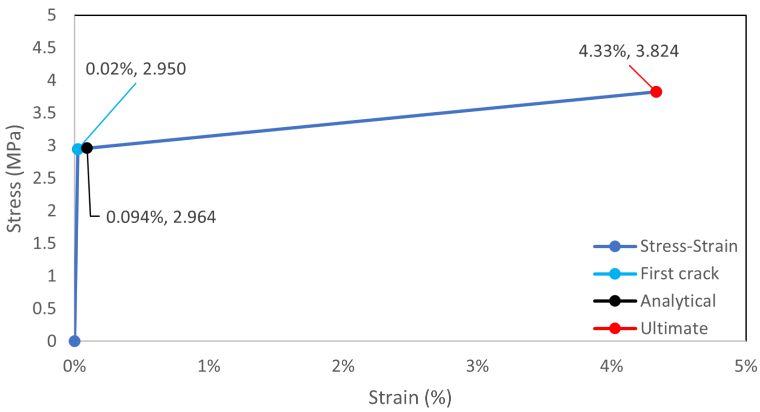

Figure 4.6: Stress-strain curve of the cracked *SHCC*.

The final results using the *SHCC* as closure pour and applying the data from Table 4.11 are shown in table 4.12 and fig. 4.7.

Dimensions	Old Bridge	*SHCC CP*	New Bridge
Elastic Modulus (MPa)	30941	3139	18461
Shrinkage (ε)	-	9.85×10^{-4}	1.57×10^{-4}

Table 4.11: Data for *SHCC* closure pour.

SHCC	Old top	Old bottom	CP top	CP bottom	New top	New bottom
item 1	0.00	0.00	3.09	3.09	2.90	2.90
item 2	-1.89	-1.89	-0.19	-0.19	-1.13	-1.13
item 3	1.37	1.37	0.05	0.05	-1.41	-1.41
item 4	1.79	-1.79	0.01	-0.01	1.03	-1.03
Total	1.26	-2.31	2.96	2.94	1.39	-0.67

Table 4.12: Results of shrinking cracked *SHCC* closure pour.

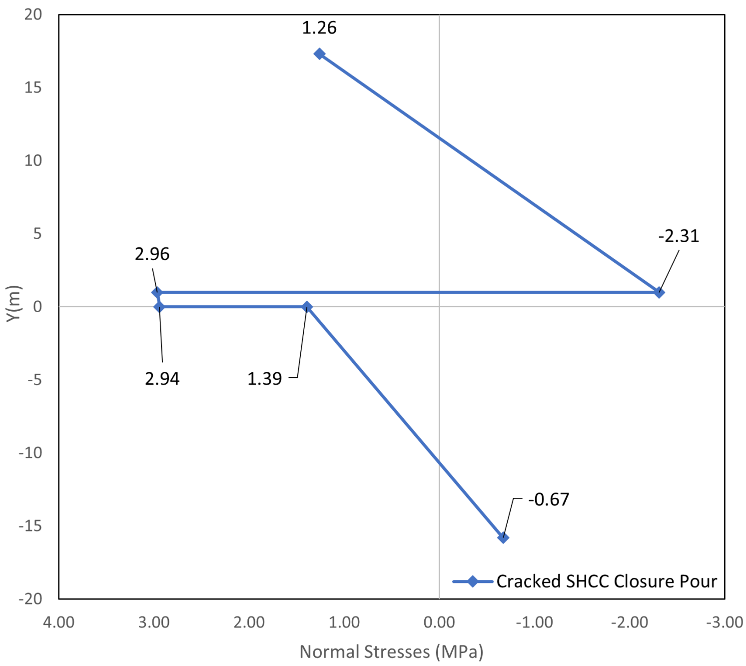

Figure 4.7: Results of shrinking cracked *SHCC* closure pour.

4.1.3 Summary

4.1.3.1 Only shrinkage is considered

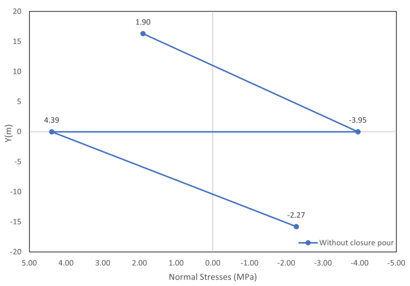

(a) No closure pour.

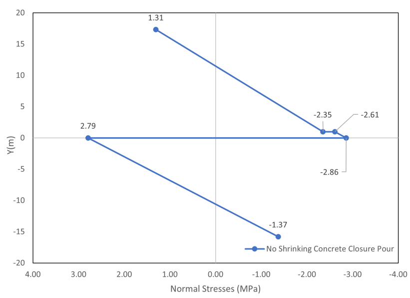

(b) No shrinking concrete closure pour.

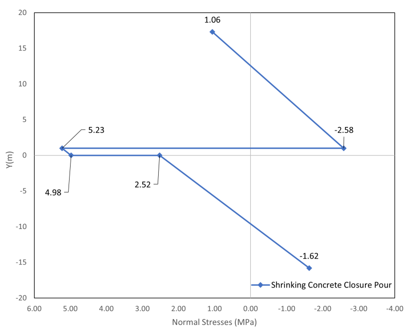

(c) Concrete shrinking closure pour.

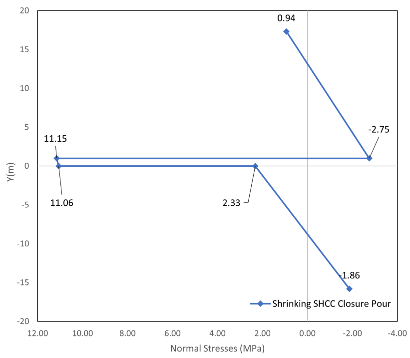

(d) SHCC shrinking closure pour.

Figure 4.8: Only shrinkage is considered.

4.1.3.2 Shrinkage, creep, and crack are considered

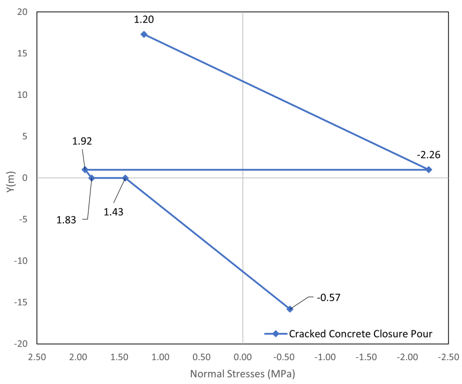

(a) Concrete closure pour.

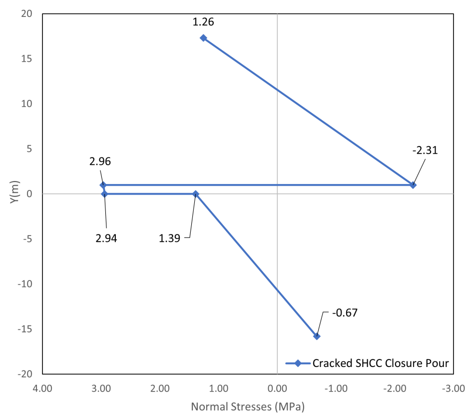

(b) *SHCC* closure pour.

Figure 4.9: Shrinkage, creep, and crack are considered.

4.2 Maximum deformation of *SHCC* analysis

As explained in Section 3.4, the modified elastic modulus was calculated through Equation 4.1 and presented with the modified elastic modulus for the new and old bridge at Table 4.13. The final normal stresses of the model are shown in Table 4.14 and in Figure 4.10

$$E_{x+1} = \frac{\sigma_x}{\varepsilon_x} = \frac{3.824}{4.33 \times 10^{-2}} = 88MPa \tag{4.1}$$

Dimensions	Old Bridge	*SHCC CP*	New Bridge
Elastic Modulus (MPa)	30941	88	18461
Shrinkage (ε)	-	4.33×10^{-2}	1.57×10^{-4}

Table 4.13: Data for the extra *SHCC* model.

Stresses	Old top	Old bottom	CP top	CP bottom	New top	New bottom
item 1	0.00	0.00	3.81	3.81	2.90	2.90
item 2	-1.93	-1.93	-0.01	-0.01	-1.15	-1.15
item 3	1.37	1.37	0.00	0.00	-1.42	-1.42
item 4	1.79	-1.79	0.00	0.00	1.04	-1.04
Total	1.24	-2.35	3.81	3.81	1.37	-0.70

Table 4.14: Results of the extra *SHCC* model.

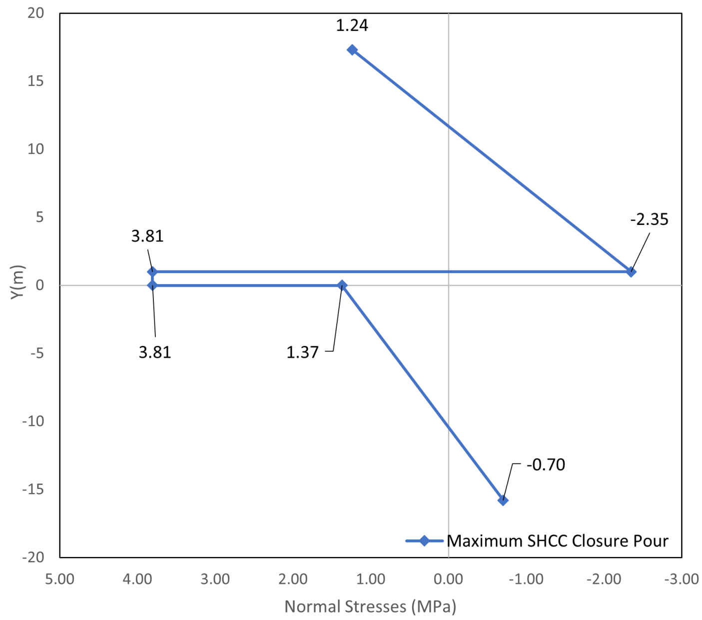

Figure 4.10: Results of the extra *SHCC* model.

4.3 Finite Element Analysis Linear Model

The following section provides the results obtained through the methodology explained in Section 3.5 and the data provided in Section F.2. To enhance clarity and facilitate comprehension, the results have been organized into distinct subsections.

1. Bridge with a concrete closure pour.
2. Bridge with a *SHCC* closure pour.

4.3.1 Model 1 with a concrete closure pour.

The summary of the data used for this model is in Table 4.15.

Dimensions	Old Bridge	Concrete *CP*	New Bridge
Elastic Modulus (MPa)	30941	11667	18461
Shrinkage (ε)	-	2.37×10^{-4}	1.57×10^{-4}

Table 4.15: Data for concrete closure pour.

4.3.1.1 Normal Stresses And Strains

The normal stresses throughout the structure, as depicted in Figure 4.11, are comparable to those displayed in the graphic of stresses at the midpoint of the span, illustrated in Figure 4.12. Similarly, the normal strains in the structure, displayed in Figure 4.13, are akin to those exhibited in the graphic of strains at the edge of the span, as shown in Figure 4.14.

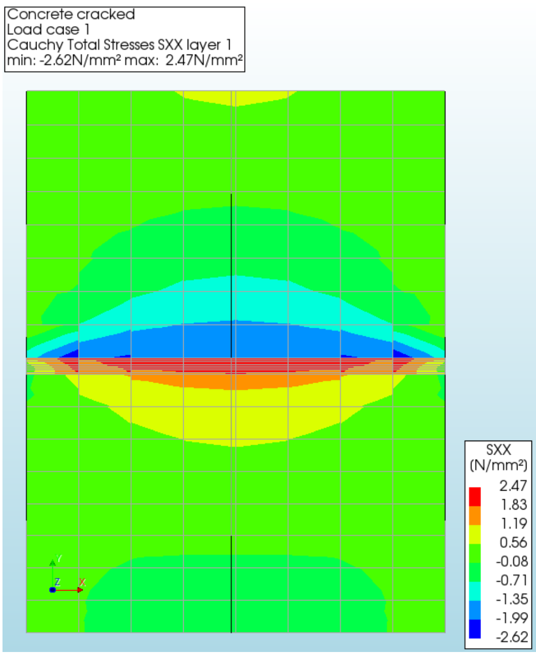

Figure 4.11: Longitudinal stresses of Model 1.

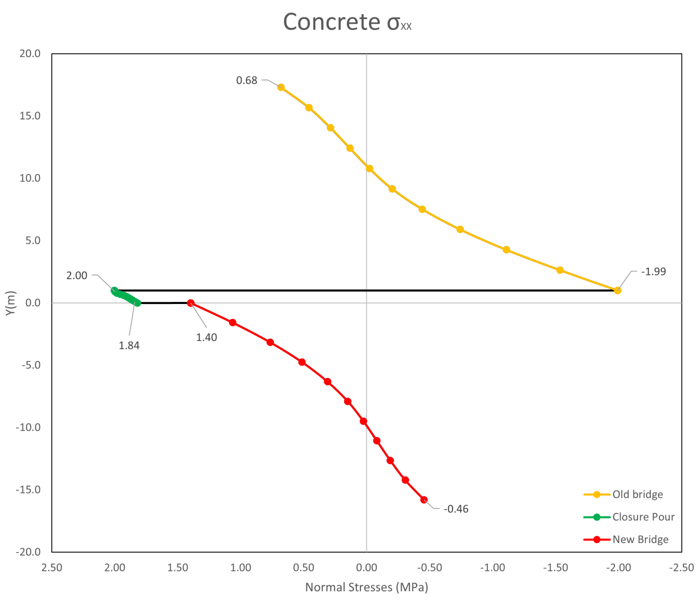

Figure 4.12: Longitudinal stresses along the mid-span of Model 1.

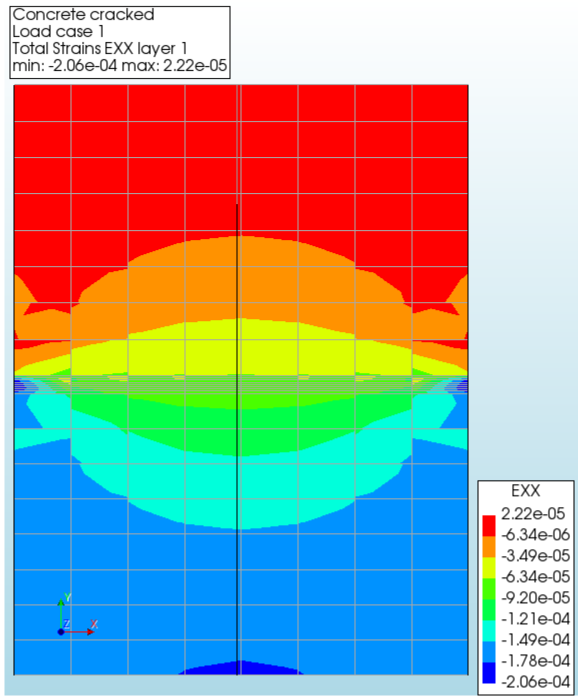

Figure 4.13: Longitudinal strains of Model 1.

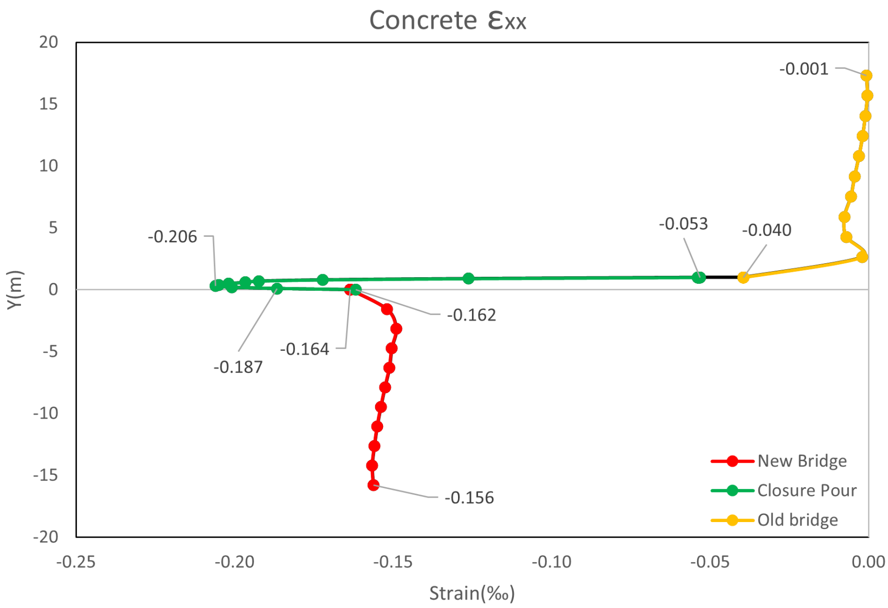

Figure 4.14: Longitudinal strains along the edge of the span of Model 1.

4.3.1.2 Shear Stresses And Strains

The shear stresses observed in the structure, as portrayed in Figure 4.15, are equivalent to those shown in a stress graphic at the span's edge, illustrated in Figure 4.16. Likewise, the shear strains in the structure, as presented in Figure 4.17, are comparable to those exhibited in a strain graphic at the edge of the span, as depicted in Figure 4.18.

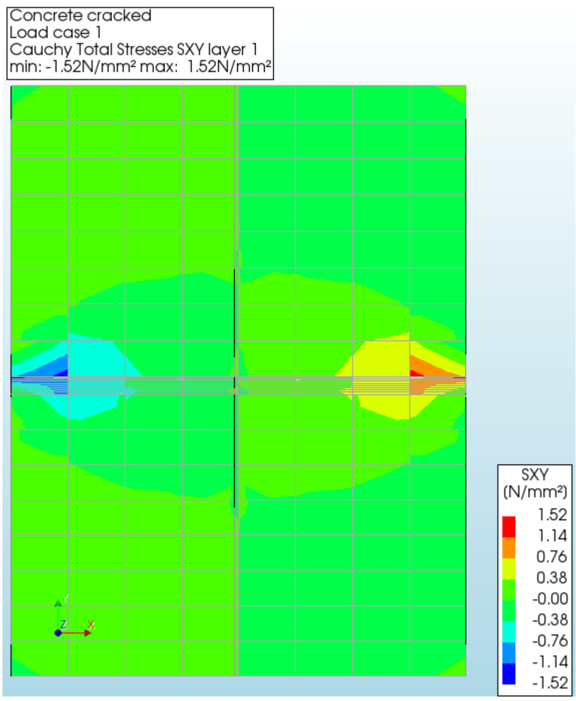

Figure 4.15: Shear stresses of Model 1.

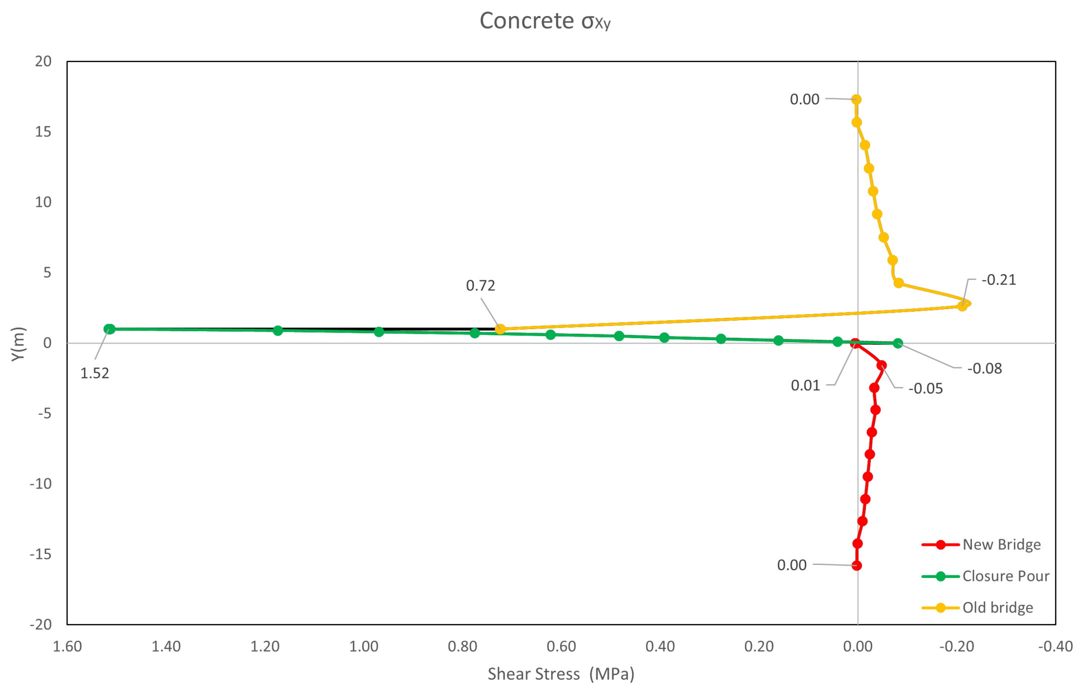

Figure 4.16: Shear stresses along the edge of the span of Model 1.

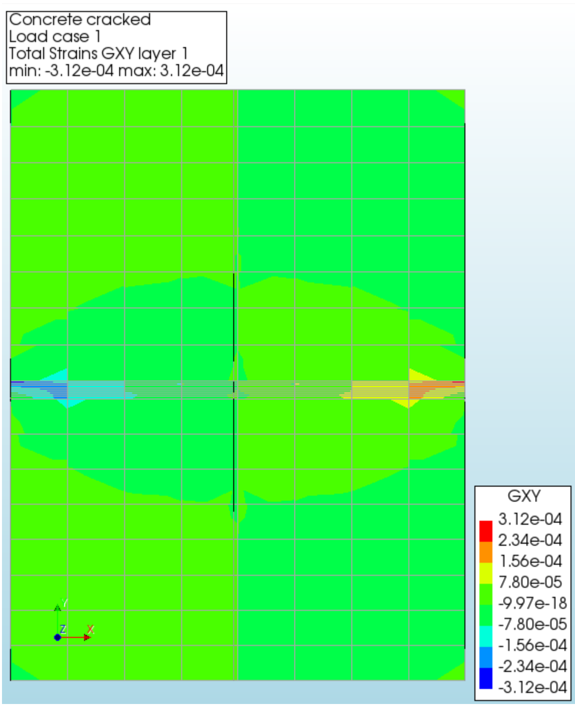

Figure 4.17: Shear strains of Model 2.

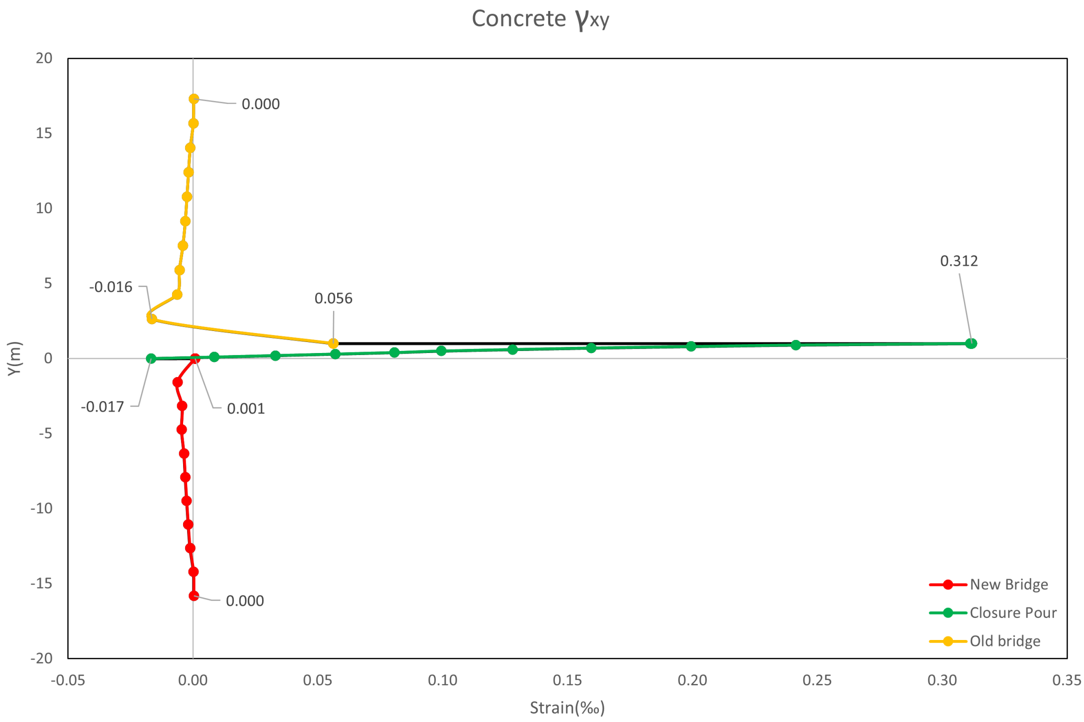

Figure 4.18: Shear strains along the edge of the span of Model 1.

4.3.2 Model 2 with a *SHCC* closure pour

The Figure 4.19 shows the stress-strain curve of the *SHCC* adopted to calculate the modified elastic modulus to account for the cracked *SHCC*. At Table 4.16, there is a summary of elastic modulus modified and shrinkage values input into the model. The value of the elastic modulus of the *SHCC* closure pour was taken from the last line of Table D.2, which was calculated applying Figure 4.19.

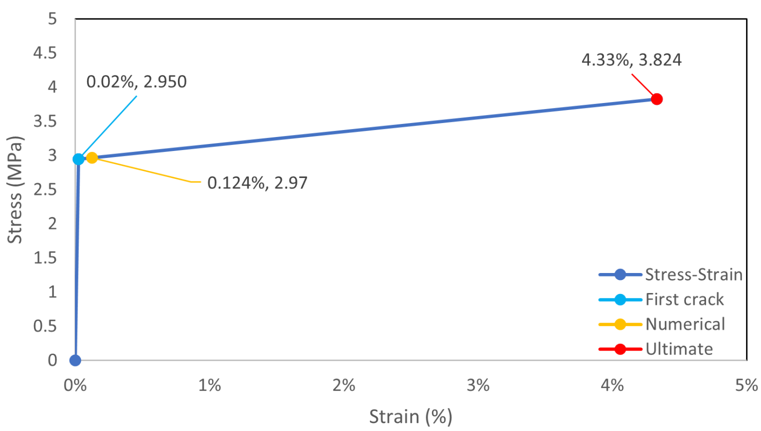

Figure 4.19: Stress-strain curve of the *FEA SHCC*.

Dimensions	Old Bridge	*SHCC CP*	New Bridge
Elastic Modulus (MPa)	30941	2402	18461
Shrinkage (ε)	-	9.85×10^{-4}	1.57×10^{-4}

Table 4.16: Data for *SHCC* closure pour.

4.3.2.1 Normal Stresses And Strains

The longitudinal stresses exhibited throughout the structure, as depicted in Figure 4.20, are similar to those illustrated in a graph featuring stresses at the midpoint of the span, displayed in Figure 4.21. Furthermore, the normal strains present in the structure, showcased in Figure 4.22, closely resemble those showcased in the strain graph at the span's edge, as depicted in Figure 4.23

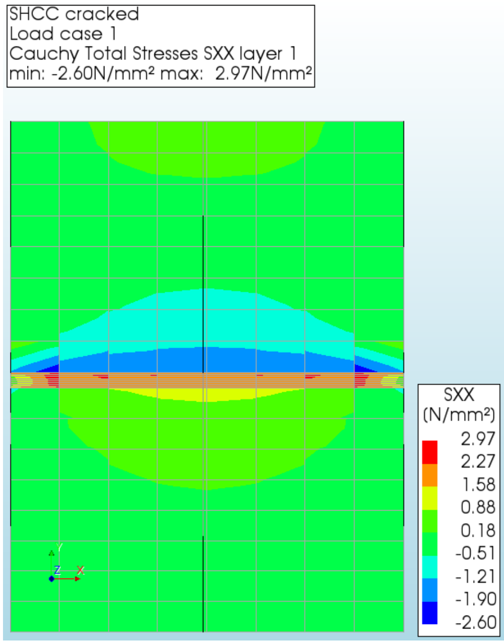

Figure 4.20: Longitudinal stresses of Model 2.

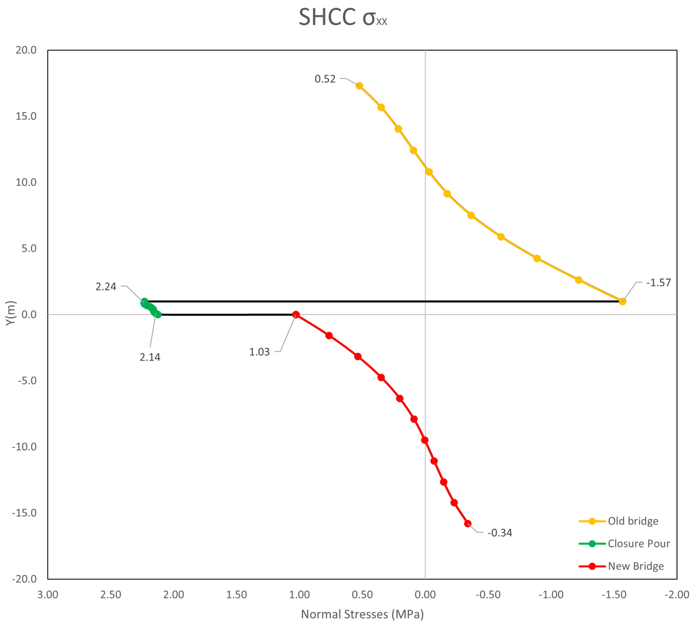

Figure 4.21: Longitudinal stresses along the mid-span of Model 2.

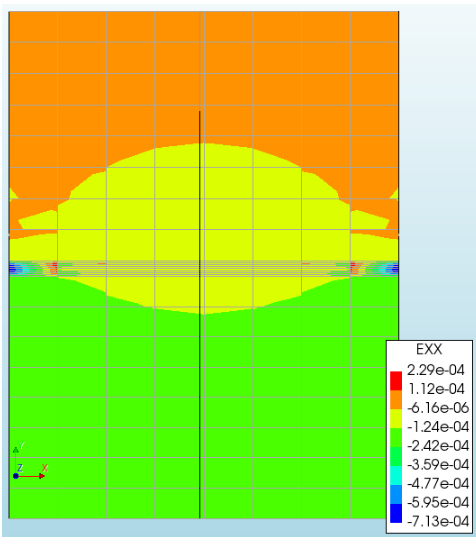

Figure 4.22: Longitudinal strains of Model 2.

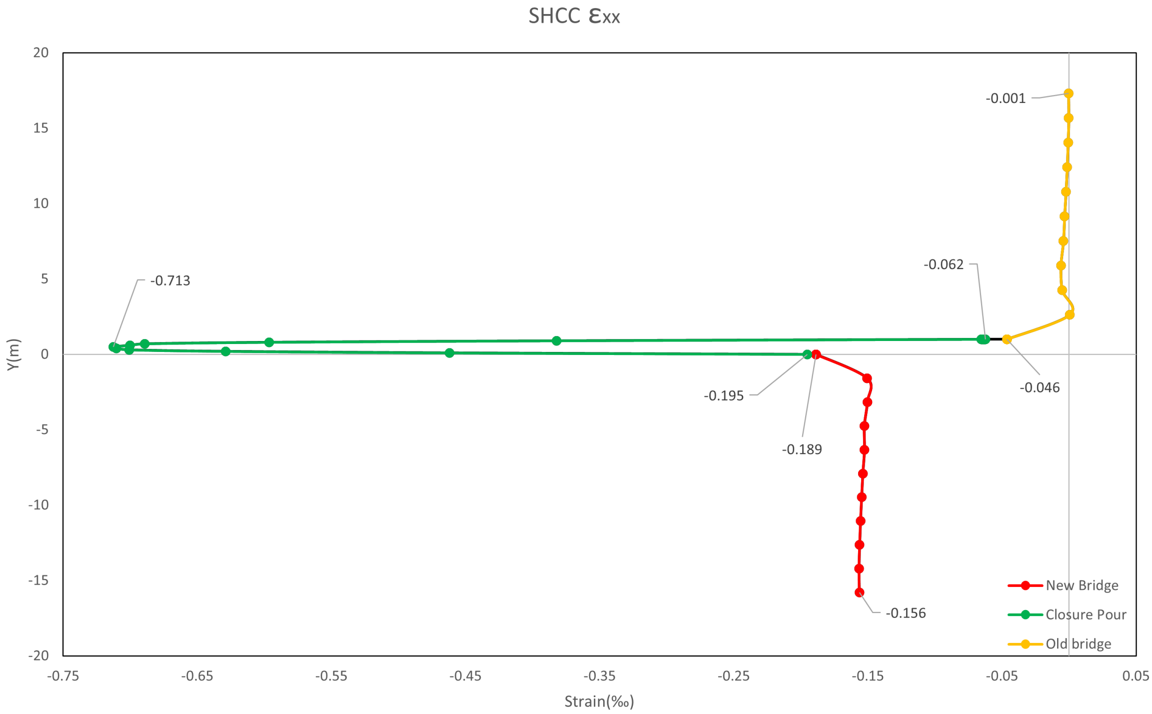

Figure 4.23: Longitudinal strains along the edge of the span of Model 2.

4.3.2.2 Shear Stresses And Strains

The shear stress and strain patterns observed in the structure, illustrated in Figure 4.24 and Figure 4.26 correspond to those displayed in stress and strain diagrams at the edge of the span, as portrayed in Figure 4.25 and Figure 4.27 respectively. Additionally, a supplementary diagram was generated to enhance the depiction of shear strains in the closure pour, as presented in Figure 4.28.

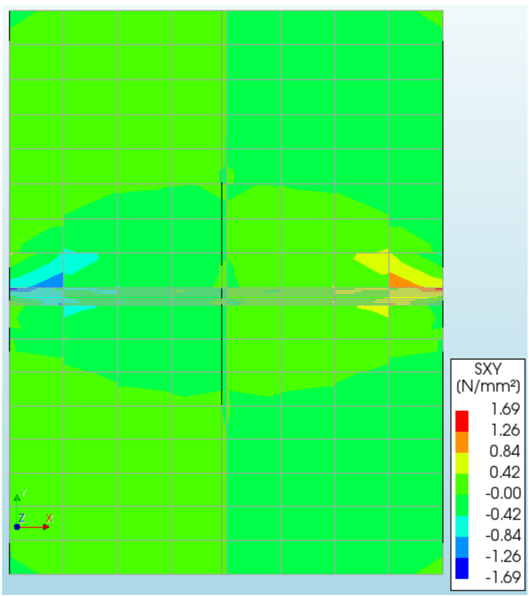

Figure 4.24: Shear stresses of Model 2.

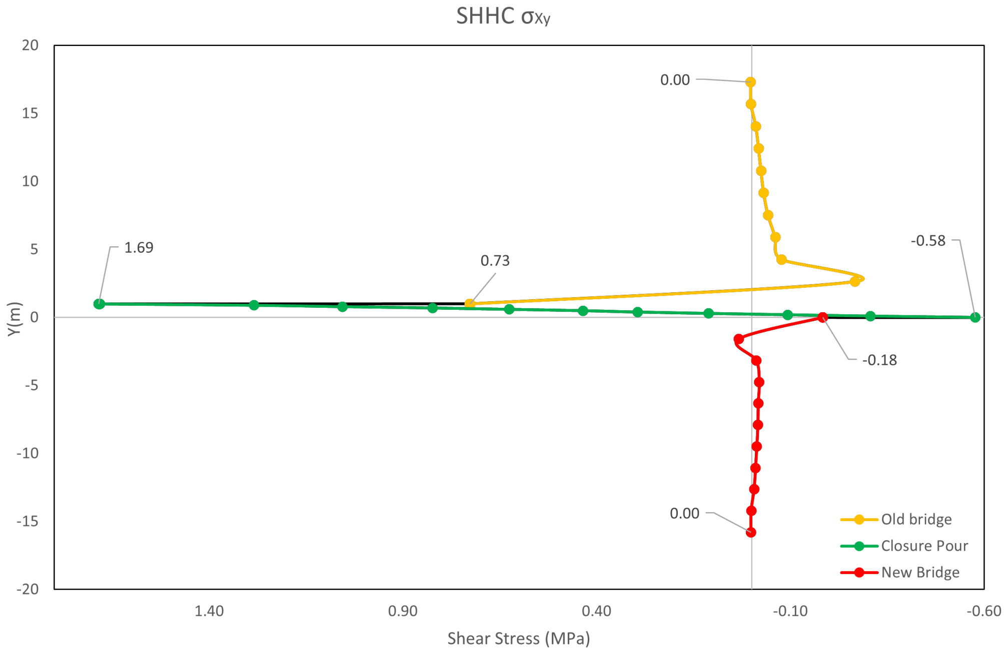

Figure 4.25: Shear stresses along the edge of the span of Model 2.

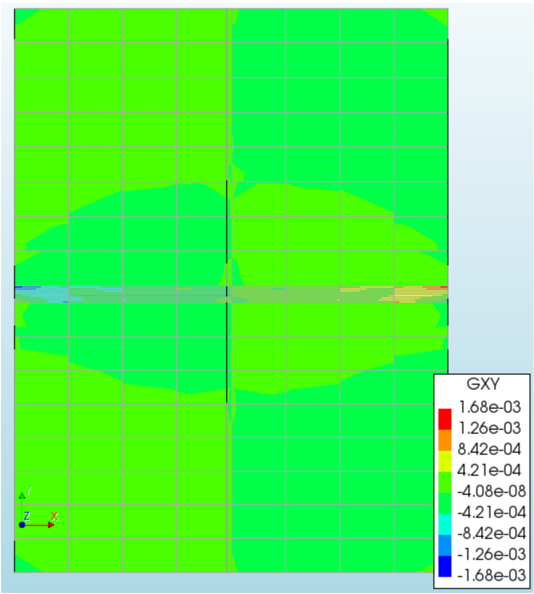

Figure 4.26: Shear strains of Model 2.

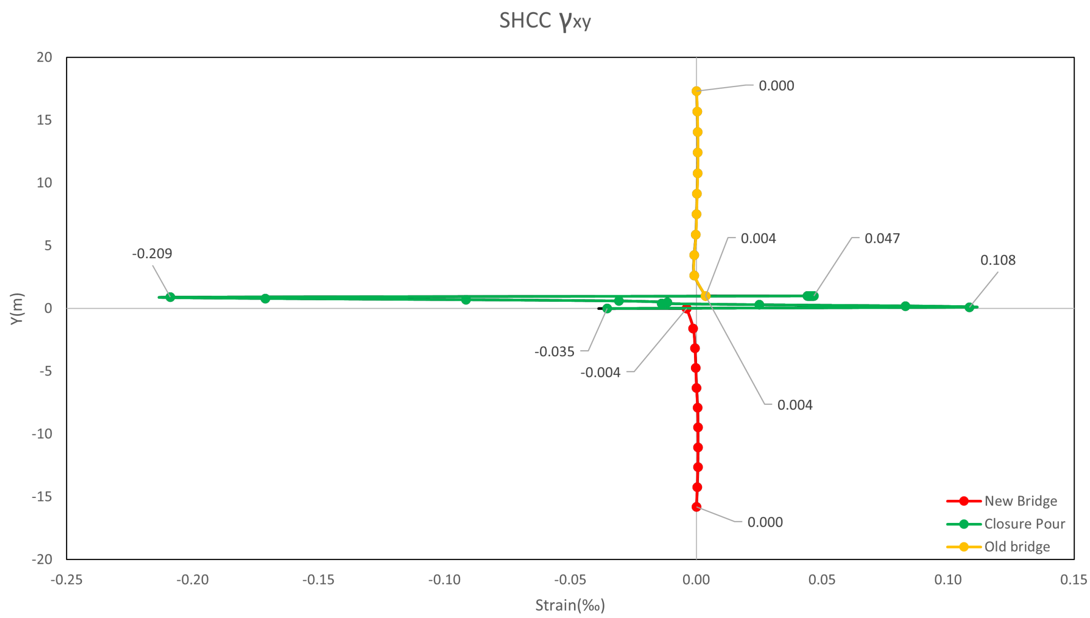

Figure 4.27: Shear strains along the edge of the span of Model 2.

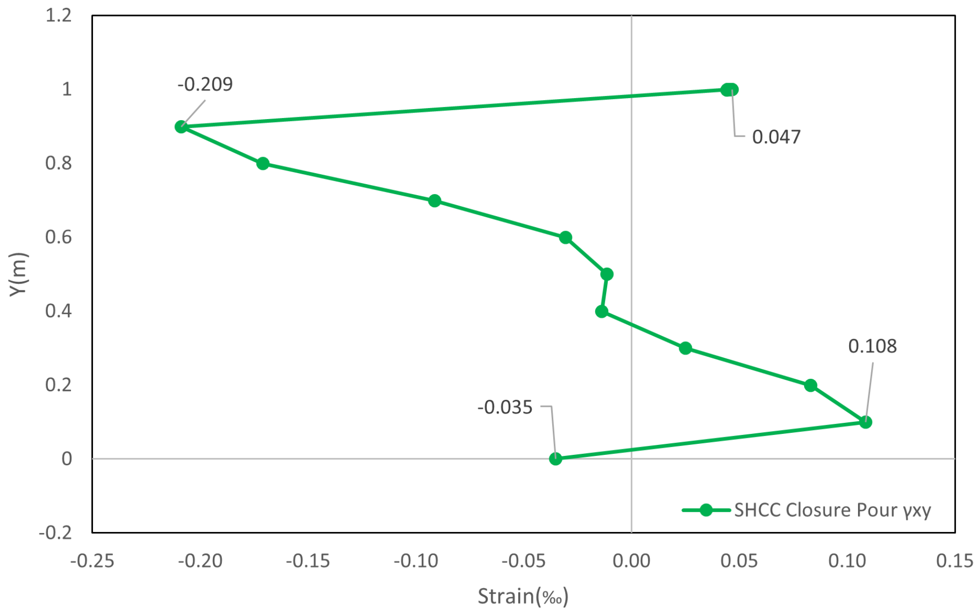

Figure 4.28: Shear strains along the edge of the span of Model 2, focusing only on the *SHCC* closure pour.

4.4 Reinforcement Design

The calculations for the reinforcement design were made in Appendix E. They result in the number of bars needed for the reinforced concrete closure pour, which is shown in Table 4.17.

Diameter	Minimum of bars	Steel Stress
$\phi = 20mm$	38	$191,90MPa$
$\phi = 25mm$	26	$179.41MPa$
$\phi = 32mm$	18	$165.76MPa$

Table 4.17: Data used for Reinforcement Design

5

Discussion

The discussion on this thesis will go over four main topics: a comparison of the analytical and numerical methods, the deformation problem, *SHCC* as a closure pour, and a comparison of concrete and *SHCC* closure pour.

5.1 Comparison of Analytical and Numerical Methods

When it comes to analyzing structures, there are various methods available. One of the most common approaches is *FEA*, which involves breaking down the design into more minor elements and using complex mathematical equations to calculate stresses and other factors. An alternative method is to use analytical calculations, which involve simplifying the system by considering it as a cross-section and reducing the 2D shell to a cross-section, thereby disregarding the span's length. According to Section 3.5, it was necessary to incorporate the use of *FEA* modeling to ensure the accuracy of analytical computations. The *FEA* linear model was crucial for validating the precision of the calculations. The *FEA* model treated the deck as a shell structure, taking into account all dimensions, including length, width, and thickness, thereby providing highly accurate results. In contrast, analytical calculations tend to treat decks as a simple cross-section, which may result in less precise outcomes.

This approach has certain limitations compared to FEA due to its lower complexity. One example is that analytical calculations assume that the maximum value of stress occurs at the midpoint of the span, which may not always be the case. In some situations, the ultimate tensile stresses may occur elsewhere, which analytical calculations would not account for. A comparison of mid-span values using concrete closure pour between the two approaches is shown in Figure 5.1. The results are reasonably similar, especially in the closure pour ($2.00MPa$ for the numerical model, while 1.92 for the analytical). However, the *FEA* model does generate a slightly higher maximum value ($2.47MPa$), as illustrated in Figure 5.2, likely due to its ability to take into account the length of the span. Ultimately, the choice of which method to use will depend on the specifics of the structure being analyzed and the goals of the analysis.

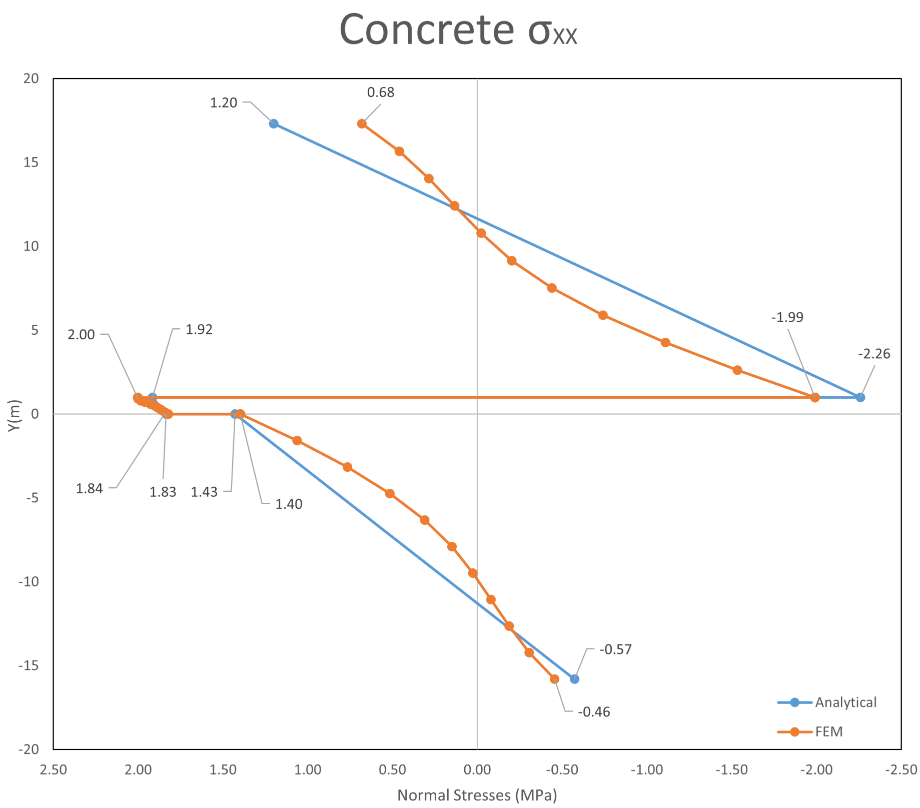

Figure 5.1: Longitudinal stresses with a concrete closure pour.

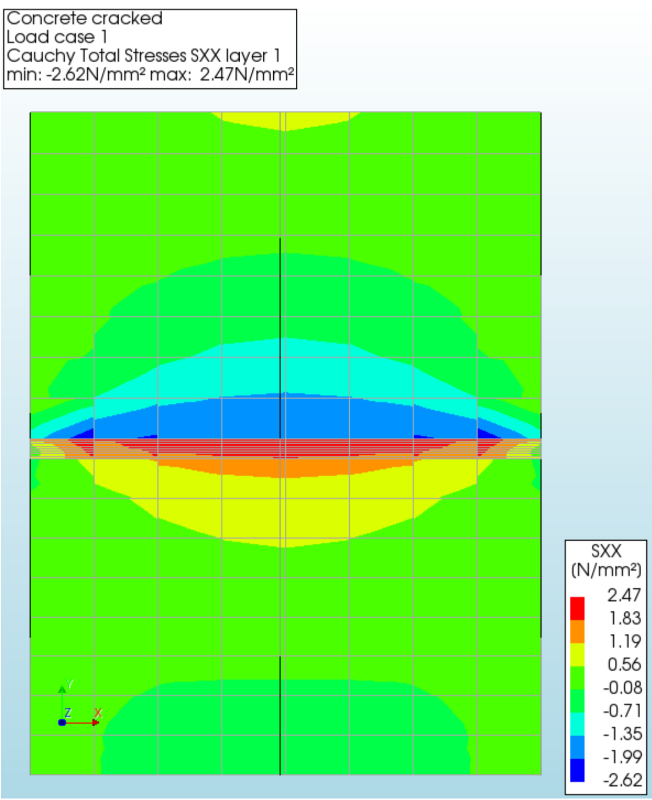

Figure 5.2: Longitudinal stresses of the concrete *FEA* model.

After conducting a thorough analysis of Figure 5.3, which provides a comparative analysis of the *SHCC*, a notable discrepancy between the methods becomes apparent. This disparity can be attributed to the fact that the stress-strain plot for cracked *SHCC* was assessed using the highest tensile value across the entire *FEA* model, as outlined in Section D.2, rather than the one at mid-span. Consequently, the ultimate tensile stress value in the analytical calculations aligns with the maximum tensile stress in the whole structure, as depicted in Figure 5.4.

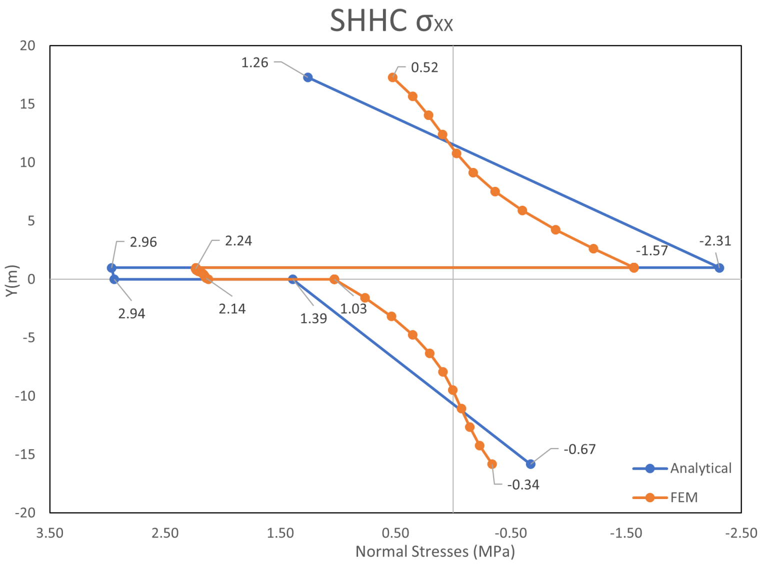

Figure 5.3: Longitudinal stresses with a *SHCC* closure pour.

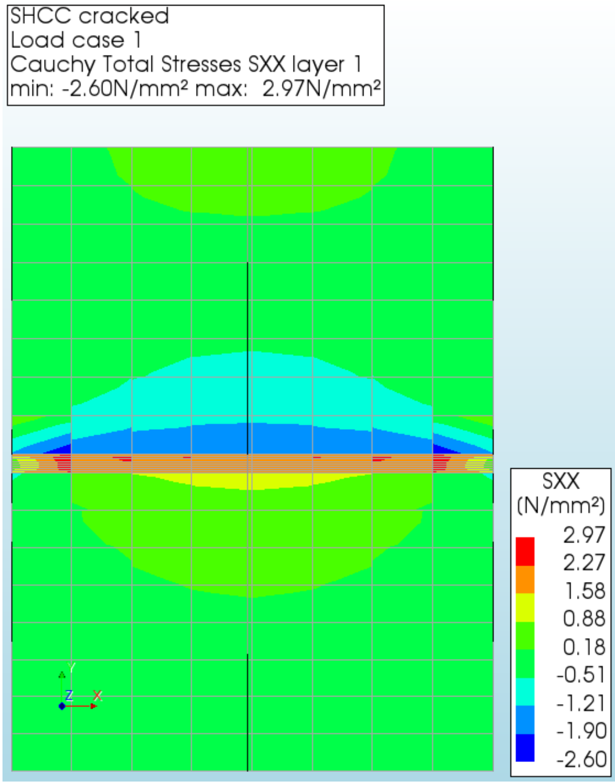

Figure 5.4: Longitudinal stresses of the *SHCC FEA* model.

Table 5.1 presents a comprehensive overview of the maximum tensile stress values depicted in figs. 5.1 to 5.4, allowing for easier comparison of these values.

Upon examination of the maximum mid-span values for concrete at Figure 5.1, a difference of 4.08% (analytical: $1.92MPa$, numerical: $2.00MPa$) is observed between the two methods. This difference indicates a slight variance in the results obtained from analytical and numerical methods. However, for *SHCC* at Figure 5.3, the difference in mid-span values is significantly higher at 27.69% (analytical: $2.96MPa$, numerical: $2.24MPa$), leading to a significant disparity in the results obtained from the two methods.

However, when comparing the maximum values of both methods, the difference in concrete is 25.06% (analytical: $1.92MPa$, numerical: $2.47MPa$), which signifies a substantial difference. On the other hand, for *SHCC*, the difference in maximum stress values obtained from the analytical and numerical methods is only 0.34% (analytical: $2.96MPa$, numerical: $2.97MPa$), likely due to the alignment of the cracked *SHCC* calculations, resulting in similar outcomes from both methods.

Stresses (MPa)	Concrete	*SHCC*
Analytical	1.92	2.96
FEA mid-span	2.00	2.24
FEA maximum	2.47	2.97

Table 5.1: Maximum tensile stress in the Analytical and Numerical Methods for Concrete and *SHCC*.

After careful examination of both sections 4.1 and 4.3, it becomes clear that certain similarities are present in the longitudinal stresses at the mid-span of the bridge widening. This observation leads to the belief that analytical calculations can be a reliable solution for basic calculations, particularly when it comes to determining the optimal material for the closure pour. However, it is also essential to acknowledge that the numerical method takes a more conservative approach, as evidenced by the higher tension results in Table 5.1.

It is vital to note that high levels of *SHCC*'s shrinkage do not pose a concern when the material has a high strain range. This aspect is critical for ensuring the stability and safety of the structure over time.

As the project progresses, it would be beneficial to incorporate a numerical model similar to the one outlined in Section 3.5. This model can provide more precise results and allow for the evaluation of shrinkage force transfer from the new bridge and closure pour to the old bridge at specific angles. Model 1, for instance, shows roughly 26 degrees (Figure 5.2), while Model 2 depicts 28 degrees (as shown in Figure 5.4).

The resulting compression stresses in the old bridge cause tension stresses in the closure pour and the new bridge at a 22-degree angle for Model 1(as depicted in Figure 5.2). However, in Model 2(as illustrated in Figure 5.4), the shrinkage force in the closure pour is significantly higher, resulting in a decrease in the tensile stresses in the new bridge, only a 9-degree angle. These findings demonstrate another significance of implementing the *FEA* model. A comprehensive understanding of stress behavior throughout the entire plate can be gained, rather than solely focusing on the mid-span through analytical calculations. Accurate identification and addressing of potential stress concentrations throughout the deck is possible, ultimately ensuring the structural integrity and safety of the system.

The outcomes of the concrete closure pour for the entire structure are consolidated in Table 5.2, which also exhibits the stress levels in each component highlighted in Figure 5.1. Correspondingly, Table 5.3 presents a rundown of the *SHCC* closure pour outcomes for the identical structure depicted in Figure 5.3.

Stresses (MPa)	Concrete Analytical	Concrete *FEA*
Old top	1.20	0.68
Old bottom	-2.26	-1.99
CP top	1.92	2.00
CP bottom	1.83	1.84
New top	1.43	1.40
New bottom	-0.57	-0.46

Table 5.2: Summary of the concrete closure pour results from Figure 5.1.

Stresses (MPa)	*SHCC* Analytical	*SHCC FEA*
Old top	1.26	0.52
Old bottom	-2.31	-1.57
CP top	2.96	2.24
CP bottom	2.94	2.14
New top	1.39	1.03
New bottom	-0.67	-0.34

Table 5.3: Summary of *SHCC* closure pour results from Figure 5.3.

5.2 Deformation Problem

As observed in Section 3.2, the issue of shrinkage and creep in widening a prestressed concrete bridge arises from the varying deformations of the old bridge, closure pour, and new bridge. To overcome this problem, a material with a higher tensile strain capable of better deformation and restoring compatibility among the elements would be a viable solution.

Furthermore, as mentioned in Section 3.2 and elaborated in Section 5.1, the normal stresses in the closure pour are induced by the difference in deformations between the two main decks of the Schipholbrug. This discrepancy in deformation, illustrated in Figure 3.1 and Figure 3.2, also manifests in the normal and shear strains and their stresses.

A comprehensive investigation of the normal stresses has been conducted and outlined in Section 5.1. This analysis has also shed light on the differences between analytical and numerical approaches. Thus, the subsequent section will delve into the topic of normal strains, shear stresses, and shear strains.

5.2.1 Normal strains

Figure 4.14 and Figure 4.23 illustrate that the normal strain behavior of both the new and old bridges remains consistent at their respective edges. The new bridge exhibits a normal strain of $-0.156‰$, while the old bridge presents a normal strain of $-0.001‰$. However, the values of compressive strains in the closure pour, and its surroundings differ despite exhibiting similar behavior.

All strains in the area are compressive, indicating a negative strain caused by shrinkage, with the exception of a small part of the old bridge. The application of shrinkage in the new bridge, as well as the closure pour, leads to greater values of compressive strain. Moreover, it can be observed that the strain in the new bridge is not centered at zero, unlike the old one.

The closure pour exhibits the highest compressive strain among the figures, owing to its greater shrinkage compared to the new bridge. Notably, the compressive strain observed in the closure pour made of *SHCC* is higher than that made of reinforced concrete. This is because *SHCC* exhibits more than four times the shrinkage of concrete (concrete: 2.37×10^{-4}, *SHCC*: 9.85×10^{-4}). Therefore, it is not surprising that the compressive strain of the closure pour is three times higher with *SHCC* (concrete: $-0.713‰$, *SHCC*: $-0.206‰$).

It is worth noting that both models display a negligible difference in strain between the closure pour and the main decks, regardless of whether they are new or old. Nevertheless, in terms of shear strain, the situation is considerably different, and a more in-depth analysis of this aspect will be presented in Section 5.2.3.

In the case of the concrete closure pour, the difference between the new bridge and the closure is minimal, with only a $0.002‰$ variation (new bridge: $-0.164‰$, closure pour: $-0.162‰$). The difference between the old bridge and the concrete is slightly higher at $0.013‰$ (old bridge: $-0.040‰$, closure pour: $-0.053‰$). For the *SHCC* closure pour, the difference between the new bridge and closure is also quite small, only $0.007‰$ (new bridge: $-0.189‰$, closure pour: $-0.195‰$). However, the difference between the old bridge and the concrete increases to $0.016‰$ (old bridge: $-0.046‰$, closure pour: $-0.062‰$).

5.2.2 Shear Stress

Figure 4.16 and Figure 4.25 illustrate that the behavior of shear stresses in the concrete and *SHCC* closure pour is quite similar. Near the closure pour, the new bridge experiences shear stresses that are almost zero. In contrast, the old bridge shows nearly identical positive shear stress levels, with only a slight 1.4% variance (concrete: $0.72MPa$, *SHCC*: $0.73MPa$). The closure pour has a small negative shear stress near the new bridge, with a difference of $0.50MPa$ (concrete: $-0.08MPa$, *SHCC*: $-0.58MPa$), but this evolves into a significant positive shear stress near the old bridge, with a difference of $0.17MPa$ (concrete: $1.52MPa$, *SHCC*: $1.69MPa$).

Moreover, both the old and new bridges experience reduced shear stress as the distance from the closure pour increases, irrespective of the closure pour type. This decrease in stress is due to the minimal difference in deformation at the span's edges, resulting in negligible stress on the bridge decks' edges ($0.00MPa$).

5.2.3 Shear Strain

Both new and old bridges exhibit consistent shear strain behavior at their respective edges, as evidenced by Figure 4.18 and Figure 4.27, regardless of whether concrete or *SHCC* closure pour is used. As predicted, there is minimal deformation at the span edges of both bridges, with no shear strains ($0.000‰$) detected on all four edges, two edges in each model of closure pour. However, near the closure pour, there are two distinct shear strain behaviors due to variations between concrete and *SHCC*, as depicted in Figure 5.5.

The *SHCC* material displays superior deformation properties, with its shear strain for the closure pour nearly matching the negative shear strain of the new bridge, differing by only $0.032‰$ (new bridge: $-0.004‰$, closure pour: $-0.035‰$). However, to compensate for this negative shear strain, the closure pour generates a positive shear strain of $0.108‰$. *SHCC* also allows for a close match between the closure pour shear strain and the old bridge's positive shear strain, with a difference of only $0.043‰$ (old bridge: $0.004‰$, closure pour: $0.047‰$). Nevertheless, to counterbalance the old bridge's positive shear strain, the closure pour generates a significantly high negative shear strain of $0.209‰$.

In contrast, concrete is a rigid material that closely mirrors the positive shear strain of the new bridge, differing only by a small margin of $0.017‰$ (new bridge: $0.001‰$, closure pour: $-0.017‰$). However, due to its inflexibility, the closure pour's shear strain follows a curve without changing direction, unlike *SHCC*, which exhibits different behavior, as illustrated in Figure 5.5, resulting in a significant tensile strain of $0.312‰$. This makes it impossible to achieve compatibility with the old bridge, which has a mere tensile strain of $0.056‰$, creating a significant difference of $0.256‰$. This deviation in strains poses practical challenges due to its unrealistic nature.

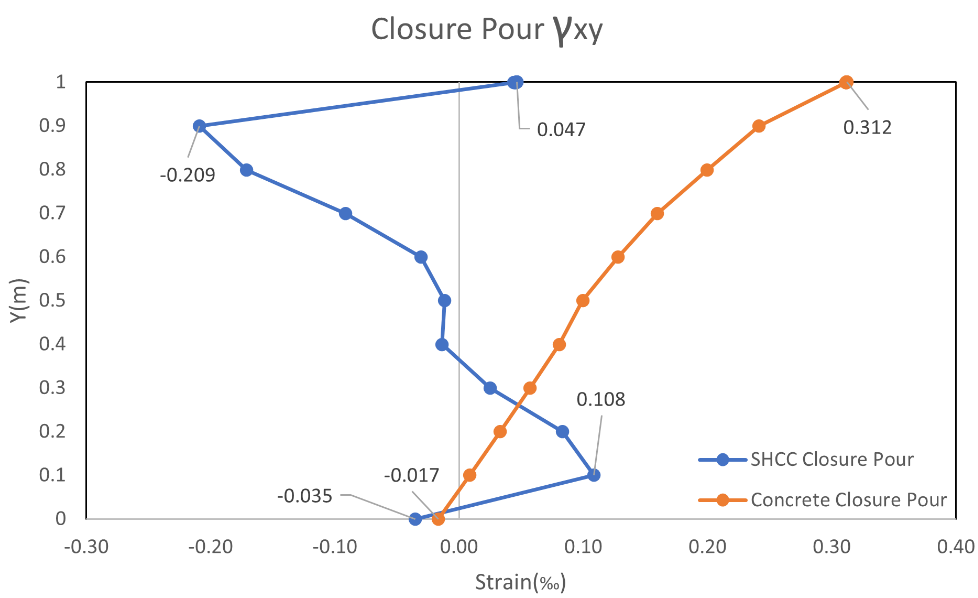

Figure 5.5: Comparison of the behavior of the shear strain, γ_{xy}.

5.3 *SHCC* as a closure pour

The primary objective of this thesis is to minimize the duration required for widening a bridge by employing *SHCC* as the closure pour. Through thorough research conducted in Chapter 2 and the outcomes obtained in Chapter 4, it has been demonstrated that *SHCC* can endure all the in-plane loads contemplated for this study associated with the various materials. In other words, *SHCC* can effectively address concerns such as creep in the main decks, shrinkage in the new bridge, and closure pour shrinkage and cracking.

5.3.1 Stress-Strain graphic

In the presented Figure 5.6, the stress-strain diagram of *SHCC* is depicted, revealing that both stress and strain measuring methods used in the study yielded comparable outcomes. Notably, the stress values exhibit a minimal variation of $0.006MPa$ (analytical: $2.964MPa$, numerical: $2.97MPa$), while the strain values only differ by a minute amount of 0.0003(analytical: 0.094%, numerical: 0.124%). These results demonstrate a high level of accuracy and reliability in the measurement techniques employed. Figure 5.6 also demonstrate that *SHCC* could suffer a deformation of 4.33%, that it still would be able to handle the stresses.

Furthermore, it is noteworthy that both stress and strain values are in close proximity to the first crack rather than the ultimate tensile stress and strain, as illustrated in Figure 5.7. This observation highlights the potential for higher loads and suggests that *SHCC* possesses durable and robust material properties. This information is of significant value to engineers and researchers interested in designing and developing materials with enhanced strength and durability. Overall, the stress-strain diagram of *SHCC* provides crucial insights into the material's properties and has the potential to inform future research and development efforts.

It is important to highlight that the calculation of the elastic modulus modification in *SHCC* resulting from cracking is based on a simplified approach that assumes a linear relationship between stress and strain, as shown in Figure 5.6. While it would be ideal to validate this assumption through experimental testing, it is commonly used in practice due to its practicality.

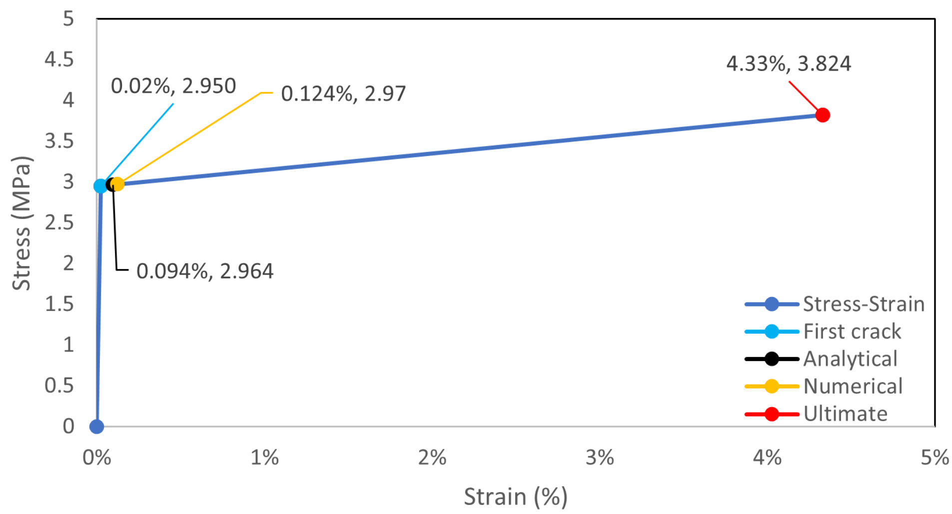

Figure 5.6: Final stress-strain graphic of *SHCC*.

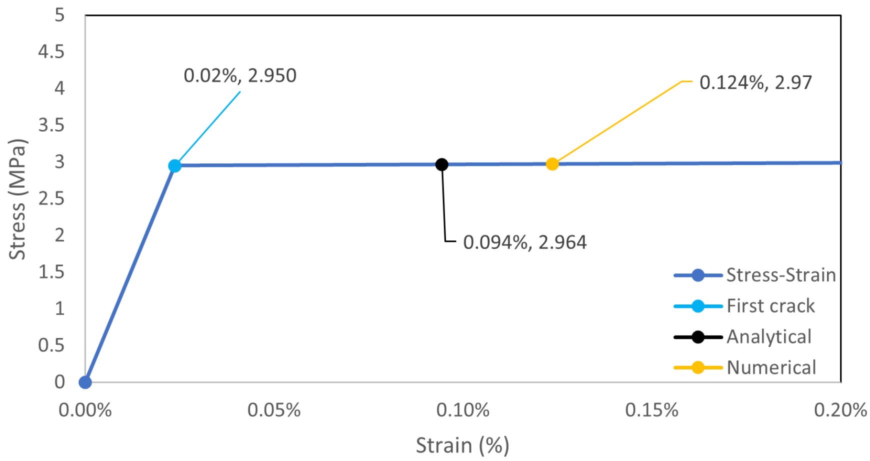

Figure 5.7: Focus on the main results of the final stress-strain graphic of *SHCC*.

5.3.2 Crack width

As mentioned in Section 2.3.4 Wang's research, which serves as the primary reference for the *SHCC* in this thesis, it was discovered that the crack width for *SHCC* is limited to a maximum of $0.05mm$. As also mentioned in Section 2.3.4, the crack widths for *SHCC* are typically below $100\mu m$ or $0.10mm$, or even lower. These values are significantly lower than the maximum crack width allowed by the codes, which is $0.20mm$ as indicated in Section 2.1.3.3.

Observations confirm that *SHCC* is an incredibly durable and dependable material with excellent crack resistance. These qualities make it an ideal choice for multiple engineering applications where strength, longevity, and reliability are crucial. Precise and detailed information about this material's crack width can assist engineers and researchers in making informed decisions about its use in their projects.

5.3.3 Maximum deformation of *SHCC* analysis

Based on the findings outlined in Section 4.2 and Figure 5.6, it is evident that *SHCC* demonstrates exceptional deformation handling abilities, surpassing the corresponding numerical model by a factor of 35. The numerical deformation recorded was 0.124%, while the maximum deformation reached was 4.331%, confirming the superiority and effectiveness of *SHCC* in such situations. Additionally, the normal stress results depicted in Figure 4.10, of $3.81MPa$, are even lower than the ultimate tensile stress illustrated in Figure 5.6 of $3.824MPa$, which technically should not happen but the difference is almost negligible.

5.3.4 Extra Model with three spans

The thesis employed a span of $25.5m$, although its length was not taken into account in the analytical calculations. It is worth noting that the results depicted in Figure 5.9 and the stress-strain curve in Figure 5.8 remained consistent regardless of whether one or three spans were used for shrinkage, creep, and crack issues.

The final elastic modulus modified for this extra model was $2507MPa$, and its calculation is at Section D.3, and it could also be taken from Figure 5.8.

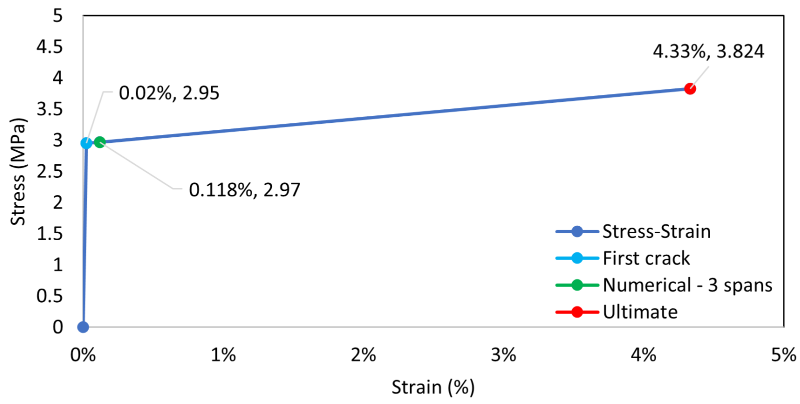

Figure 5.8: Stress-strain curve of three spans model of *SHCC*.

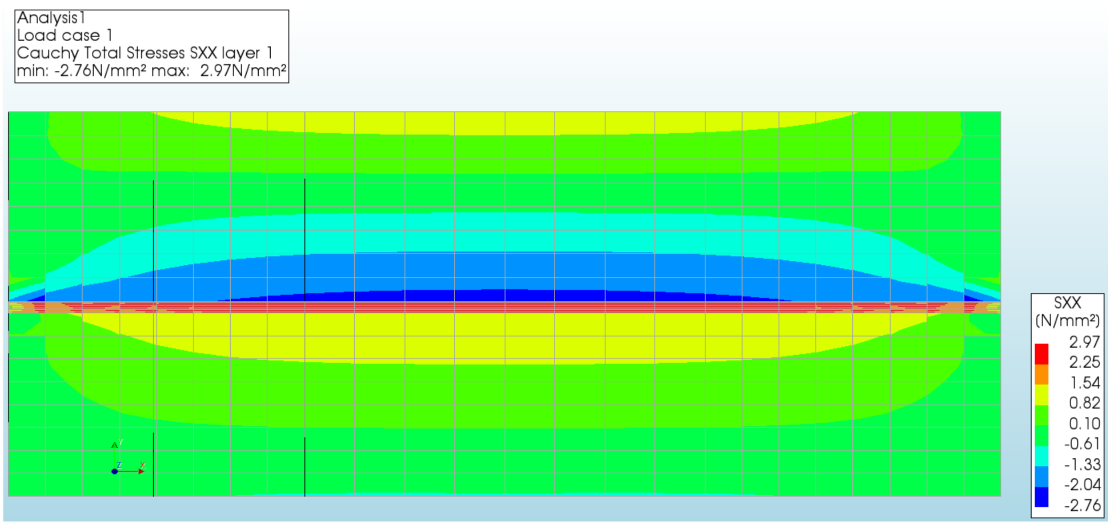

Figure 5.9: Longitudinal stresses with cracked *SHCC* of three spans.

The diagram presented in Figure 5.10 illustrates the deformation resulting from the shrinkage strain.

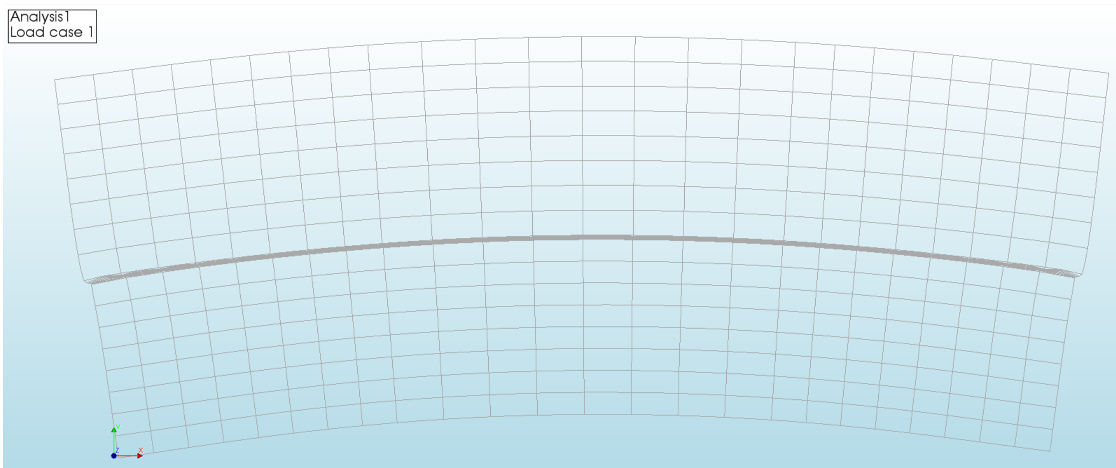

Figure 5.10: Line diagram of the deformation of cracked *SHCC* of three spans.

5.4 Comparison Of Concrete And *SHCC* As A Closure Pour.

According to Section 5.1, Section 5.2, and Section 5.3, both closure pours could potentially resolve the deformation issue. The normal and shear stresses and strains fall comfortably within acceptable ranges, though some may raise concerns about the shear strains in the reinforced concrete closure pour.

Additionally, reinforced concrete is a highly favored option for closure pour in the Netherlands, thanks to its well-established properties, cost-effectiveness, and long-lasting durability. It is, however, essential to note that the *C40/50* concrete variant is susceptible to cracking if its tension stress exceeds $3.5MPa$, as clearly indicated in Table F.1.

The results of the reinforcement design conducted in Appendix E are outlined in Section 4.4, which confirms that the reinforced concrete meets the necessary crack width of $0.20mm$, as stated in Section 2.1.3.3. Additionally, Table 4.17 offers three reinforcement choices. It is important to consider that the closure pour has a one-meter width, and even two layers with nine $32mm$ diameter bars in each layer already constitute a significant amount of reinforcement.

Despite the fact that concrete closure pour experiences lower stresses compared to *SHCC* closure pour (concrete: $2.47Pa$, *SHCC*: $2.97MPa$), the considerable amount of reinforcement required for concrete is ultimately no match for *SHCC*. This is due to the fact that *SHCC* does not require reinforcement to address crack width issues, which reduces implementation time and labor costs - a crucial factor in the Netherlands.

The utilization of the *SHCC* closure pour presents a promising solution for the reduction of construction time required for bridge widening projects. This observation is due to the fact that the highest stress values obtained through both analytical and numerical methods (analytical: $2.96MPa$, numerical: $2.97MPa$) are significantly lower (by at least 25%) than the ultimate tensile strength of the *SHCC* material, which is measured at $3.824MPa$, as presented in Figure 5.6. It is also worth noting that the maximum strain values for both methods (analytical: 0.094%, numerical: 0.124%) are significantly lower (by over 188%) than the ultimate strain of 4.331%.

Moreover, as described in Section 5.3.3, the material has been shown to withstand strains up to 35 times higher than those predicted by analytical and numerical models. These findings indicate that the SHCC closure pour can be effectively utilized to shorten the construction period of bridge widening projects while maintaining the material's integrity.

The main goal of this thesis is to reduce the time required to widen a bridge by utilizing *SHCC* as the closure pour and incorporating a two-month waiting period. Through extensive research conducted in Chapter 2, through the methodology in Chapter 3, and the results obtained in Chapter 4, it has been shown that *SHCC* is capable of withstanding all in-plane loads considered in this study, regardless of the materials involved. Therefore, *SHCC* is a reliable solution for concerns such as creep in the primary decks, shrinkage in the new bridge, and closure pour shrinkage and cracking.

6 Conclusion & Recommendations

6.1 Conclusion

The main goal of this thesis was to evaluate analytically and numerically if *SHCC* could be used as a closure pour to reduce the construction time of widening a bridge. The goal was to reduce the time between the completion of the new bridge and casting the closure pour from 6-9 months to 2 months. The fact that the structure is totally restrained establishes the main problem of widening a bridge due to the new *SHCC* and the new concrete necessity to creep and shrinkage and the old bridge to be stationary.

The longitudinal stress calculations at the mid-span for the bridge widening project can be done both analytically and numerically. Although the analytical method is reliable, the numerical approach is considered more cautious as it yields higher tension outcomes. For the bridge widening project, stress calculations at the mid-span can be achieved using both analytical and numerical methods. While the analytical approach is dependable, the numerical technique is deemed more prudent as it generates slightly higher tension outcomes. As the project advances, it would be advantageous to integrate a numerical model. This model can furnish more accurate results and facilitate the assessment of shrinkage force transfer from the new bridge and closure pour to the old bridge at distinct angles. Ultimately, engineers and designers should choose the path that best suits their specific needs and goals, recognizing that both analytical and numerical methods have their strengths and weaknesses. In conclusion, these findings emphasize the importance of selecting the appropriate method and ensuring that calculations are accurate and precise to obtain reliable results.

Reinforced concrete is a commonly used material for closure pour in the Netherlands, owing to its established qualities, cost-effectiveness, and durability. However, it is essential to note that the $C40/50$ concrete variant used in this thesis experiences cracking since its tension stress exceeds $3.5MPa$ before cracking. This cracking necessitates the application of reinforcements to maintain a crack width of $0.20mm$. To achieve this, two layers of nine $32mm$ diameter bars in each layer are required, which is a significant amount of reinforcement, particularly for a one-meter-wide closure pour. Ultimately, when compared to concrete, *SHCC* proves to be a superior option as it performs without the need for reinforcements.

6.1.1 Sub-Research Question

What is the analytical calculation method for determining the stresses that arise from bridge widening based on the imposed deformation, and can this method be validated using numerical models?

For the thesis, a composite structure mechanics approach was employed, with the use of imposed deformation as the methodology. An advanced version of the original "Pink Book" method was developed and can be found in Section 3.1.1. Through analytical calculations, the longitudinal stresses at the mid-span of a widening bridge were determined, as showcased in Section 4.1. As discussed in Section 5.1, the numerical model, explained in Section 3.5, affirmed the results of the analytical calculations, particularly at the mid-span of the numerical calculations. The *FEA* model adopted a more conservative approach, leading to higher tension stresses. It was previously assumed that the maximum stress value occurred at the midpoint of the span, but this assertion has since been disproven.

Is it possible to determine if SHCC would be a suitable and durable replacement for concrete in terms of handling the stresses caused by imposed deformation?

Based on the research outlined in Chapter 2 and the findings detailed in Chapter 4, it has been established that *SHCC* is capable of withstanding all in-plane loads considered in this study across a variety of materials. These results mean that *SHCC* can effectively address issues like creep in the main decks, shrinkage in the new bridge, and closure pour shrinkage and cracking. Furthermore, *SHCC* is a more elastic material which prevents issues of compatibility, especially in the shear strains. Additionally, various authors have commented on the fact that *SHCC* generally exhibits crack widths below $0.10mm$, or even less, as noted in Section 3.1.2. These measurements fall well below the maximum crack width allowed by current standards, which is $0.20mm$, as evidenced in Section 2.1.3.3. Hence, the presence of cracks in *SHCC* is not a significant obstacle. It is important to note, however, that there is currently no research demonstrating that *SHCC* can maintain its durability for a century.

The figure presented in Figure 5.6 indicates the likelihood of cracking in *SHCC*. However, it is worth noting that this should not be a considerable concern for *SHCC* due to its exceptional crack-bridging fibers, strain-hardening property, and its crack width remaining below $0.10mm$. These unique qualities enable *SHCC* to endure cracking and maintain its structural integrity under various circumstances.

Based on the visual representation presented in Figure 5.6 and in Figure 5.7, it seems highly improbable for *SHCC* to encounter any failure. The stress and strain measurements are significantly distant from the ultimate tensile strength and strain of the material used. Even if the deformation of the material increased 35 times, *SHCC* would still be able to handle such deformations, as mentioned in Section 5.3.3. Thus, *SHCC* can serve as a dependable closure pour, successfully alleviating the shrinkage and creep stresses on both the old and new bridge, along with its self-shrinkage.

6.1.2 Main Research Question

Can the construction time needed for widening a prestressed concrete bridge be reduced by applying *SHCC* as a closure pour?

The main objective of the investigation was to discover a means of shortening the duration of bridge-widening endeavors from six months to a mere two months. The solution entailed implementing a specific form of concrete, referred to as *SHCC*, as a closure pour. The findings indicated that this innovative approach was effective in handling in-plane loads and alleviating common concerns such as creep, shrinkage, and cracking. By utilizing the *SHCC* closure pour method, construction time for bridge widening projects can be significantly reduced. Additionally, the material's stress and strain values are much lower than its ultimate strength, implying that it can maintain its integrity while minimizing construction periods.

Overall, this innovative construction method utilizing *SHCC* closure pour can be considered a safe, efficient, and reliable option for concrete bridge widening projects seeking to minimize construction time without compromising on quality and safety.

6.2 Recommendations

The following recommendations are worth considering for future research endeavors.

- It is important to investigate the impact of repeated freezing and thawing on the tensile stress versus strain curves of *SHCC*. The purpose of this investigation is to enhance the performance of *SHCC* as a closure pour. Previous studies have identified freezing and thawing as a potential concern for this material, as noted in Section 2.1.3.2.
- The question of whether *SHCC* can withstand being used as a closure pour for 100 years has yet to be fully resolved. It is a matter that requires further investigation and exploration in order to guarantee that it will perform optimally.

- Conducting a thorough analytical calculation is crucial when examining the issue of shear stress arising from longitudinal stresses resulting from shrinkage and creep. It is imperative to carefully investigate this matter in order to address and mitigate any potential complications properly.

References

[1] *Rijkswaterstaat - Bridges*. https://www.rijkswaterstaat.nl/wegen/wegbeheer/bruggen. Accessed: 2022-08-11.

[2] *Online Bezoekerscentrum Weguitbreiding Schiphol-Amsterdam-Almere (SAA) Kernel Description*. https://bezoekerscentrum.rijkswaterstaat.nl/SchipholAmsterdamAlmere/. Accessed: 2022-08-03.

[3] Vincent T. H. CHU. *A Self-Learning Manual Mastering Different Fields of Civil Engineering Works (VC-Q&A Method)*. 2010.

[4] J.C. Walraven and C.R. Braam. *Prestressed concrete*. Technische Universiteit Delft, Faculteit der Civiele Techniek, Vakgroep, 2019.

[5] *National Annex to NEN-EN 1992-1-1+C2 Eurocode 2: Design of concrete structures - Part 1-1: General rules and rules for buildings*. European Committee Standardization. 2020.

[6] Bing Tu et al. "Time-variant reliability analysis of widened deteriorating prestressed concrete bridges considering shrinkage and creep". In: *Engineering Structures* 153 (Dec. 2017), pp. 1–16. ISSN: 0141-0296. DOI: 10.1016/J.ENGSTRUCT.2017.09.060.

[7] *Guide for Widening Highway Bridges*. American Concrete Institute. 2013.

[8] *MEMO TO DESIGNERs - 9-3 WIDENING EXISTING BRIDGES*. Caltrans. 2010.

[9] A. Vosogh, A. Sadeghian, and M. Hassan. "Design Challenges of the Widening of an Existing Bridge with Post-tensioned Concrete Deck". In: *Lecture Notes in Civil Engineering* 244 (2022), pp. 135–146. ISSN: 23662565. DOI: 10.1007/978-981-19-0656-5{_}12/FIGURES/15. URL: https://link.springer.com/chapter/10.1007/978-981-19-0656-5_12.

[10] Qing Jie Wen. "Long-term effect analysis of prestressed concrete box-girder bridge widening". In: *Construction and Building Materials* 25.4 (Apr. 2011), pp. 1580–1586. ISSN: 0950-0618. DOI: 10.1016/J.CONBUILDMAT.2010.09.041.

[11] *Drafting and Design Presentation Standards Volume 3: Structural Drafting Standards: Chapter 8: Bridge Widening*. The State of Queensland (Department of Transport and Main Roads). 2019.

[12] Y. H. Chai and H. J. Hung. "Waiting Period for Closure Pours in Bridge Widening or Staged Construction". In: *Journal of Bridge Engineering* 21.5 (May 2016), p. 04016006. ISSN: 1084-0702. DOI: 10.1061/(ASCE)BE.1943-5592.0000875/ASSET/0EB56A9B-2A2B-4CAE-A322-8C057C1EB294/ASSETS/IMAGES/LARGE/FIGURE13.JPG. URL: https://ascelibrary.org/doi/abs/10.1061/%28ASCE%29BE.1943-5592.0000875https://ascelibrary.org/doi/10.1061/%28ASCE%29BE.1943-5592.0000875.

[13] Michael M. Sprinkel et al. "Failure and repair of deck closure pour on interstate 81". In: *Transportation Research Record* 2150 (Jan. 2010), pp. 119–128. ISSN: 03611981. DOI: 10.3141/2150-15.

[14] Adam M. Neville and J. J. Brooks. "Concrete technology". In: (2010), p. 442.

[15] Hyun Do Yun. "Effect of accelerated freeze–thaw cycling on mechanical properties of hybrid PVA and PE fiber-reinforced strain-hardening cement-based composites (SHCCs)". In: *Composites Part B: Engineering* 52 (Sept. 2013), pp. 11–20. ISSN: 1359-8368. DOI: 10.1016/J.COMPOSITESB.2013.03.021.

[16] Hyun Do Yun et al. "Tensile behavior of synthetic fiber-reinforced strain-hardening cement-based composite (SHCC) after freezing and thawing exposure". In: *Cold Regions Science and Technology* 67.1-2 (June 2011), pp. 49–57. ISSN: 0165-232X. DOI: 10.1016/J.COLDREGIONS.2011.02.002.

[17] *Eurocode 2: Design of concrete structures - Part 1-1 : General rules and rules for buildings*. European Committee Standardization. 2004.

[18] *Richtlijnen Ontwerp Kunstwerken Versie 2.0*. Rijkswaterstaat. 2021.

[19] Seung Gyu Kim, Yeong Seong Park, and Yong Hak Lee. "Comparison of Concrete Creep in Compression, Tension, and Bending under Drying Condition". In: *Materials* 12.20 (Oct. 2019). ISSN: 19961944. DOI: 10.3390/MA12203357. URL: /pmc/articles/PMC6829212//pmc/articles/PMC6829212/?report=abstracthttps://www.ncbi.nlm.nih.gov/pmc/articles/PMC6829212/.

[20] J.C. Walraven et al. *Concrete Structures under Temperature and Shrinkage Deformations – Theory and Practice*. Technische Universiteit Delft, Faculteit der Civiele Techniek, Vakgroep, 2016.

[21] P.K. Mehta and Paulo J. M. Monteiro. *Concrete: Microstructure, Properties, and Materials*. Third. New York: McGraw-Hill, 2001. ISBN: 0071462899.

[22] Yongzhen Li et al. *Predicting of the Stiffness of Cracked Reinforced Concrete Structures*. 2010.

[23] Gideon P.A.G. Van Zijl et al. "Durability of strain-hardening cement-based composites (SHCC)". In: *Materials and Structures/Materiaux et Constructions* 45.10 (Oct. 2012), pp. 1447–1463. ISSN: 13595997. DOI: 10.1617/S11527-012-9845-Y/FIGURES/9. URL: https://link.springer.com/article/10.1617/s11527-012-9845-y.

[24] Jelle Bezemer. "The Effect of Height Scaling on the Flexural Crack Width Controlling Behavior of Hybrid R/SHCC Beams: A Numerical and Experimental study". PhD thesis. 2022. URL: https://repository.tudelft.nl/islandora/object/uuid%3A0288df65-0cf5-4a3c-bc65-d7e2ff3d4719.

[25] M. Lukovic. "Influence of interface and strain hardening cementitious composite (SHCC) properties on the performance of concrete repairs". PhD thesis. 2016. DOI: 10.4233/UUID:28B07D9B-C704-47FA-9BA3-CD9FDE10130A. URL: https://repository.tudelft.nl/islandora/object/uuid%3A28b07d9b-c704-47fa-9ba3-cd9fde10130a.

[26] Victor C. Li. "Engineered Cementitious Composites (ECC) Material, Structural, and Durability Performance". In: (2008). URL: http://deepblue.lib.umich.edu/handle/2027.42/84661.

[27] Victor C. Li. "From Micromechanics to Structural Engineering - the Design of Cementitous Composites for Civil Engineering Applications". In: (1993). URL: http://deepblue.lib.umich.edu/handle/2027.42/84735.

[28] Mo Li, M. Sahmaran, and Victor C. Li. "Effect of Cracking and Healing on Durability of Engineered Cementitious Composites Under Marine Environment". In: (2007). URL: http://deepblue.lib.umich.edu/handle/2027.42/84776.

[29] *208-HFC : High performance fibre reinforced cementitious composites*. URL: https://www.rilem.net/groupe/208-hfc-high-performance-fibre-reinforced-cementitious-composites-216.

[30] R K Tai. "Upscaling of Strain-Hardening Cementitious Composites". PhD thesis. 2015. URL: https://repository.tudelft.nl/islandora/object/uuid%3Aa0d63c1a-dbcf-4141-bb8a-6c7ac1063eed.

[31] Chang Wu, Christopher K.Y. Leung, and Victor C. Li. "Derivation of crack bridging stresses in engineered cementitious composites under combined opening and shear displacements". In: *Cement and Concrete Research* 107 (May 2018), pp. 253–263. ISSN: 0008-8846. DOI: 10.1016/J.CEMCONRES.2018.02.027.

[32] Penggang Wang et al. "Research on Bonding and Shrinkage Properties of SHCC-Repaired Concrete Beams". In: *Materials (Basel, Switzerland)* 13.7 (Apr. 2020). ISSN: 1996-1944. DOI: 10.3390/MA13071757. URL: https://pubmed.ncbi.nlm.nih.gov/32283740/.

[33] Giovanni Martinola, Martin F. Baeuml, and Folker H. Wittmann. "Modified ECC by means of internal impregnation". In: *Journal of Advanced Concrete Technology* 2.2 (2004), pp. 207–212. ISSN: 13468014. DOI: 10.3151/JACT.2.207.

[34] Bartosz Budnik. *Shear capacity of innovative hybrid concrete structures with SHCC lamellas applied laterally*. 2023. URL: https://repository.tudelft.nl/islandora/object/uuid%3Ad50e6a6c-e5ff-41c9-8a4d-3fdd4899c5cf.

[35] Jun Zhang et al. “Engineered cementitious composite with characteristic of low drying shrinkage”. In: *Cement and Concrete Research* 39.4 (Apr. 2009), pp. 303–312. ISSN: 0008-8846. DOI: 10.1016/J.CEMCONRES.2008.11.012.

[36] Martin B. WEIMANN and Victor C. LI. “DRYING SHRINKAGE AND CRACK WIDTH OF ENGINEERED CEMENTITIOUS COMPOSITES (ECC)”. In: *Brittle Matrix Composites 7* (Jan. 2003), pp. 37–46. DOI: 10.1533/9780857093103.37.

[37] Dirk Jacobus, Adriaan De Jager, and G P A G Van Zijl. “Assessment of SHCC overlay retrofitting of unreinforced load bearing masonry for seismic resistance”. PhD thesis. 2018. URL: http://hdl.handle.net/10019.1/104946.

[38] Gideon P.A.G. van Zijl and Dirk J.A. de Jager. “Improved ductility of SHCC retrofitted unreinforced load bearing masonry via a strip-debonded approach”. In: *Journal of Building Engineering* 24 (July 2019), p. 100722. ISSN: 2352-7102. DOI: 10.1016/J.JOBE.2019.02.014.

[39] Othman Harrass. “Interfacial behavior of hybrid SHCC-Concrete beams with a joint at midspan”. PhD thesis. 2020. URL: https://repository.tudelft.nl/islandora/object/uuid%3Af5b2c7f1-fc84-459b-8a61-3eb3bc43254e.

[40] Shantanu Singh. “Influence of Interface and Type of Strain Hardening Cementitious Composite (SHCC) on Crack Control in SHCC-Concrete Hybrid Beams”. PhD thesis. 2019. URL: https://repository.tudelft.nl/islandora/object/uuid%3A5d59fd89-6ec4-405e-9fda-b247f1ae8789.

[41] H.W. Reinhardt. “Imposed deformation and cracking”. In: *IABSE reports = Rapports AIPC = IVBH Berichte* (1991). DOI: 10.5169/seals-47626. URL: https://doi.org/10.5169/seals-47626.

[42] *DIANA User’s Manuals*. URL: https://manuals.dianafea.com/d107/en/index-en.html.

[43] Movares Nederland B.V. ir. Q.C. de Rijke. *Kenmerk KW-QCR-060029573 - Versie 1.0*. Hoofdafdeling Droge Infrastructuur, afdeling Bruggenbouw. Rijkswaterstaat Bouwdienst, 2006.

A

Appendix A: New Bridge Shrinkage

To calculate the shrinkage effect of the new bridge, it was calculated the shrinkage of the new bridge at two, four, and six months, and at 100 years and then calculate the stresses caused by the shrinkage due to the difference with 100 years since that is the durability that needs to be guarantee. The value of infinity was added as an extra value.

A.1 Shrinkage at 2 months

Some values were necessary from table F.2, which are:

$$A = 14.22m^2$$
$$u(perimeter) = 15.8 \times 2 + 0.90 \times 2 = 33.4m$$

Also, it was calculated h_0, which is the notional size (mm) of the cross-section, which is defined at 3.1.4(6) of NEN-EN 1992-1-1[17], to then find k_h, coefficient depending on the notional size.

$$h_0 = \frac{2 \times A}{u} = \frac{2 \times 14.22}{33.4} = 0.851m = 851mm \tag{A.1}$$

Since h_0 is bigger than 500, according to table 3.3 of NEN-EN 1992-1-1[17], the value for k_h should be 0.70.

Knowing that the f_{ck} is 50MPa, from table 1 and that formula for the f_{cm} is the following:

$$f_{cm}(t) = f_{ck}(t) + 8 = 50 + 8 = 58MPa \tag{A.2}$$

A.1.1 Drying Shrinkage

Annex B.2 of NEN-EN 1992-1-1[17] determined the drying shrinkage.

$$RH_0 = 100\%$$
$$\beta_{RH} = 1.55 \times [1 - (\frac{RH}{RH_0})^3] = 1.55 \times [1 - (\frac{0.8}{1})^3] = 0.76 \tag{A.3}$$

$$\alpha_{ds1} = 4 \text{(for class N)}$$
$$\alpha_{ds2} = 0.12 \text{(for class N)}$$
$$f_{cm0} = 10MPa$$

$$\varepsilon_{cd,0} = 0.85 \times [(220 + 110 \times \alpha_{ds1}) \times e^{-\alpha_{ds2} \times \frac{f_{cm}}{f_{cm0}}}] \times 10^{-6} \times \beta_{RH} \tag{A.4}$$
$$\varepsilon_{cd,0} = 0.85 \times [(220 + 110 \times 4) \times e^{-0.12 \times \frac{58}{10}}] \times 10^{-6} \times 0.76$$
$$\varepsilon_{cd,0} = 0.21 \times 10^{-3}$$

Also the item 3.1.4(6) of NEN-EN 1992-1-1[17]. Given that t_s is two days and t is sixty days, it was calculated:

$$\beta_{ds}(t,t_s) = \frac{(t-t_s)}{(t-t_s)+0.04\sqrt{h_0^3}} \tag{A.5}$$
$$\beta_{ds}(t,t_s) = \frac{(60-2)}{(60-2)+0.04\sqrt{851^3}}$$
$$\beta_{ds}(t,t_s) = 5.52\times10^{-2}$$

$$\varepsilon_{cd}(t) = \beta_{ds}(t,t_s)\times k_h\times\varepsilon_{cd,0} \tag{A.6}$$
$$\varepsilon_{cd}(t) = 5.52\times10^{-2}\times0.7\times0.21\times10^{-3}$$
$$\varepsilon_{cd}(t) = 8.17\times10^{-6}$$

A.1.2 Autogenous Shrinkage

The item 3.1.4(6) of NEN-EN 1992-1-1[17] was used again for the autogenous shrinkage.

$$\varepsilon_{ca}(t) = 2.5\times(f_{ck}-10)\times10^{-6} = 2.5\times(50-10)\times10^{-6} = 1\times10^{-4} \tag{A.7}$$

$$\beta_{as}(t) = 1-e^{-0.2\times t^{0.5}} \tag{A.8}$$
$$\beta_{as}(t) = 1-e^{-0.2\times60^{0.5}} = 0.788$$

$$\varepsilon_{ca}(t) = \beta_{as}(t)\times\varepsilon_{ca}(t) \tag{A.9}$$
$$\varepsilon_{ca}(t) = 0.788\times10^{-4} \tag{A.10}$$

A.1.3 Final Shrinkage

The final shrinkage, $\varepsilon_{cs}(t)$ again follow from the item 3.1.4(6).

$$\varepsilon_{cs}(t) = \varepsilon_{cd}(t)+\varepsilon_{ca}(t) \tag{A.11}$$
$$\varepsilon_{cs}(t) = 8.17\times10^{-6}+0.788\times10^{-4} = 8.69\times10^{-5}$$
$$\varepsilon_{cs}(t) = 0.0869\times10^{-3}$$

A.2 Shrinkage at 4 months

A.2.1 Drying Shrinkage

Annex B.2 of NEN-EN 1992-1-1[17] determined the drying shrinkage.

$$RH_0 = 100\%$$

$$\beta_{RH} = 1.55\times[1-(\frac{RH}{RH_0})^3] = 1.55\times[1-(\frac{0.8}{1})^3] = 0.76 \tag{A.12}$$

$\alpha_{ds1} = 4$(for class N)

$\alpha_{ds2} = 0.12$(for class N)

$f_{cm0} = 10MPa$

$$\varepsilon_{cd,0} = 0.85 \times [(220 + 110 \times \alpha_{ds1}) \times e^{-\alpha_{ds2} \times \frac{f_{cm}}{f_{cm0}}}] \times 10^{-6} \times \beta_{RH} \tag{A.13}$$
$$\varepsilon_{cd,0} = 0.85 \times [(220 + 110 \times 4) \times e^{-0.12 \times \frac{58}{10}}] \times 10^{-6} \times 0.76$$
$$\varepsilon_{cd,0} = 0.21 \times 10^{-3}$$

Also the item 3.1.4(6) of NEN-EN 1992-1-1[17]. Given that t_s is two days and t is 120 days, it was calculated:

$$\beta_{ds}(t, t_s) = \frac{(t - t_s)}{(t - t_s) + 0.04\sqrt{h_0^3}} \tag{A.14}$$
$$\beta_{ds}(t, t_s) = \frac{(120 - 2)}{(120 - 2) + 0.04\sqrt{851^3}}$$
$$\beta_{ds}(t, t_s) = 10.6 \times 10^{-2}$$

$$\varepsilon_{cd}(t) = \beta_{ds}(t, t_s) \times k_h \times \varepsilon_{cd,0} \tag{A.15}$$
$$\varepsilon_{cd}(t) = 10.6 \times 10^{-2} \times 0.7 \times 0.21 \times 10^{-3}$$
$$\varepsilon_{cd}(t) = 15.7 \times 10^{-6}$$

A.2.2 Autogenous Shrinkage

The item 3.1.4(6) of NEN-EN 1992-1-1[17] was used once more for the autogenous shrinkage.

$$\varepsilon_{ca}(t) = 2.5 \times (f_{ck} - 10) \times 10^{-6} = 2.5 \times (50 - 10) \times 10^{-6} = 1 \times 10^{-4} \tag{A.16}$$

$$\beta_{as}(t) = 1 - e^{-0.2 \times t^{0.5}} \tag{A.17}$$
$$\beta_{as}(t) = 1 - e^{-0.2 \times 120^{0.5}} = 0.888$$

$$\varepsilon_{ca}(t) = \beta_{as}(t) \times \varepsilon_{ca}(t) \tag{A.18}$$
$$\varepsilon_{ca}(t) = 0.888 \times 10^{-4} \tag{A.19}$$

A.2.3 Final Shrinkage

The final shrinkage, $\varepsilon_{cs}(t)$ again follow from the item 3.1.4(6).

$$\varepsilon_{cs}(t) = \varepsilon_{cd}(t) + \varepsilon_{ca}(t) \tag{A.20}$$
$$\varepsilon_{cs}(t) = 15.7 \times 10^{-6} + 0.888 \times 10^{-4} = 1.05 \times 10^{-4}$$
$$\varepsilon_{cs}(t) = 0.105 \times 10^{-3}$$

A.3 Shrinkage at 6 months

A.3.1 Drying Shrinkage

Annex B.2 of NEN-EN 1992-1-1[17] determined the drying shrinkage.

$$RH_0 = 100\%$$

$$\beta_{RH} = 1.55 \times [1 - (\frac{RH}{RH_0})^3] = 1.55 \times [1 - (\frac{0.8}{1})^3] = 0.76 \tag{A.21}$$

$$\alpha_{ds1} = 4\text{(for class N)}$$
$$\alpha_{ds2} = 0.12\text{(for class N)}$$
$$f_{cm0} = 10MPa$$

$$\varepsilon_{cd,0} = 0.85 \times [(220 + 110 \times \alpha_{ds1}) \times e^{-\alpha_{ds2} \times \frac{f_{cm}}{f_{cm0}}}] \times 10^{-6} \times \beta_{RH} \tag{A.22}$$
$$\varepsilon_{cd,0} = 0.85 \times [(220 + 110 \times 4) \times e^{-0.12 \times \frac{58}{10}}] \times 10^{-6} \times 0.76$$
$$\varepsilon_{cd,0} = 0.21 \times 10^{-3}$$

Also the item 3.1.4(6) of NEN-EN 1992-1-1[17]. Given that t_s is two days and t is 180 days, it was calculated:

$$\beta_{ds}(t, t_s) = \frac{(t - t_s)}{(t - t_s) + 0.04\sqrt{h_0^3}} \tag{A.23}$$
$$\beta_{ds}(t, t_s) = \frac{(180 - 2)}{(180 - 2) + 0.04\sqrt{851^3}}$$
$$\beta_{ds}(t, t_s) = 15.2 \times 10^{-2}$$

$$\varepsilon_{cd}(t) = \beta_{ds}(t, t_s) \times k_h \times \varepsilon_{cd,0} \tag{A.24}$$
$$\varepsilon_{cd}(t) = 15.2 \times 10^{-2} \times 0.7 \times 0.21 \times 10^{-3}$$
$$\varepsilon_{cd}(t) = 22.5 \times 10^{-6}$$

A.3.2 Autogenous Shrinkage

The item 3.1.4(6) of NEN-EN 1992-1-1[17] was used once more for the autogenous shrinkage.

$$\varepsilon_{ca}(t) = 2.5 \times (f_{ck} - 10) \times 10^{-6} = 2.5 \times (50 - 10) \times 10^{-6} = 1 \times 10^{-4} \tag{A.25}$$

$$\beta_{as}(t) = 1 - e^{-0.2 \times t^{0.5}} \tag{A.26}$$
$$\beta_{as}(t) = 1 - e^{-0.2 \times 180^{0.5}} = 0.932$$

$$\varepsilon_{ca}(t) = \beta_{as}(t) \times \varepsilon_{ca}(t) \tag{A.27}$$
$$\varepsilon_{ca}(t) = 0.932 \times 10^{-4} \tag{A.28}$$

A.3.3 Final Shrinkage

The final shrinkage, $\varepsilon_{cs}(t)$ again follow from the item 3.1.4(6).

$$\varepsilon_{cs}(t) = \varepsilon_{cd}(t) + \varepsilon_{ca}(t) \tag{A.29}$$
$$\varepsilon_{cs}(t) = 22.5 \times 10^{-6} + 0.932 \times 10^{-4} = 1.16 \times 10^{-4}$$
$$\varepsilon_{cs}(t) = 0.116 \times 10^{-3}$$

A.4 Shrinkage at 100 years

A.4.1 Drying Shrinkage

Annex B.2 of NEN-EN 1992-1-1[17] was used to determine the drying shrinkage.

$$RH_0 = 100\%$$

$$\beta_{RH} = 1.55 \times [1 - (\frac{RH}{RH_0})^3] = 1.55 \times [1 - (\frac{0.8}{1})^3] = 0.76 \tag{A.30}$$

$$\alpha_{ds1} = 4 \text{(for class N)}$$
$$\alpha_{ds2} = 0.12 \text{(for class N)}$$
$$f_{cm0} = 10MPa$$

$$\varepsilon_{cd,0} = 0.85 \times [(220 + 110 \times \alpha_{ds1}) \times e^{-\alpha_{ds2} \times \frac{f_{cm}}{f_{cm0}}}] \times 10^{-6} \times \beta_{RH} \tag{A.31}$$
$$\varepsilon_{cd,0} = 0.85 \times [(220 + 110 \times 4) \times e^{-0.12 \times \frac{58}{10}}] \times 10^{-6} \times 0.76$$
$$\varepsilon_{cd,0} = 0.21 \times 10^{-3}$$

Also the item 3.1.4(6) of NEN-EN 1992-1-1[17]. Given that t_s is two days and t is 100 years (36500 days), it was calculated:

$$\beta_{ds}(t, t_s) = \frac{(t - t_s)}{(t - t_s) + 0.04\sqrt{h_0^3}} \tag{A.32}$$
$$\beta_{ds}(t, t_s) = \frac{(36500 - 2)}{(36500 - 2) + 0.04\sqrt{851^3}}$$
$$\beta_{ds}(t, t_s) = 9.74 \times 10^{-1}$$

$$\varepsilon_{cd}(t) = \beta_{ds}(t, t_s) \times k_h \times \varepsilon_{cd,0} \tag{A.33}$$
$$\varepsilon_{cd}(t) = 9.74 \times 10^{-1} \times 0.7 \times 0.21 \times 10^{-3}$$
$$\varepsilon_{cd}(t) = 144 \times 10^{-6}$$

A.4.2 Autogenous Shrinkage

The item 3.1.4(6) of NEN-EN 1992-1-1[17] was used once more for the autogenous shrinkage.

$$\varepsilon_{ca}(t) = 2.5 \times (f_{ck} - 10) \times 10^{-6} = 2.5 \times (50 - 10) \times 10^{-6} = 1 \times 10^{-4} \tag{A.34}$$

$$\beta_{as}(t) = 1 - e^{-0.2 \times t^{0.5}} \tag{A.35}$$
$$\beta_{as}(t) = 1 - e^{-0.2 \times 36500^{0.5}} = 1.00$$

$$\varepsilon_{ca}(t) = \beta_{as}(t) \times \varepsilon_{ca}(t) \tag{A.36}$$
$$\varepsilon_{ca}(t) = 1.00 \times 10^{-4} \tag{A.37}$$

A.4.3 Final Shrinkage

The final shrinkage, $\varepsilon_{new}(t)$ again follow from the item 3.1.4(6).

$$\varepsilon_{new}(t) = \varepsilon_{cd}(t) + \varepsilon_{ca}(t) \tag{A.38}$$
$$\varepsilon_{new}(t) = 144 \times 10^{-6} + 1.00 \times 10^{-4} = 2.44 \times 10^{-4}$$
$$\varepsilon_{new}(t) = 0.244 \times 10^{-3}$$

A.5 Summary Of New Bridge's Shrinkage

The values of the second column of table A.1 were taken from section appendices A.1.3, A.2.3, A.3.3 and A.4.3, with these values, the third column was calculated.

Time	$\varepsilon_{new}(t,2)$	$\varepsilon_{new}(100years,2)-\varepsilon_{new}(t,2)$
2 months	8.69×10^{-5}	1.57×10^{-4}
4 months	1.05×10^{-4}	1.39×10^{-4}
6 months	1.16×10^{-4}	1.28×10^{-4}
100 years	2.44×10^{-4}	

Table A.1: Shrinkage of the new bridge at different times.

B

Appendix B: Concrete Closure Pour Shrinkage

In this Appendix, it was calculated the shrinkage of the concrete closure pour. Thus, following the same procedure from section A.4, the shrinkage will be calculated only at 100 years since the difference of shrinkage of 99.5 years or 100 years is minimal and irrelevant.

B.1 Shrinkage at 100 years

Some values were necessary from table F.2, which are:

$$A = 0.90m^2$$
$$u(perimeter) = 1 \times 2 = 2m$$

Also, it was calculated h_0, which is the notional size (mm) of the cross-section, which is defined at 3.1.4(6) of NEN-EN 1992-1-1[17], to then find k_h, coefficient depending on the notional size.

$$h_0 = \frac{2 \times A}{u} = \frac{2 \times 0.90}{2} = 0.900m = 900mm \quad \text{(B.1)}$$

Since h_0 is bigger than 500, according to table 3.3 of NEN-EN 1992-1-1[17], the value for k_h should be 0.70.

Knowing that the f_{ck} is 40MPa, from Table F.1 since the closure pour is made of a C40/50 concrete and that formula for the f_{cm} is the following:

$$f_{cm}(t) = f_{ck}(t) + 8 = 40 + 8 = 48MPa \quad \text{(B.2)}$$

B.1.1 Drying Shrinkage

Annex B.2 of NEN-EN 1992-1-1[17] determined the drying shrinkage.

$$RH_0 = 100\%$$
$$\beta_{RH} = 1.55 \times [1 - (\frac{RH}{RH_0})^3] = 1.55 \times [1 - (\frac{0.8}{1})^3] = 0.76 \quad \text{(B.3)}$$

$$\alpha_{ds1} = 4 \text{(for class N)}$$

$$\alpha_{ds2} = 0.12 \text{(for class N)}$$

$$f_{cm0} = 10MPa$$

$$\varepsilon_{cd,0} = 0.85 \times [(220 + 110 \times \alpha_{ds1}) \times e^{-\alpha_{ds2} \times \frac{f_{cm}}{f_{cm0}}}] \times 10^{-6} \times \beta_{RH} \tag{B.4}$$
$$\varepsilon_{cd,0} = 0.85 \times [(220 + 110 \times 4) \times e^{-0.12 \times \frac{48}{10}}] \times 10^{-6} \times 0.76$$
$$\varepsilon_{cd,0} = 0.24 \times 10^{-3}$$

Also the item 3.1.4(6) of NEN-EN 1992-1-1[17]. Given that t_s is two days and t is 100 years, which is equal to 36500 days, it was calculated:

$$\beta_{ds}(t, t_s) = \frac{(t - t_s)}{(t - t_s) + 0.04\sqrt{h_0^3}} \tag{B.5}$$
$$\beta_{ds}(t, t_s) = \frac{(36500 - 2)}{(36500 - 2) + 0.04\sqrt{900^3}}$$
$$\beta_{ds}(t, t_s) = 0.97$$

$$\varepsilon_{cd}(t) = \beta_{ds}(t, t_s) \times k_h \times \varepsilon_{cd,0} \tag{B.6}$$
$$\varepsilon_{cd}(t) = 0.97 \times 0.70 \times 0.24 \times 10^{-3}$$
$$\varepsilon_{cd}(t) = 0.162 \times 10^{-3}$$

B.1.2 Autogenous Shrinkage

Item 3.1.4(6) of NEN-EN 1992-1-1[17] was used once more for the autogenous shrinkage.

$$\varepsilon_{ca}(t) = 2.5 \times (f_{ck} - 10) \times 10^{-6} = 2.5 \times (40 - 10) \times 10^{-6} = 0.75 \times 10^{-4} \tag{B.7}$$

$$\beta_{as}(t) = 1 - e^{-0.2 \times t^{0.5}} \tag{B.8}$$
$$\beta_{as}(t) = 1 - e^{-0.2 \times 36500^{0.5}} = 1$$

$$\varepsilon_{ca}(t) = \beta_{as}(t) \times \varepsilon_{ca}(t) \tag{B.9}$$
$$\varepsilon_{ca}(t) = 1 \times 0.75 \times 10^{-4} = 0.75 \times 10^{-4} \tag{B.10}$$

B.1.3 Final Shrinkage

The final shrinkage, $\varepsilon_{cs}(t)$ again follow from the item 3.1.4(6).

$$\varepsilon_{cs}(t) = \varepsilon_{cd}(t) + \varepsilon_{ca}(t) \tag{B.11}$$
$$\varepsilon_{cs}(t) = 0.162 \times 10^{-3} + 0.75 \times 10^{-4} = 2.37 \times 10^{-4}$$
$$\varepsilon_{cs}(t) = 2.37 \times 10^{-4}$$

B.2 Shrinkage of the concrete closure pour

Time	Shrinkage Strain
100 years	2.37×10^{-4}

Table B.1: Shrinkage of the closure pour at different times.

C

Appendix C: Creep Calculations

C.1 Old Bridge

For the old bridge, the same procedure was done following the steps of the new bridge at Section C.2. The calculations are shown below.

Knowing that the f_{ck} is $37MPa$, from Table F.1 since the closure pour is made of a C40/50 concrete and that formula for the f_{cm} is the following:

$$f_{cm}(t) = f_{ck}(t) + 8 = 37 + 8 = 45MPa \tag{C.1}$$

Following the formulas of Annex B.1(1) of NEN-EN 1992-1-[17], the creep was calculated, and the alphas were found, the f_{cm} was taken from Equation C.1.

$$\alpha_1 = [\frac{35}{f_{cm}}]^{0.7} = [\frac{35}{45}]^{0.7} = 0.84 \tag{C.2}$$

$$\alpha_2 = [\frac{35}{f_{cm}}]^{0.2} = [\frac{35}{45}]^{0.2} = 0.95 \tag{C.3}$$

$$\alpha_3 = [\frac{35}{f_{cm}}]^{0.5} = [\frac{35}{45}]^{0.5} = 0.88 \tag{C.4}$$

Also, it was calculated h_0, which is the notional size (mm) of the cross-section, which is defined at 3.1.4(6) of NEN-EN 1992-1-1[17], to then find k_h, coefficient depending on the notional size.

$$h_0 = \frac{2 \times A}{u} = \frac{2 \times 14.68}{34.42} = 0.853m = 853mm \tag{C.5}$$

For the calculation, h_0 was taken from Equation C.5 and φ_{RH} was used the following formula since $f_{cm} > 35MPa$.

$$\varphi_{RH} = [1 + \frac{1 - RH/100}{0.1 \times \sqrt[3]{h_0}} \times \alpha_1] \times \alpha_2 \tag{C.6}$$

$$\varphi_{RH} = [1 + \frac{1 - 80/100}{0.1 \times \sqrt[3]{853}} \times 0.84] \times 0.95 = 1.12$$

$$\beta(f_{cm}) = \frac{16.8}{\sqrt{f_{cm}}} = \frac{16.8}{\sqrt{45}} = 2.50 \tag{C.7}$$

$$t_0 = 3$$

$$\beta(t_0) = \beta(3) = \frac{1}{(0.1 + t_0^{0.2})} = \frac{1}{(0.1 + 3^{0.2})} = 0.74 \tag{C.8}$$

$$\varphi_0 = \varphi_{RH} \times \beta(f_{cm}) \times \beta(t_0) \tag{C.9}$$
$$\varphi_0 = 1.12 \times 2.50 \times 0.74 = 2.08$$

$$\beta_H = 1.5 \times [1 + (0.012 \times RH)^{18}] \times h_0 + 250 \times \alpha_3 \leq 1500 \times \alpha_3 \tag{C.10}$$
$$\beta_H = 1.5 \times [1 + (0.012 \times 0.8)^{18}] \times 853 + 250 \times 0.88 \leq 1500 \times 0.88$$
$$\beta_H = 1499.9 \leq 1322.9 \Rightarrow \beta_H = 1322.9$$

C.1.1 Creep coefficient at 54 years

Calculating the creep for 54 years ($365 \times 54 = 19710$) (19710 days):

$$\beta_c(t, t_0) = [\frac{(t - t_0)}{(\beta_H + t - t_0)}]^{0.3} = [\frac{(19710 - 3)}{(1322.9 + 19710 - 3)}]^{0.3} = 0.98 \tag{C.11}$$

$$\varphi(t, t_0) = \varphi_0 \times \beta_c(t, t_0) \tag{C.12}$$
$$\varphi(19710, 3) = 2.08 \times 0.98 = 2.04$$

C.1.2 Creep coefficient at 100 years

Calculating the creep for 100 years ($365 \times 100 = 36500$) (36500 days):

$$\beta_c(t, t_0) = [\frac{(t - t_0)}{(\beta_H + t - t_0)}]^{0.3} = [\frac{(36500 - 3)}{(1322.9 + 36500 - 3)}]^{0.3} = 0.99 \tag{C.13}$$

$$\varphi(t, t_0) = \varphi_0 \times \beta_c(t, t_0) \tag{C.14}$$
$$\varphi(36500, 3) = 2.08 \times 0.99 = 2.06$$

C.1.3 Old bridge creep coefficient at different times and its Elastic Modulus modified

The data presented in the second column of table C.1 was gathered from various sections, namely sections appendices C.1.1 and C.1.2.

Time	Creep Coefficient (φ)
54 years	2.04
100 years	2.06

Table C.1: Creep Coefficient (φ) of the Old Bridge.

The values of 54 years and 100 years were utilized to determine the difference in creep between the two time periods, resulting in a value of $\varphi = 0.02$, as evident in Table C.1. In reference to chapter 6.3.3 from the "Blue Book"[4], equation C.15 was employed to compute the modified Young's Modulus via creep.

$$E_{old,creep} = \frac{E_{old}}{1 + \varphi} = \frac{31.5 \times 10^3}{1 + 0.02} = 30941 N/mm^2 \tag{C.15}$$

C.2 New Bridge

The majority of concrete creep values remain unaffected by the final age of the concrete. As a result, calculations were made and subsequently separated based on the final age of the concrete.

Following the formulas of Annex B.1(1) of NEN-EN 1992-1-[17], the creep was calculated, and the alphas were found, the f_{cm} was taken from Equation A.2

$$\alpha_1 = [\frac{35}{f_{cm}}]^{0.7} = [\frac{35}{58}]^{0.7} = 0.70 \tag{C.16}$$

$$\alpha_2 = [\frac{35}{f_{cm}}]^{0.2} = [\frac{35}{58}]^{0.2} = 0.90 \tag{C.17}$$

$$\alpha_3 = [\frac{35}{f_{cm}}]^{0.5} = [\frac{35}{58}]^{0.5} = 0.78 \tag{C.18}$$

For the calculation, h_0 was taken from equation A.1 and φ_{RH} was used the following formula since $f_{cm} > 35MPa$.

$$\varphi_{RH} = [1 + \frac{1 - RH/100}{0.1 \times \sqrt[3]{h_0}} \times \alpha_1] \times \alpha_2 \tag{C.19}$$
$$\varphi_{RH} = [1 + \frac{1 - 80/100}{0.1 \times \sqrt[3]{851}} \times 0.70] \times 0.90 = 1.04$$

$$\beta(f_{cm}) = \frac{16.8}{\sqrt{f_{cm}}} = \frac{16.8}{\sqrt{58}} = 2.21 \tag{C.20}$$

$$\beta(t_0) = \frac{1}{(0.1 + t_0^{0.2})} = \frac{1}{(0.1 + 3^{0.2})} = 0.74 \tag{C.21}$$

$$\varphi_0 = \varphi_{RH} \times \beta(f_{cm}) \times \beta(t_0) \tag{C.22}$$
$$\varphi_0 = 1.04 \times 2.21 \times 0.74 = 1.70$$

$$\beta_H = 1.5 \times [1 + (0.012 \times RH)^{18}] \times h_0 + 250 \times \alpha_3 \leq 1500 \times \alpha_3 \tag{C.23}$$
$$\beta_H = 1.5 \times [1 + (0.012 \times 0.8)^{18}] \times 851 + 250 \times 0.78 \leq 1500 \times 0.78$$
$$\beta_H = 1471.4 \leq 1165.2 \Rightarrow \beta_H = 1165.2$$

C.2.1 Creep coefficient at 2 months

Calculating the creep for two months (60 days):

$$\beta_c(t, t_0) = [\frac{(t - t_0)}{(\beta_H + t - t_0)}]^{0.3} = [\frac{(60 - 3)}{(1165.2 + 60 - 3)}]^{0.3} = 0.40 \tag{C.24}$$

$$\varphi(t, t_0) = \varphi_0 \times \beta_c(t, t_0) \tag{C.25}$$
$$\varphi(60, t_0) = 1.70 \times 0.40 = 0.68$$

C.2.2 Creep coefficient at 4 months

Calculating the creep for four months (120 days):

$$\beta_c(t, t_0) = [\frac{(t - t_0)}{(\beta_H + t - t_0)}]^{0.3} = [\frac{(120 - 3)}{(1165.2 + 120 - 3)}]^{0.3} = 0.49 \tag{C.26}$$

$$\varphi(t, t_0) = \varphi_0 \times \beta_c(t, t_0) \tag{C.27}$$
$$\varphi(120, t_0) = 1.70 \times 0.49 = 0.83$$

C.2.3 Creep coefficient at 6 months

Calculating the creep for six months (180 days):

$$\beta_c(t,t_0) = [\frac{(t-t_0)}{(\beta_H+t-t_0)}]^{0.3} = [\frac{(180-3)}{(1165.2+180-3)}]^{0.3} = 0.54 \tag{C.28}$$

$$\begin{gathered}\varphi(t,t_0) = \varphi_0 \times \beta_c(t,t_0) \\ \varphi(180,t_0) = 1.70 \times 0.54 = 0.93\end{gathered} \tag{C.29}$$

C.2.4 Creep coefficient at 100 years

Calculating the creep for 100 years ($365 \times 100 = 36500$) (36500 days):

$$\beta_c(t,t_0) = [\frac{(t-t_0)}{(\beta_H+t-t_0)}]^{0.3} = [\frac{(36500-3)}{(1165.2+36500-3)}]^{0.3} = 0.99 \tag{C.30}$$

$$\begin{gathered}\varphi(t,t_0) = \varphi_0 \times \beta_c(t,t_0) \\ \varphi(36500,t_0) = 1.70 \times 0.99 = 1.69\end{gathered} \tag{C.31}$$

C.2.5 New bridge creep coefficient at different times and its Elastic Modulus modified

The values of 2 months and 100 years were utilized to determine the difference in creep between the two time periods, resulting in a value of $\varphi = 1.00$, as evident in Table C.2. In reference to chapter 6.3.3 from the "Blue Book"[4], equation C.32 was employed to compute the modified Young's Modulus via creep.

$$E_{new,creep} = \frac{E_{new}}{1+\varphi} = \frac{37 \times 10^3}{1+1.00} = 18461N/mm^2 \tag{C.32}$$

The data presented in the second column of table C.2 was gathered from various sections, namely sections appendices C.2.1 to C.2.4. The figures in the third column were calculated by subtracting the value corresponding to 100 years from the relevant age. The fourth column was the value of the modified Young's Modulus by creep for the corresponding age such as calculated in Equation C.32.

Final age	$\varphi_{(t,3)}$	$\varphi_{(100,3)} - \varphi_{(t,3)}$	$E_{(100y)}$
2 months	0.68	1.00	18461
4 months	0.83	0.85	19972
6 months	0.93	0.76	21077
100 years	1.69	0.00	37000

Table C.2: Creep Coefficient (φ) of the New Bridge.

D

Appendix D: Calculations Of *SHCC* Cracked

According to Section 2.3.6, the stress-strain graphic is depicted in Figure 2.8 and Figure D.1 was used to calculate the new stress and strain for a cracked *SHCC*.

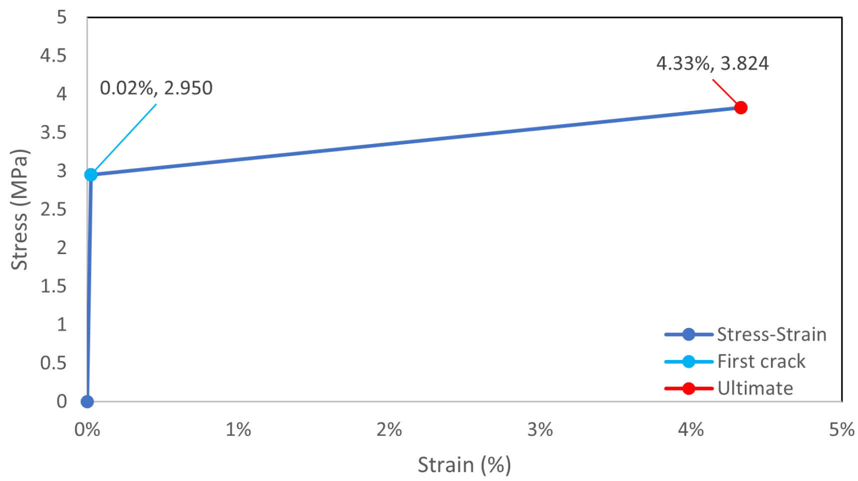

Figure D.1: Simplified stress-strain curve of the *SHCC*.

The methodology of this calculation follows Section 3.1.4. However, each calculation of the stress utilized distinct values, all of which began with the assumption that the old and new bridge would experience creep, but the *SHCC* would remain crack-free. Based on this assumption, an iterative method was set in motion that considered the highest tensile stresses in the closure pour as determined by this technique, which for the *FEA* model does not mean at mid-span. The reason for that was explained at Chapter 5. The calculations are in Section D.1 and Section D.2. And the final values were used at Section 4.1.2.2 and Section 4.3.2.

At Section D.3, there are the calculations of a three-span model. Its final value is shown at Section 5.3.4.

D.1 Analytical Calculations

The calculation was an iterative process. It started by adopting the stress of the case that the old and new bridge would creep, but the *SHCC* would not crack ($11.6MPa$), as shown in Figure D.2. Then, the strain that this stress would have if elastic modulus was kept at $12421MPa$, which was 0.093%. Applying the rule of three with the first cracking strength and first cracking strain and ultimate tensile strength and ultimate tensile strain, resulting in a stress of $2.964MPa$. Knowing the stress and strain at a certain juncture, it was possible to calculate the modified elastic modulus for this juncture. The modified elastic modulus was applied to the model, and a new stress was established. It was applied the eqs. (D.1) and (D.2), where "x" is the number of the trial; ε is the strain; σ_M is the stress determined by the model; E_x is the elastic modulus adopted at the model in each trial and the forthcoming trial will incorporate the elastic modulus E_{x+1}, calculated at Equation D.3, as part of its model.

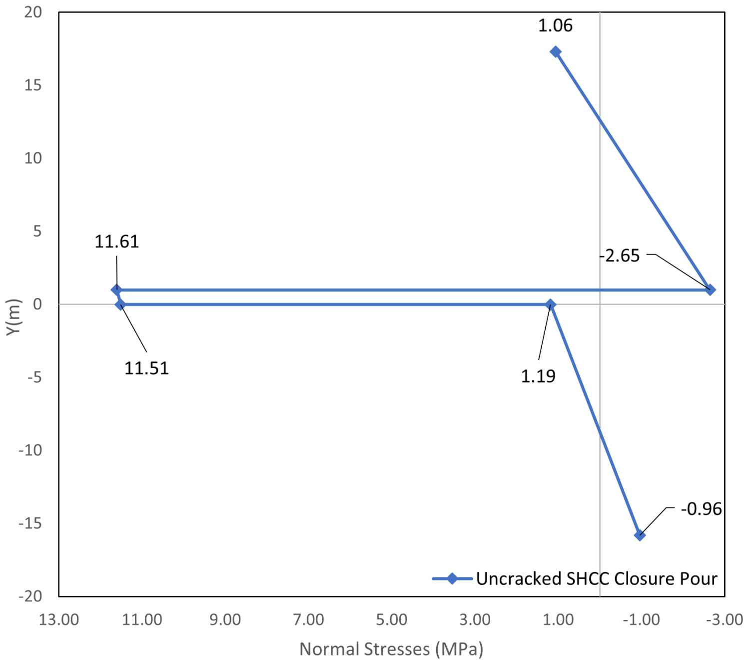

Figure D.2: Results of shrinking uncracked *SHCC* closure pour.

$$\varepsilon_x = \frac{\sigma_M}{E_x} \tag{D.1}$$

$$\sigma_x = \frac{(\varepsilon_x - \varepsilon_t) \times (f_{tu} - F_t)}{(\varepsilon_{tu} - \varepsilon_t)} + F_t \tag{D.2}$$

$$E_{x+1} = \frac{\sigma_x}{\varepsilon_x} \tag{D.3}$$

The procedure of the 1st trial will be shown in eqs. (D.4) to (D.6), and then the rest follow the same procedure.

$$\varepsilon_x = \frac{\sigma_M}{E_x} = \frac{11.606}{12421} = 0.093\% \tag{D.4}$$

$$\sigma_x = \frac{(\varepsilon_x - \varepsilon_t) \times (f_{tu} - F_t)}{(\varepsilon_{tu} - \varepsilon_t)} + F_t = \frac{(0.093\% - 0.0237\%) \times (3.824 - 2.950)}{(4.331\% - 0.0237\%)} + 2.950 = 2.964MPa \tag{D.5}$$

$$E_{x+1} = \frac{\sigma_x}{\varepsilon_x} = \frac{2.964}{0.093\%} = 3172MPa \tag{D.6}$$

This procedure was tested until both stresses (σ_M and σ_x) had the same result, meaning that the final result was also part of the graphic as shown in the 4th trial of Table D.1.

	E_x (MPa)	σ_M(MPa)	ε_x(%)	σ_x(MPa)
1st trial	12421	11.606	0.093	2.964
2nd trial	3172	2.995	0.094	2.964
3rd trial	3140	2.965	0.094	2.964
4th trial	**3139**	**2.964**	**0.094**	**2.964**

Table D.1: Iterative procedure.

At Figure D.3, the red dot was the final stress and strain calculated.

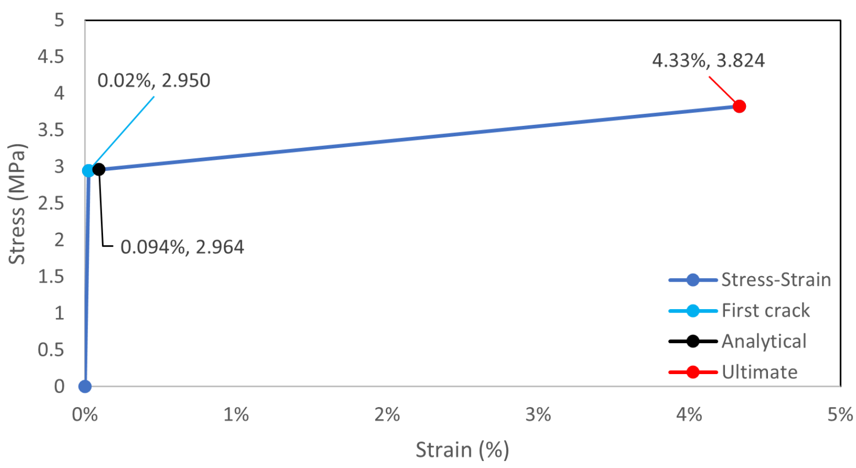

Figure D.3: Stress-strain curve of the cracked *SHCC*.

D.2 *FEA* Linear Model

The calculation was an iterative process. It started by adopting the stress if *SHCC* would not crack $(13.19MPa)$, as shown in Figure D.4. Then, the strain that this stress would have if elastic modulus was kept at $12421MPa$, which was 0.106%. Applying the rule of three with the first cracking strength and first cracking strain and ultimate tensile strength and ultimate tensile strain, resulting in a stress of $2.967MPa$. Knowing the stress and strain at a certain juncture, it was possible to calculate the modified elastic modulus for this juncture. The modified elastic modulus was applied to the model, and a new stress was established. It was applied the eqs. (D.7) and (D.8), where "x" is the number of the trial; ε is the strain; σ_M is the stress determined by the model; E_x is the elastic modulus adopted at the model in each trial and the forthcoming trial will incorporate the elastic modulus E_{x+1}, calculated at Equation D.9, as part of its model.

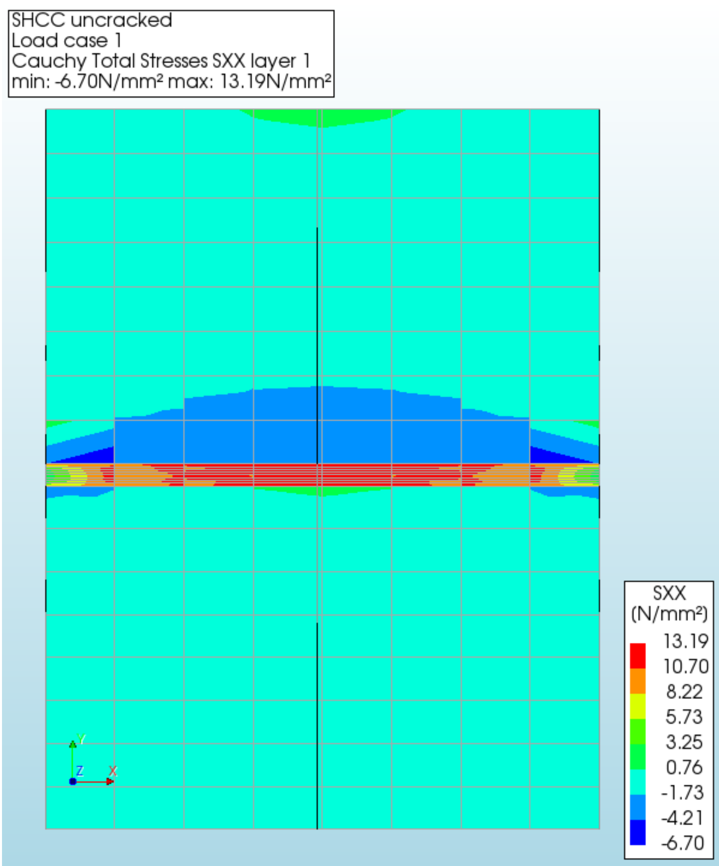

Figure D.4: Results of shrinking uncracked *SHCC* closure pour.

$$\varepsilon_x = \frac{\sigma_M}{E_x} \tag{D.7}$$

$$\sigma_x = \frac{(\varepsilon_x - \varepsilon_t) \times (f_{tu} - F_t)}{(\varepsilon_{tu} - \varepsilon_t)} + F_t \tag{D.8}$$

$$E_{x+1} = \frac{\sigma_x}{\varepsilon_x} \tag{D.9}$$

The procedure of the 1st trial will be shown in eqs. (D.10) to (D.12), and then the rest follow the same procedure.

$$\varepsilon_x = \frac{\sigma_M}{E_x} = \frac{13.19}{12421} = 0.106\% \tag{D.10}$$

$$\sigma_x = \frac{(\varepsilon_x - \varepsilon_t) \times (f_{tu} - F_t)}{(\varepsilon_{tu} - \varepsilon_t)} + F_t = \frac{(0.106\% - 0.0237\%) \times (3.824 - 2.950)}{(4.331\% - 0.0237\%)} + 2.950 = 2.967MPa \tag{D.11}$$

$$E_{x+1} = \frac{\sigma_x}{\varepsilon_x} = \frac{2.967}{0.106\%} = 2794MPa \tag{D.12}$$

This procedure was tested until both stresses (σ_M and σ_x) had the same result, meaning that the final result was also part of the graphic as shown in the 4th trial of Table D.2.

	E_x (MPa)	σ_M(MPa)	ε_x(%)	σ_x(MPa)
1st trial	12421	13.19	0.106	2.967
2nd trial	2794	3.27	0.122	2.970
3rd trial	2426	2.98	0.124	2.970
4th trial	**2402**	**2.97**	**0.124**	**2.970**

Table D.2: Iterative procedure.

At Figure D.5, the red dot was the final stress and strain calculated.

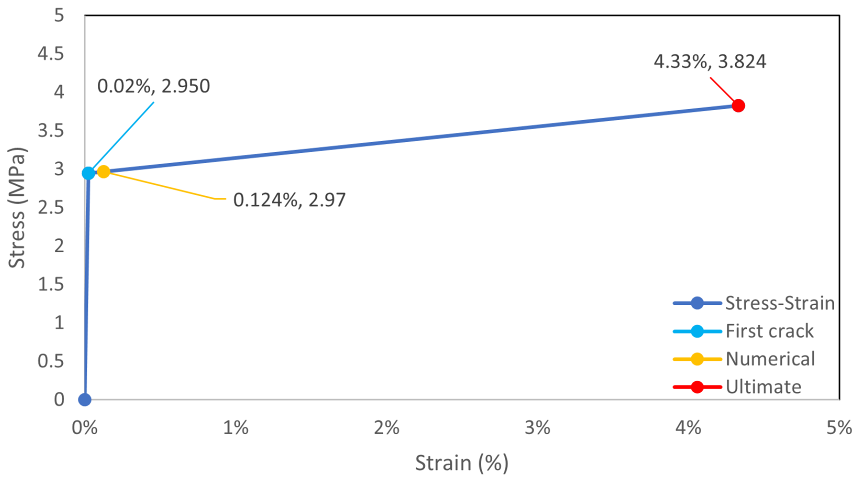

Figure D.5: Stress-strain curve of the cracked *SHCC*.

D.3 *FEA* Linear Model - Three Spans

The calculation was an iterative process. It started by adopting the stress if *SHCC* would not crack $(12.7MPa)$, as shown in Figure D.6. Then, the strain that this stress would have if elastic modulus were kept at $12421MPa$, which was 0.102%. Applying the rule of three with the first cracking strength and first cracking strain and ultimate tensile strength and ultimate tensile strain, resulting in a stress of $2.966MPa$. Knowing the stress and strain at a certain point, it was possible to calculate the modified elastic modulus for this stage. The modified elastic modulus was applied to the model, and a new stress was established. It was applied the eqs. (D.13) and (D.14), where "x" is the number of the trial; ε is the strain; σ_M is the stress determined by the model; E_x is the elastic modulus adopted at the model in each trial and the forthcoming trial will incorporate the elastic modulus E_{x+1}, calculated at Equation D.15, as part of its model.

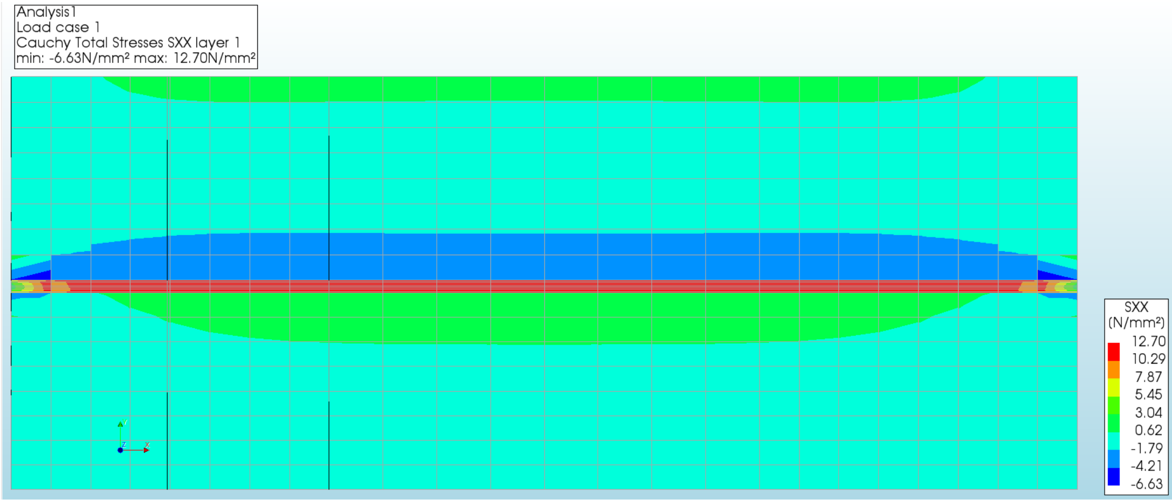

Figure D.6: Results of shrinking uncracked *SHCC* closure pour with three spans.

$$\varepsilon_x = \frac{\sigma_M}{E_x} \tag{D.13}$$

$$\sigma_x = \frac{(\varepsilon_x - \varepsilon_t) \times (f_{tu} - F_t)}{(\varepsilon_{tu} - \varepsilon_t)} + F_t \tag{D.14}$$

$$E_{x+1} = \frac{\sigma_x}{\varepsilon_x} \tag{D.15}$$

The procedure of the 1st trial will be shown in eqs. (D.16) to (D.18), and then the rest follow the same procedure.

$$\varepsilon_x = \frac{\sigma_M}{E_x} = \frac{12.70}{12421} = 0.102\% \tag{D.16}$$

$$\sigma_x = \frac{(\varepsilon_x - \varepsilon_t) \times (f_{tu} - F_t)}{(\varepsilon_{tu} - \varepsilon_t)} + F_t = \frac{(0.102\% - 0.0237\%) \times (3.824 - 2.950)}{(4.331\% - 0.0237\%)} + 2.950 = 2.966MPa \tag{D.17}$$

$$E_{x+1} = \frac{\sigma_x}{\varepsilon_x} = \frac{2.966}{0.102\%} = 2901MPa \tag{D.18}$$

This procedure was tested until both stresses (σ_M and σ_x) had the same result, meaning that the final result was also part of the graphic as shown in the 4th trial of Table D.3.

	E_x (MPa)	σ_M(MPa)	ε_x(%)	σ_x(MPa)
1st trial	12421	12.7	0.102%	2.966
2nd trial	2901	3.4	0.117%	2.969
3rd trial	2533	3.00	0.118%	2.969
4th trial	**2507**	**2.97**	**0.118%**	**2.969**

Table D.3: Iterative procedure.

At Figure D.7, the red dot was the final stress and strain calculated.

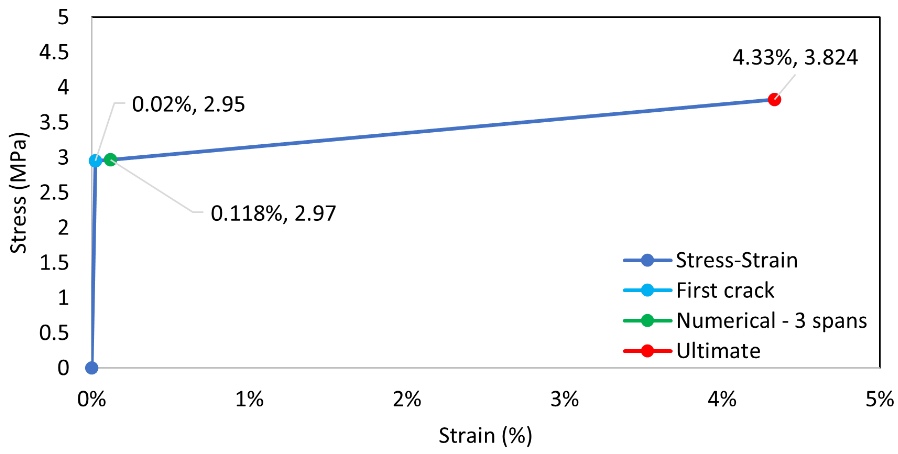

Figure D.7: Stress-strain curve of the three spans model of cracked *SHCC*.

E

Appendix E: Reinforcement Design

E.1 Methodology

The calculation of the crack width was made following the Eurocode, defined in section 7.3.4 of NEN-EN 1992-1-1[17].

The formula of the crack width, w_k, is shown in Equation E.1, which depends on the maximum crack spacing, $s_{r,max}$, and on the mean strains of concrete, ε_{cm}, and reinforced steel, ε_{sm}.

$$w_k = s_{r,max}(\varepsilon_{sm} - \varepsilon_{cm}) \tag{E.1}$$

The difference of strains of the steel and concrete are calculated through Equation E.2.

$$\varepsilon_{\mathrm{sm}} - \varepsilon_{\mathrm{cm}} = \frac{\sigma_{\mathrm{s}} - k_{\mathrm{t}} \frac{f_{\mathrm{ct,eff}}}{\rho_{\mathrm{p,eff}}} \left(1 + \alpha_{\mathrm{e}} \rho_{\mathrm{p,eff}}\right)}{E_{\mathrm{s}}} \geq 0,6 \frac{\sigma_{\mathrm{s}}}{E_{\mathrm{s}}} \tag{E.2}$$

Knowing that α_e is the ratio E_s/E_c and that $\rho_{p,eff}$ depends on the areas of the materials and the basic formula is shown in Equation E.3

$$\rho_{\mathrm{p,eff}} = \frac{A_s + \xi_1 \times A_p'}{A_{\mathrm{c,eff}}} \tag{E.3}$$

Since the closure pour is made of reinforced concrete and has no prestress, A_p' is zero, modifying Equation E.3 to Equation E.4

$$\rho_{\mathrm{p,eff}} = \frac{A_s}{A_{\mathrm{c,eff}}} \tag{E.4}$$

To calculate $\rho_{p,eff}$, the effective area of concrete was calculated it was used Equation E.5 and Equation E.6

$$A_{\mathrm{c,eff}} = w \times h_{c,ef} \tag{E.5}$$

$$\begin{aligned} h_{c,ef,1} &= 2.5(h-d) \\ h_{c,ef,2} &= \frac{h-x}{3} \\ h_{c,ef,3} &= h/2 \\ h_{c,ef} &= \min(h_{c,ef,1}, h_{c,ef,2}, h_{c,ef,3}) \end{aligned} \tag{E.6}$$

The formula of the maximum crack spacing, $s_{r,max}$, is shown in Equation E.7.

$$s_{r,\max} = k_3 c + k_1 k_2 k_4 \phi / \rho_{\mathrm{p,eff}} \tag{E.7}$$

E.2 Calculations

The reinforcement design methodology outlined in Section E.1 was utilized by analyzing the data provided in Table E.1. Which enabled the calculation of the necessary quantity of steel bars for each diameter option ($\phi = 20mm$, $\phi = 25mm$, $\phi = 32mm$), as well as their corresponding stress levels (σ_s). In addition, the maximum allowable crack width for reinforced concrete, as discussed in Section 2.1.3.3, was assumed to be $0.20mm$, as illustrated in the table mentioned above.

Data for calculations:

Variable	Values with units
A'_p	$0m^2$
A_s	$\pi \times \phi^2/4$
E_c	$35000MPa$
E_s	$200000MPa$
c	$60mm$
d	$800mm$
h	$900mm$
k_1	0.8
k_2	1.0
k_3	3.4
k_4	0.425
k_t	0.4
$f_{ct,eff}$	$3.5MPa$
w	$1000mm$
w_k	$0.20mm$
x	$0mm$ (no compressive zone)
ϕ	$20mm$/$25mm$/$32mm$

Table E.1: Data used for Reinforcement Design

Through an iterative process, the outcome of this process is shown at Table E.2, which is the diameter, the minimum amount of bars up to the immediate following whole number, and the steel stress.

Diameter	Minimum of bars	Steel Stress
$\phi = 20mm$	38	$191,90MPa$
$\phi = 25mm$	26	$179.41MPa$
$\phi = 32mm$	18	$165.76MPa$

Table E.2: Data used for Reinforcement Design

F

Appendix F: Data For Calculations

F.1 Data For Analytical Calculations

For the horizontal stress calculations, some information is needed, such as the cross-section dimensions, shrinkage of the new bridge, and the creep of the new and old bridge. The elastic modulus of the crack concrete closure pour was assumed to be $1/3$ of the original as mentioned on Section 2.2.3.

F.1.1 Cross-Section Dimensions

According to the file "20060530_KWQCR060029573" of the project "IF 137380 Kenmerk KW-QCR-060029573"[43], the old bridge was assumed to be a K450, resulting in the following values of table F.1 for the old bridge. The new bridge's concrete was assumed to be a C50/60. And for the closure pour assumed a lower compressive strength than the new bridge, resulting in a concrete C40/50. Afterward, the closure pour material will be deeply analyzed. With the following characteristics for both types of concrete, according to table 3.1 of NEN-EN 1992-1-1[17], and follows its dimensions:

Concrete characteristics	Old Bridge	Concrete *CP*	New Bridge
f_{ck} (MPa)	37.00	40/50	50/60
f_{ctk} (MPa)	2.05	2.5	2.9
f_{ctm} (MPa)	2.84	3.5	4.1
E_{cm} (GPa)	31.5	35	37

Table F.1: Concrete characteristics.

For the *SHCC*, the values were taken for Table 2.1, therefore the elastic modulus of *SHCC* is $E_{SHCC} = 12421MPa$ and the shrinkage strain after 100 years is $\varepsilon_{SHCC} = 0.985 \times 10^{-3}$.

The dimensions from table F.2 were taken from figure 1.4, which was given by Rijswaterstaat and simplified in the figs. 1.11, 1.12 and 1.15.

Dimensions	Old Bridge	Closure Pour	New Bridge
w (m)	16.30	1	15.80
t (m)	0.9	0.9	0.9
Area (m^2)	14.68	0.9	14.22
u (m)	34.4	3.8	33.4
S (m^3)	39.9	0.15	37.45

Table F.2: Cross-Section Dimensions.

F.1.2 Final values of shrinkage and creep

The values of shrinkage of the new bridge were taken from Table A.1 and repeated in Table F.3.

Time	ε_{new}
2 months	1.57×10^{-4}
100 years	2.44×10^{-4}

Table F.3: Shrinkage of the new bridge at different times.

The values of shrinkage of the concrete closure pour were taken from Table B.1 and repeated in Table F.4.

Time	ε_{cp}
100 years	2.37×10^{-4}

Table F.4: Shrinkage of the closure pour at different times.

The creep values were taken from Equation C.15 for the old bridge and repeated at Equation F.1, and at Table C.2 are the values of creep for the new bridge, and repeated at Table F.5.

$$E_{old,creep} = \frac{E_{old}}{1+\varphi} = \frac{31.5 \times 10^3}{1+0.02} = 30941 N/mm^2 \tag{F.1}$$

Final age	$\varphi_{(t,3)}$	$\varphi_{(100,3)} - \varphi_{(t,3)}$	$E_{(100y)}$
2 months	0.68	1.00	18461
4 months	0.83	0.85	19972
6 months	0.93	0.76	21077
100 years	1.69	0.00	37000

Table F.5: Creep Coefficient (φ) of the New Bridge.

F.2 Data For the Numerical Model

It was assumed that the Poisson's ratio is always 0.2 for both concrete and *SHCC*. The geometry of the plates, just as their dimension, was based on the original bridge, and the thickness was considered constant, as shown in the Table F.6 and also in Figure 3.25.

Dimensions	Old Bridge	Closure Pour	New Bridge
L (m)	25.5	25.5	25.5
w (m)	16.3	1.0	15.8
t (m)	0.9	0.9	0.9

Table F.6: Cross-Section Dimensions.

The element class of the model was chosen as "Regular Curved Shells" because the decks of the bridge were modeled as plates. Thus, this element class enables the plates to undergo both in and out-of-plane loads and are able to bend. The class of the model was selected, "Concrete and Masonry," since it is the easiest manner to input different values for the elastic modulus. The material model chosen was "Linear Elastic Isotropic" because it is linear. And isotropic because it was considered at a structural level that concrete and *SHCC* behave equally in the three directions, as shown in Table F.7.

	All Components
Element Class	Regular Curved Shells
Material Class	Concrete and Masonry
Material Model	Linear Elastic Isotropic

Table F.7: Element class, Material Class, and Material model.

The type of the finite element is shown in Table F.8, which shows eight edge divisions for the creation of the mesh of the model, which in total used 64 elements in each component(old bridge, closure pour, and new bridge), each part had a different size of elements. Therefore, a total of 192 quadratic elements were used.

Type of the finite element	CQ40S
	8-node quadrilateral isoparametric curved shell element
Degrees of freedom	40 (5×8) (5 per node, u_x, u_y, u_z, ρ_x, ρ_y)
Interpolation scheme	Quadratic
Integration scheme	2x2x2 Gauss
Shape dimension	3D
Topological dimension	2D
Stress components	σ_{xx}, σ_{yy}, σ_{zz}, σ_{xy}, σ_{xz}, σ_{yz}
Inclusion of shear deformations	yes
Edge divisions	8
Total number of elements	192
Total number of nodes	641

Table F.8: Type of the finite element.

Its original material according to Section F.1.1, just as the modified elastic modulus and the assumed Poisson's ratio is shown in Table F.9.

Model part	Original Material	Young's Modulus Modified	Poisson's ratio
Old Bridge	Concrete K450	30941 Mpa	0.2
Concrete Closure Pour	Concrete C40/50	11667 MPa	0.2
SHCC Closure Pour	SHCC from [32]	2402 MPa	0.2
New Bridge	Concrete C50/60	18461 MPa	0.2

Table F.9: Original Material, Young's Modulus Modified and Poisson's Ratio.

Despite being aware that the shrinkage and creep of the concrete and the shrinkage of the *SHCC* is not linear, it was calculated and just used the final values for simplification purposes. Shrinkage was turned into a prescribed strain load, and creep was applied, modifying the corresponding materials' elastic modulus. The crack of the concrete closure pour was also accounted for by modifying its Young's modulus. The crack of the *SHCC* was calculated at Section D.2, and its final value is on the Table F.9. The elastic modulus of each element is shown in Table F.9.

Two loads were applied to account for the shrinkage of the new bridge and the closure pour, each to account for one of the shrinkages. The type of load used was prescribed strain so that the shrinkage previously applied in Section 3.3 could be included in this model, and the design could be comparable to the previously mentioned chapter. The final values of the strain applied were taken from Table F.3 for the new bridge, from Table F.4 for the concrete closure pour, and from Table 2.1 for the *SHCC* closure pour and shown in the Table F.10.

	Strain Applied
New Bridge	1.57×10^{-4}
Concrete Closure Pour	2.37×10^{-4}
SHCC Closure Pour	9.85×10^{-4}

Table F.10: Strains applied as prescribed strain in the model.

G

Appendix G: Calculations Of Each Analytical Method

G.1 Method item 1 - No closure pour

Described at Section 3.3.2, the steps of the calculations, along with their final results, will be presented.

These are the horizontal stress calculations for the old and new bridges, considering that only the new bridge would shrink and assuming that the bridges will be connected as soon as the new bridge is cast. Therefore, the structure will be affected by the total shrinkage (100 years).

Following the procedure shown in Section 3.3.2, to calculate the force N^* from Equation 3.7, it was used $\varepsilon_{new} = 2.44 \times 10^{-4}$ from Table A.1. $E_{new} = 37GPa = 37000N/mm^2$ from Table F.1 and $A_{new} = 14.22m^2$ from Table F.2. Resulting in the Equation G.1 below:

$$N^* = \varepsilon_{new} \times E_{new} \times A_{new} = 2.44 \times 10^{-4} \times 37000 \times 14.22 = 128.5MN \tag{G.1}$$

For the calculation of the moment, Equation 3.7, it is necessary to the value of "e", defined in 3.3.2 along with z_{new}, z_{old} and z_{total} and shown in figs. 3.11 and 3.12. Knowing that the axial stiffnesses are taken from the Table F.2 and that according to definitions $z_{new} = 7.90m$. $z_{old} = 23.96m$, it was possible to calculate z_{total} using Equation 3.8 and applying the numbers, the result is in Equation G.2.

$$z_{total} = \frac{z_{new} \times EA_{new} + z_{old} \times EA_{old}}{EA_{new} + EA_{old}} = \frac{7.90 \times 526 \times 10^3 + 23.96 \times 462 \times 10^3}{526 \times 10^3 + 462 \times 10^3} = 15.41m \tag{G.2}$$

$$e = z_{total} - z_{new} = 15.41 - 7.90 = 7.51m \tag{G.3}$$

$$M^* = N^* \times e = 128.5 \times 7.51 = 964.8MNm \tag{G.4}$$

Once the N^* and M^* are calculated, the stresses that they caused were calculated. These stresses induced by the imposed deformation are:

1. Due to the axial tensile force only on the layer that suffered the action;
2. In virtue of the force that N^* caused in the total structure;
3. Because of the stresses originating due to the M^* on the entire structure;
4. As a consequence of the moment M^* per layer.

For item 1, the stresses were only calculated on the new bridge, which was the layer that suffered the shrinkage. It was use the Equation 3.12.

$$\sigma_{wb} = \sigma_{wo} = \frac{N^*}{A_{new}} = \frac{128.5}{14.22} = 9.03N/mm^2 \tag{G.5}$$

For item 2, it was first calculated the force per layer and then the stresses caused in each layer. For the old bridge, it was used eqs. (3.9) and (3.14), and for the new bridge, it was used eqs. (3.13) and (3.15). It also used the axial stiffness from Table F.2.

Old bridge:

$$N_{old} = \frac{(EA)_{old}}{(EA)_{total}} \times N^* = \frac{462 \times 10^3}{989 \times 10^3} \times 128.5 = 60.09MN \tag{G.6}$$

$$\sigma_{wb} = \sigma_{wo} = -\frac{N_{old}}{A_o} = \frac{-60.09}{14.68} = -4.09N/mm^2 \tag{G.7}$$

New bridge:

$$N_{new} = N^* - N_{old} = 128.5 - 60.09 = 68.38MN \tag{G.8}$$

$$\sigma_{wb} = \sigma_{wo} = -\frac{N_{new}}{A_{new}} = \frac{-68.38}{14.22} = -4.81N/mm^2 \tag{G.9}$$

At item 3, it was used the Equation 3.10 to calculate the force in the old bridge that the bending moment produced in the entire structure, and Equation 3.17 was used to calculate the stresses, which the force originated. A similar force happened in the new bridge, and the formulas used for that were eqs. (3.16) and (3.18).

$(EI)_{total} = 84.6MNm^2$

Old bridge:

$$N_{old} = \frac{M^*}{(EI)_{total}} \times (EA)_{old} \times a_{old} = \frac{964.8}{84.6 \times 10^6} \times 462 \times 10^3 \times 8.55 = 45.04MN \tag{G.10}$$

$$\sigma_{wb} = \sigma_{wo} = +\frac{N_{old}}{A_{old}} = +\frac{45.04}{14.68} = 3.07N/mm^2 \tag{G.11}$$

New bridge:

$$N_{new} = \frac{M^*}{(EI)_{total}} \times (EA)_{new} \times a_{new} = \frac{964.8}{84.6 \times 10^6} \times 526 \times 10^3 \times 7.51 = 45.04MN \tag{G.12}$$

$$\sigma_{wb} = \sigma_{wo} = -\frac{N_{new}}{A_{new}} = -\frac{45.04}{14.22} = -3.17N/mm^2 \tag{G.13}$$

At item 4, a moment was calculated per layer for the old and new bridges, using the eqs. (3.11) and (3.19), respectively. Also, their stresses were calculated using eqs. (3.20) and (3.21), where S_{old} and S_{new} are the associated section modulus of each part of the cross-section, shown in Table F.2.

Old bridge:

$$M_{old} = M^* \times \frac{(EI)_{old}}{(EI)_{total}} = 964.8 \times \frac{10.25 \times 10^6}{84.6 \times 10^6} = 116.85MN \tag{G.14}$$

$$\sigma_{wb} = -\sigma_{wo} = -\frac{M_{old}}{S_{old}} = -\frac{116.85}{39.90} = -2.93N/mm^2 \tag{G.15}$$

New bridge:

$$M_{new} = M^* \times \frac{(EI)_{new}}{(EI)_{total}} = 964.8 \times \frac{10.95 \times 10^6}{84.6 \times 10^6} = 124.77MN \tag{G.16}$$

$$\sigma_{wb} = -\sigma_{wo} = -\frac{M_{new}}{S_{new}} = -\frac{124.77}{37.45} = -3.33N/mm^2 \tag{G.17}$$

Final horizontal stresses

The Table G.1 summarized all the stresses calculated above, and Figure G.1 is the graphic of the stresses.

Stresses (MPa)	Old top	Old bottom	New top	New bottom
item 1	0.00	0.00	9.03	9.03
item 2	-4.09	-4.09	-4.81	-4.81
item 3	3.07	3.07	-3.17	-3.17
item 4	2.93	-2.93	3.33	-3.33
Total	1.90	-3.95	4.39	-2.27

Table G.1: Results without a closure pour.

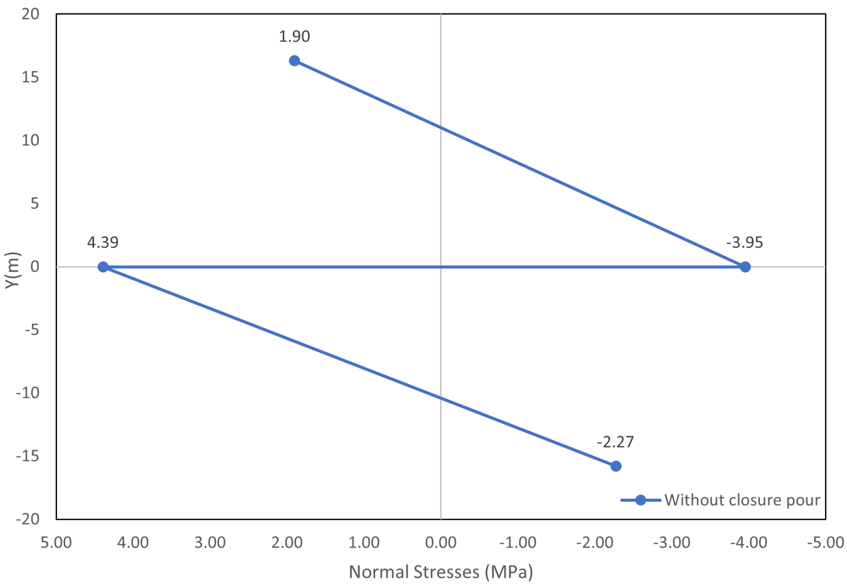

Figure G.1: Results without a closure pour.

G.2 Method item 2 - No shrinking closure pour

Described at Section 3.3.3, the steps of the calculations, along with their final results, will be presented.

These are the horizontal stress calculations for the old, the new bridge, and the closure pour, considering that the new bridge and the closure pour would shrink and assuming that the closure pour is cast 2 months after the new bridge is done. Therefore, the shrinkage of the closure pour will be of 100 years, and the shrinkage of the new bridge will be the same as the last example, which is 100 years minus two months.

Following the procedure shown in Section 3.3.3, to calculate the force N^* from Equation 3.22, it was used $\varepsilon_{new} = 1.57 \times 10^{-4}$ from table Table A.1. $E_{new} = 37GPa = 37000N/mm^2$ from Table F.1 and $A_{new} = 14.22m^2$ from table Table F.2. Resulting in the Equation G.18 below:

$$N^* = \varepsilon_{new} \times E_{new} \times A_{new} = 1.57 \times 10^{-4} \times 37,000 \times 14.22 = 82.7MN \tag{G.18}$$

For the calculation of the moment, Equation 3.23, it is necessary to the value of "e", defined in 3.3.3 along with z_{new}, z_{cp}, z_{old}, and z_{total} and shown in figs. 3.17 and 3.18. Knowing that the axial stiffnesses are taken from the Table F.2 and that according to definitions $z_{new} = 7.90m$, $z_{cp} = 16.30m$ $z_{old} = 24.96m$, it was possible to calculate z_{total} using Equation 3.24 and applying the numbers, the result is in Equation G.19.

$$z_{total} = \frac{z_{new} \times EA_{new} + z_{cp} \times EA_{cp} + z_{old} \times EA_{old}}{EA_{new} + EA_{cp} + EA_{old}} =$$
$$= \frac{7.90 \times 526 \times 10^3 + 16.30 \times 32 \times 10^3 + 24.96 \times 462 \times 10^3}{526 \times 10^3 + 32 \times 10^3 + 462 \times 10^3} = 15.89m \tag{G.19}$$

$$e = z_{total} - z_{new} = 15.89 - 7.90 = 7.99m \tag{G.20}$$

$$M^* = N^* \times e = 82.7 \times 7.99 = 661.1MNm \tag{G.21}$$

Once the N^* and M^* are calculated, the stresses that they caused were calculated. These stresses induced by the imposed deformation are:

1. Due to the axial tensile force only on the layer that suffered the action;
2. In virtue of the force that N^* caused in the total structure;
3. Because of the stresses originating due to the M^* on the entire structure;
4. As a consequence of the moment M^* per layer.

For item 1, the stresses were only calculated on the new bridge. It was the layer that suffered the shrinkage, and it was used the Equation 3.28.

$$\sigma_{wb} = \sigma_{wo} = \frac{N^*}{A_{new}} = \frac{82.7}{14.22} = 5.82N/mm^2 \tag{G.22}$$

For item 2, it was first calculated the force per layer and then the stresses caused in each layer. For the old bridge, it was used eqs. (3.25) and (3.31). For the new bridge, it was used eqs. (3.29) and (3.32), and for the closure pour, it was used eqs. (3.30) and (3.33). It also used the axial stiffness from Table F.2.

Old bridge:

$$N_{old} = \frac{(EA)_{old}}{(EA)_{total}} \times N^* = \frac{462 \times 10^3}{1020 \times 10^3} \times 82.7 = 37.50MN \tag{G.23}$$

$$\sigma_{wb} = \sigma_{wo} = -\frac{N_{old}}{A_{old}} = \frac{-37.50}{14.68} = -2.55N/mm^2 \tag{G.24}$$

New bridge:

$$N_{new} = \frac{(EA)_{new}}{(EA)_{total}} \times N^* = \frac{526 \times 10^3}{1020 \times 10^3} \times 82.7 = 42.67MN \tag{G.25}$$

$$\sigma_{wb} = \sigma_{wo} = -\frac{N_{new}}{A_{new}} = \frac{-42.67}{14.22} = -3.00N/mm^2 \tag{G.26}$$

Closure pour:

$$N_{cp} = N^* - N_{old} - N_{new} = 82.7 - 37.50 - 42.67 = 2.55MN \tag{G.27}$$

$$\sigma_{wb} = \sigma_{wo} = -\frac{N_{cp}}{A_{cp}} = \frac{-2.55}{0.90} = -2.84N/mm^2 \tag{G.28}$$

At item 3, it was used the Equation 3.26 to calculate the force in the old bridge that the bending moment produced in the entire structure, and Equation 3.36 was used to calculate the stresses, which the force originated. A similar force happened in the new bridge and in the closure pour, and the formulas used for that were eqs. (3.34) and (3.37) for the new bridge and eqs. (3.35) and (3.38) for the closure pour.

$(EI)_{total} = 92.8MNm^2$

Old bridge:

$$N_{old} = \frac{M^*}{(EI)_{total}} \times (EA)_{old} \times a_{old} = \frac{661.1}{92.8 \times 10^6} \times 462 \times 10^3 \times 9.06 = 29.86MN \tag{G.29}$$

$$\sigma_{wb} = \sigma_{wo} = +\frac{N_{old}}{A_{old}} = +\frac{29.86}{14.68} = 2.03N/mm^2 \quad \text{(G.30)}$$

New bridge:

$$N_{new} = \frac{M^*}{(EI)_{total}} \times (EA)_{new} \times a_{new} = \frac{661.1}{92.8 \times 10^6} \times 526 \times 10^3 \times 7.99 = 29.95MN \quad \text{(G.31)}$$

$$\sigma_{wb} = \sigma_{wo} = -\frac{N_{new}}{A_{new}} = -\frac{29.95}{14.22} = -2.11N/mm^2 \quad \text{(G.32)}$$

Closure pour:

$$N_{cp} = \frac{M^*}{(EI)_{total}} \times (EA)_{cp} \times a_{cp} = \frac{661.1}{92.8 \times 10^6} \times 526 \times 10^3 \times 0.41 = 0.09MN \quad \text{(G.33)}$$

$$\sigma_{wb} = \sigma_{wo} = \frac{N_{cp}}{A_{cp}} = \frac{0.09}{0.90} = 0.10N/mm^2 \quad \text{(G.34)}$$

At item 4, a moment was calculated per layer for the old bridge, new bridge, and closure pour, using the eqs. (3.27), (3.39) and (3.40), respectively. Also, their stresses were calculated using eqs. (3.41) to (3.43), where S_{old}, S_{new}, and S_{cp} are the associated section modulus of each part of the cross-section, shown in table Table F.2.

Old bridge:

$$M_{old} = M^* \times \frac{(EI)_{old}}{(EI)_{total}} = 661.1 \times \frac{10.25 \times 10^6}{92.8 \times 10^6} = 73.03MN \quad \text{(G.35)}$$

$$\sigma_{wb} = -\sigma_{wo} = -\frac{M_{old}}{S_{old}} = -\frac{73.03}{39.90} = -1.83N/mm^2 \quad \text{(G.36)}$$

New bridge:

$$M_{new} = M^* \times \frac{(EI)_{new}}{(EI)_{total}} = 661.1 \times \frac{10.95 \times 10^6}{92.8 \times 10^6} = 77.98MN \quad \text{(G.37)}$$

$$\sigma_{wb} = -\sigma_{wo} = -\frac{M_{new}}{S_{new}} = -\frac{77.98}{37.45} = -3.33N/mm^2 \quad \text{(G.38)}$$

Closure pour:

$$M_{cp} = M^* \times \frac{(EI)_{cp}}{(EI)_{total}} = 661.1 \times \frac{0.003 \times 10^6}{92.8 \times 10^6} = 0.02MN \quad \text{(G.39)}$$

$$\sigma_{wb} = -\sigma_{wo} = -\frac{M_{cp}}{S_{cp}} = -\frac{0.02}{0.15} = -0.12N/mm^2 \quad \text{(G.40)}$$

Final horizontal stresses

The table Table G.2 summarized all the stresses calculated above and figure Figure G.2 is the graphic of the stresses.

Stresses (MPa)	Old top	Old bottom	CP top	CP bottom	New top	New bottom
Item item 1	0.00	0.00	0.00	0.00	5.82	5.82
Item item 2	-2.55	-2.55	-2.84	-2.84	-3.00	-3.00
Item item 3	2.03	2.03	0.10	0.10	-2.11	-2.11
Item item 4	1.83	-1.83	0.12	-0.12	2.08	-2.08
Total	1.31	-2.35	-2.61	-2.86	2.79	-1.37

Table G.2: Results of no shrinking concrete closure pour.

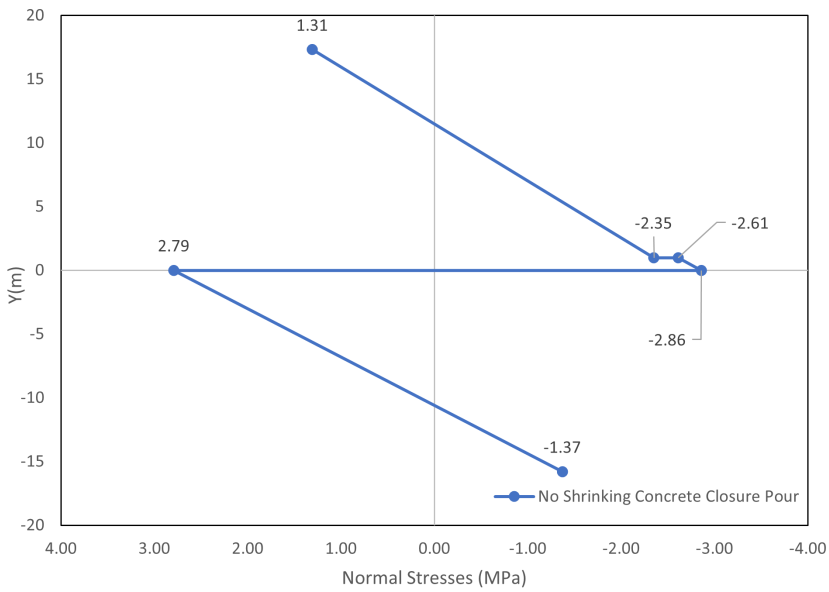

Figure G.2: Results of no shrinking concrete closure pour.

G.3 Method item 3 - Shrinking closure pour

Described at Section 3.3.4, the steps of the calculations, along with their final results, will be presented.

These are the horizontal stress calculations for the old, the new bridge, and the closure pour, considering that the new bridge and the closure pour would shrink and assuming that the closure pour is cast 2 months after the new bridge is done. Therefore, the shrinkage of the closure pour will be of 100 years, and the shrinkage of the new bridge will be the same as the last example, which is 100 years minus two months.

Following the procedure shown in Section 3.3.4, to calculate the force N_1^* from Equation 3.44 and the force N_2^* was calculated from Equation 3.45, it was used $\varepsilon_{new} = 1.57 \times 10^{-4}$ from Table A.1. $E_{new} = 37GPa = 37000N/mm^2$ from Table F.1 and $A_{new} = 14.22m^2$ from Table F.2. Resulting in the Equation G.41 below:

$$N_1^* = \varepsilon_{new} \times E_{new} \times A_{new} = 1.57 \times 10^{-4} \times 37,000 \times 14.22 = 82.7MN \tag{G.41}$$

To calculate N_2^* from Equation 3.45, it was used $\varepsilon_{cp} = 2.37 \times 10^{-4}$ from Table B.1. $E_{cp} = 35GPa = 35,000N/mm^2$ from Table F.1 and $A_{cp} = 0.90m^2$ from Table F.2.

$$N_2^* = \varepsilon_{cp} \times E_{cp} \times A_{cp} = 2.37 \times 10^{-4} \times 35,000 \times 0.90 = 7.5MN \tag{G.42}$$

$$N^* = N_1^* + N_2^* = 82.7 + 7.5 = 90.2MN \tag{G.43}$$

For the calculation of the moment, Equation 3.46, it is necessary to the value of "e_1" and "e_2", defined in 3.3.4 along with z_{new}, z_{cp}, z_{old} and z_{total} and shown in figs. 3.23 and 3.24. Knowing that the axial stiffnesses are taken from the Table F.2 and that according to definitions $z_{new} = 7.90m$, $z_{cp} = 16.30m$ $z_{old} = 24.96m$, it was possible to calculate z_{total} using Equation 3.47 and applying the numbers, the result is in Equation G.44.

$$z_{total} = \frac{z_{new} \times EA_{new} + z_{cp} \times EA_{cp} + z_{old} \times EA_{old}}{EA_{new} + EA_{cp} + EA_{old}} =$$
$$= \frac{7.90 \times 526 \times 10^3 + 16.30 \times 32 \times 10^3 + 24.96 \times 462 \times 10^3}{526 \times 10^3 + 32 \times 10^3 + 462 \times 10^3} = 15.89m \tag{G.44}$$

$$
\begin{aligned}
e_1 &= z_{total} - z_{new} = 15.89 - 7.90 = 7.99m \\
e_2 &= z_{total} - z_{cp} = 15.89 - 16.30 = -0.41m
\end{aligned} \tag{G.45}
$$

$$M^* = N_1^* \times e_1 + N_2^* \times e_2 = 82.7 \times 7.99 + 7.5 \times -0.41 = 658.0MNm \tag{G.46}$$

Once the N^* and M^* are calculated, the stresses that they caused were calculated. These stresses induced by the imposed deformation are:

1. Due to the axial tensile force only on the layer that suffered the action;
2. In virtue of the force that N^* caused in the total structure;
3. Because of the stresses originating due to the M^* on the entire structure;
4. As a consequence of the moment M^* per layer.

For item 1, the stresses were only calculated on the new bridge and on the closure pour. They were the layers that suffered the shrinkage. It used the formulas eqs. (3.51) and (3.52).

$$\sigma_{wb} = \sigma_{wo} = \frac{N_1^*}{A_{new}} = \frac{82.7}{14.22} = 5.82N/mm^2 \tag{G.47}$$

$$\sigma_{wb} = \sigma_{wo} = \frac{N_2^*}{A_{cp}} = \frac{7.5}{0.9} = 8.30N/mm^2 \tag{G.48}$$

For item 2, it was first calculated the force per layer and then the stresses caused in each layer. For the old bridge, it was used eqs. (3.48) and (3.55), for the new bridge, it was used eqs. (3.53) and (3.56) and for the closure pour, it was used eqs. (3.54) and (3.57). It also used the axial stiffness from Table F.2.

Old bridge:

$$N_{old} = \frac{(EA)_{old}}{(EA)_{total}} \times N^* = \frac{462 \times 10^3}{1020 \times 10^3} \times 90.2 = 40.89MN \tag{G.49}$$

$$\sigma_{wb} = \sigma_{wo} = -\frac{N_{old}}{A_{old}} = \frac{-40.89}{14.68} = -2.79N/mm^2 \tag{G.50}$$

New bridge:

$$N_{new} = \frac{(EA)_{new}}{(EA)_{total}} \times N^* = \frac{526 \times 10^3}{1020 \times 10^3} \times 90.2 = 46.53MN \tag{G.51}$$

$$\sigma_{wb} = \sigma_{wo} = -\frac{N_{new}}{A_{new}} = \frac{-46.53}{14.22} = -3.27N/mm^2 \tag{G.52}$$

Closure pour:

$$N_{cp} = N^* - N_{old} - N_{new} = 90.2 - 40.89 - 46.53 = 2.79MN \tag{G.53}$$

$$\sigma_{wb} = \sigma_{wo} = -\frac{N_{cp}}{A_{cp}} = \frac{-2.79}{0.90} = -3.10N/mm^2 \tag{G.54}$$

At item 3, it was used the Equation 3.49 to calculate the force in the old bridge that the bending moment produced in the entire structure, and Equation 3.60 was used to calculate the stresses, which the force originated. A similar force happened in the new bridge and in the closure pour, and the formulas used for that were eqs. (3.58) and (3.61) for the new bridge and eqs. (3.59) and (3.62) for the closure pour.

$(EI)_{total} = 92.8MNm^2$

Old bridge:

$$N_{old} = \frac{M^*}{(EI)_{total}} \times (EA)_{old} \times a_{old} = \frac{658.0}{92.8 \times 10^6} \times 462 \times 10^3 \times 9.06 = 29.72MN \tag{G.55}$$

$$\sigma_{wb} = \sigma_{wo} = +\frac{N_{old}}{A_{old}} = +\frac{29.72}{14.68} = 2.02N/mm^2 \tag{G.56}$$

New bridge:

$$N_{new} = \frac{M^*}{(EI)_{total}} \times (EA)_{new} \times a_{new} = \frac{658.0}{92.8 \times 10^6} \times 526 \times 10^3 \times 7.99 = 29.81MN \quad \text{(G.57)}$$

$$\sigma_{wb} = \sigma_{wo} = -\frac{N_{new}}{A_{new}} = -\frac{29.81}{14.22} = -2.10N/mm^2 \quad \text{(G.58)}$$

Closure pour:

$$N_{cp} = \frac{M^*}{(EI)_{total}} \times (EA)_{cp} \times a_{cp} = \frac{658.0}{92.8 \times 10^6} \times 526 \times 10^3 \times -0.41 = -0.09MN \quad \text{(G.59)}$$

$$\sigma_{wb} = \sigma_{wo} = \frac{N_{cp}}{A_{cp}} = \frac{-0.09}{0.90} = -0.10N/mm^2 \quad \text{(G.60)}$$

At item 4, a moment was calculated per layer for the old bridge, new bridge, and closure pour, using the eqs. (3.50), (3.63) and (3.64), respectively. Also, their stresses were calculated using equations eqs. (3.65) to (3.67), where S_{old}, S_{new}, and S_{cp} are the associated section modulus of each part of the cross-section, shown in Table F.2.

Old bridge:

$$M_{old} = M^* \times \frac{(EI)_{old}}{(EI)_{total}} = 658.0 \times \frac{10.25 \times 10^6}{92.8 \times 10^6} = 72.69MN \quad \text{(G.61)}$$

$$\sigma_{wb} = -\sigma_{wo} = -\frac{M_{old}}{S_{old}} = -\frac{72.69}{39.90} = -1.82N/mm^2 \quad \text{(G.62)}$$

New bridge:

$$M_{new} = M^* \times \frac{(EI)_{new}}{(EI)_{total}} = 658.0 \times \frac{10.95 \times 10^6}{92.8 \times 10^6} = 77.62MN \quad \text{(G.63)}$$

$$\sigma_{wb} = -\sigma_{wo} = -\frac{M_{new}}{S_{new}} = -\frac{77.62}{37.45} = -2.07N/mm^2 \quad \text{(G.64)}$$

Closure pour:

$$M_{cp} = M^* \times \frac{(EI)_{cp}}{(EI)_{total}} = 658.0 \times \frac{0.003 \times 10^6}{92.8 \times 10^6} = 0.02MN \quad \text{(G.65)}$$

$$\sigma_{wb} = -\sigma_{wo} = -\frac{M_{cp}}{S_{cp}} = -\frac{0.02}{0.15} = -0.12N/mm^2 \quad \text{(G.66)}$$

Final horizontal stresses

The Table G.3 summarized all the stresses calculated above, and Figure G.3 is the graphic of the stresses.

Stresses (MPa)	Old top	Old bottom	CP top	CP bottom	New top	New bottom
Item item 1	0.00	0.00	8.30	8.30	5.82	5.82
Item item 2	-2.79	-2.79	-3.10	-3.10	-3.27	-3.27
Item item 3	2.02	2.02	-0.10	-0.10	-2.10	-2.10
Item item 4	1.82	-1.82	0.12	-0.12	2.07	-2.07
Total	1.06	-2.58	5.23	4.98	2.52	-1.62

Table G.3: Results of shrinking concrete closure pour.

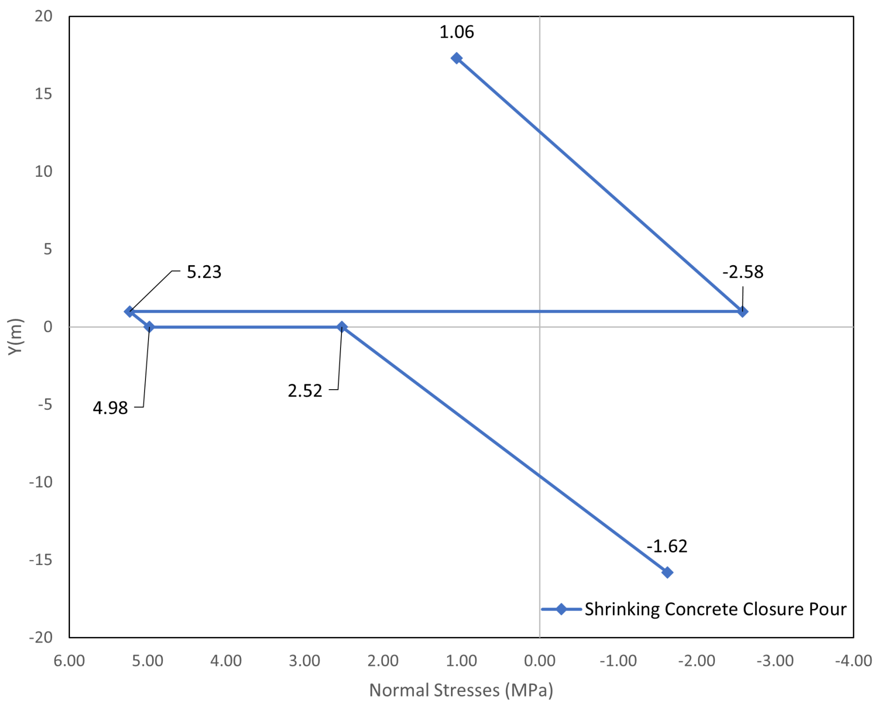

Figure G.3: Results of shrinking concrete closure pour.

G.4 Results of *SHCC* closure pour with only shrinkage

For the results using a *SHCC* closure pour only the Method 3 will be presented since it is the one closer to reality.

Also, due to the fact that the principle is the same and the only value changing is the elastic modulus and the shrinkage, which are presented at Section F.1.1 and again at Table G.4.

Dimensions	Old Bridge	Closure Pour	New Bridge
Elastic Modulus (MPa)	31500	12421	37000
Shrinkage (ε)	-	9.85E-04	1.57E-04

Table G.4: Data for *SHCC* closure pour.

Thus, final stresses will be presented in Table G.5 and in Figure G.4.

Stresses	Old top	Old bottom	CP top	CP bottom	New top	New bottom
Item	0.00	0.00	12.24	12.24	5.82	5.82
Item	-2.95	-2.95	-1.16	-1.16	-3.47	-3.47
Item	2.05	2.05	0.04	0.04	-2.12	-2.12
Item	1.84	-1.84	0.04	-0.04	2.09	-2.09
Total	0.94	-2.75	11.15	11.06	2.33	-1.86

Table G.5: Results of shrinking *SHCC* closure pour.

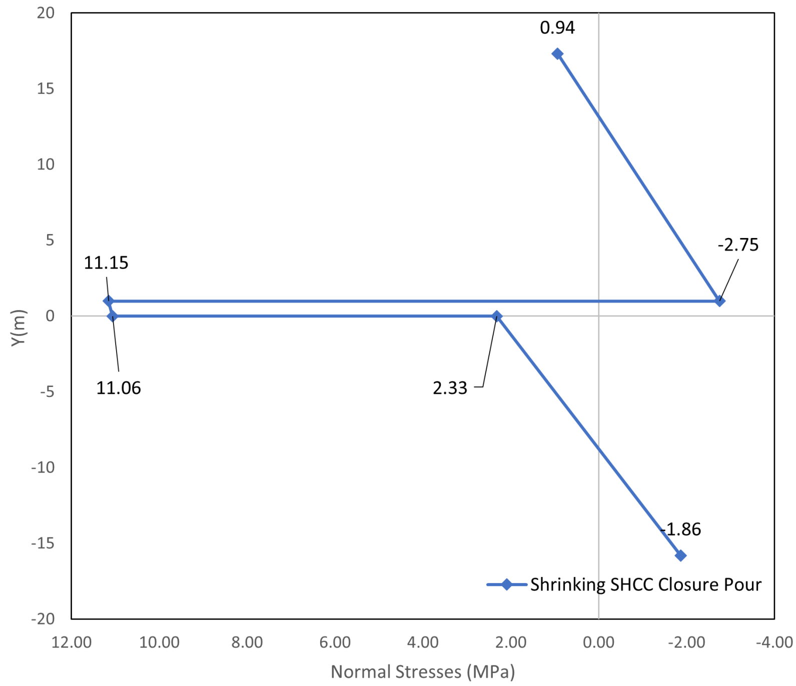

Figure G.4: Results of shrinking *SHCC* closure pour.

G.5 Shrinkage, creep, and crack are considered at a concrete closure pour.

G.5.1 Without including crack

To incorporate the effects of crack and creep, the steps outlined in Method 3 were followed in accordance with the guidelines provided in Section G.3. The elastic modulus of both the old and new bridges was adjusted to account for the creep, which was determined using the values obtained from appendices C.1 and C.2. Subsequently, new stresses were calculated to ensure that the closure pour resulted in cracks. The data for this new calculation is at Table G.6, and the results are at Table G.7 and Figure G.5.

Dimensions	Old Bridge	Concrete *CP*	New Bridge
Elastic Modulus (MPa)	30941	35000	18461
Shrinkage (ε)	-	2.37×10^{-4}	1.57×10^{-4}

Table G.6: Data for concrete closure pour.

Concrete	Old top	Old bottom	CP top	CP bottom	New top	New bottom
Item	0.00	0.00	8.30	8.30	2.90	2.90
Item	-2.02	-2.02	-2.28	-2.28	-1.20	-1.20
Item	1.30	1.30	-0.53	-0.53	-1.31	-1.31
Item	1.67	-1.67	0.12	-0.12	0.97	-0.97
Total	0.96	-2.39	5.60	5.37	1.36	-0.58

Table G.7: Results of shrinking uncracked concrete closure pour without including crack.

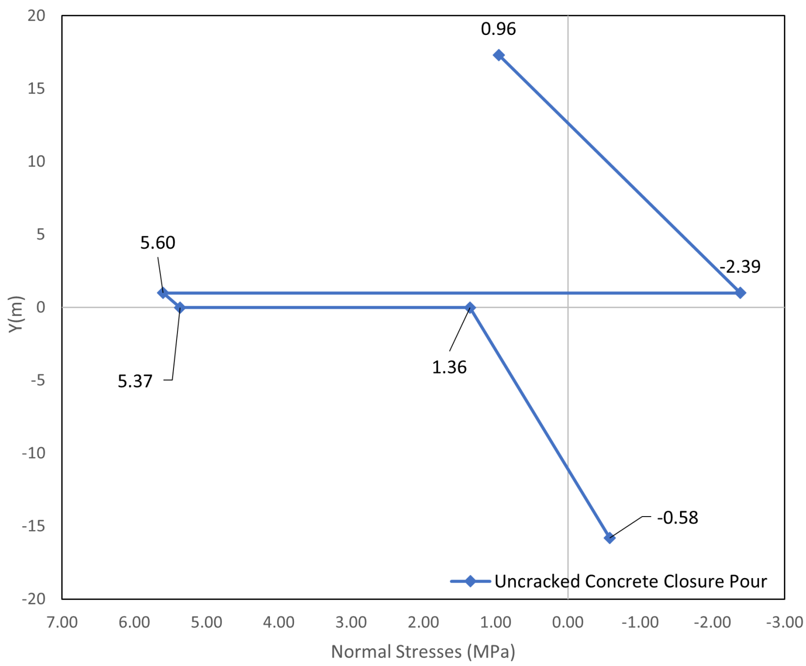

Figure G.5: Results of shrinking uncracked concrete closure pour.

Based on the data presented in Table G.7 and Figure G.5, it can be concluded that the maximum tensile stresses observed in the concrete closure pour reach $5.60MPa$. This value is higher than the f_{ctm} value of $C40/50$, which is $3.5MPa$. As a result, concrete cracking will occur, rendering the concrete closure pour impractical for reducing the casting time required for bridge widening. These findings are consistent with the information provided in Section 3.1.2.

G.5.2 Including Crack

After detecting cracks in the concrete, all the stresses in the entire bridge were recalculated for later comparison with *SHCC*. The elastic modulus of concrete was adjusted to account for cracks by reducing it to one-third of its original value ($35000/3 = 11667MPa$). The data in Table G.8 was used to determine the values for the old bridge, concrete closure pour, and new bridge during the shrinking process. The final results can be found in Table G.9 and Figure G.6.

Dimensions	Old Bridge	Concrete *CP*	New Bridge
Elastic Modulus (MPa)	30941	11667	18461
Shrinkage (ε)	-	2.37×10^{-4}	1.57×10^{-4}

Table G.8: Data for concrete closure pour.

Stresses (MPa)	Old top	Old bottom	*CP* top	*CP* bottom	New top	New bottom
item 1	0.00	0.00	2.77	2.77	2.90	2.90
item 2	-1.86	-1.86	-0.70	-0.70	-1.11	-1.11
item 3	1.33	1.33	-0.19	-0.19	-1.36	-1.36
item 4	1.73	-1.73	0.04	-0.04	1.00	-1.00
Total	1.20	-2.26	1.92	1.83	1.43	-0.57

Table G.9: Results of shrinking cracked concrete closure pour.

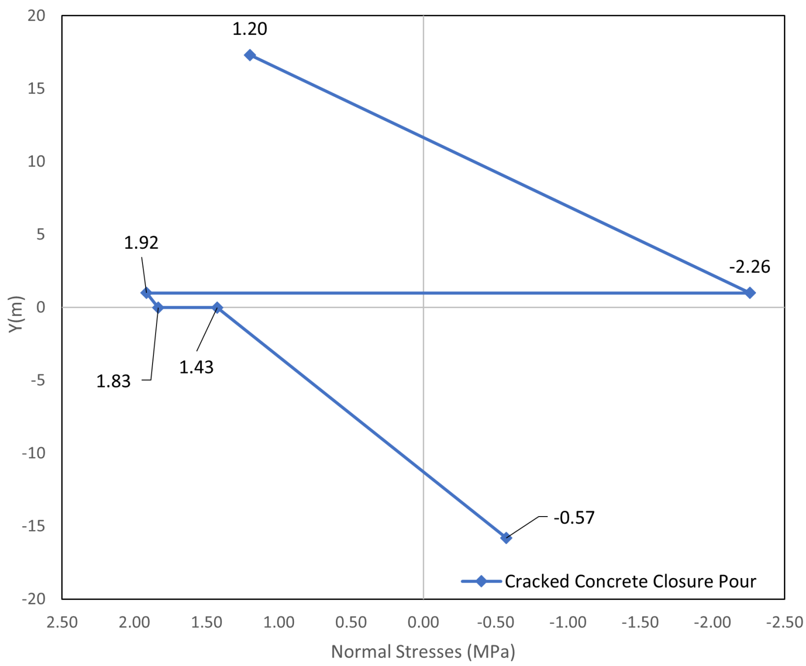

Figure G.6: Results of shrinking cracked concrete closure pour.

G.6 Shrinkage, creep, and crack are considered at a *SHCC* closure pour.

G.6.1 Without including crack

To incorporate the effects of crack and creep, the steps outlined in Method 3 were followed in accordance with the guidelines provided in Section G.3. The elastic modulus of both the old and new bridges was adjusted to account for the creep, which was determined using the values obtained from appendices C.1 and C.2. Subsequently, new stresses were calculated to ensure that the *SHCC* closure pour resulted in cracks. The data for this new calculation is at Table G.10, and the results are at Table G.11 and Figure G.7.

Dimensions	Old Bridge	*SHCC CP*	New Bridge
Elastic Modulus (MPa)	30941	12421	18461
Shrinkage (ε)	-	9.85×10^{-4}	1.57×10^{-4}

Table G.10: Data for *SHCC* closure pour.

SHCC	Old top	Old bottom	CP top	CP bottom	New top	New bottom
item 1	0.00	0.00	12.24	12.24	2.90	2.90
item 2	-2.22	-2.22	-0.89	-0.89	-1.33	-1.33
item 3	1.43	1.43	0.22	0.22	-1.46	-1.46
item 4	1.86	-1.86	0.05	-0.05	1.07	-1.07
Total	1.06	-2.65	11.61	11.51	1.19	-0.96

Table G.11: Results of shrinking uncracked *SHCC* closure pour.

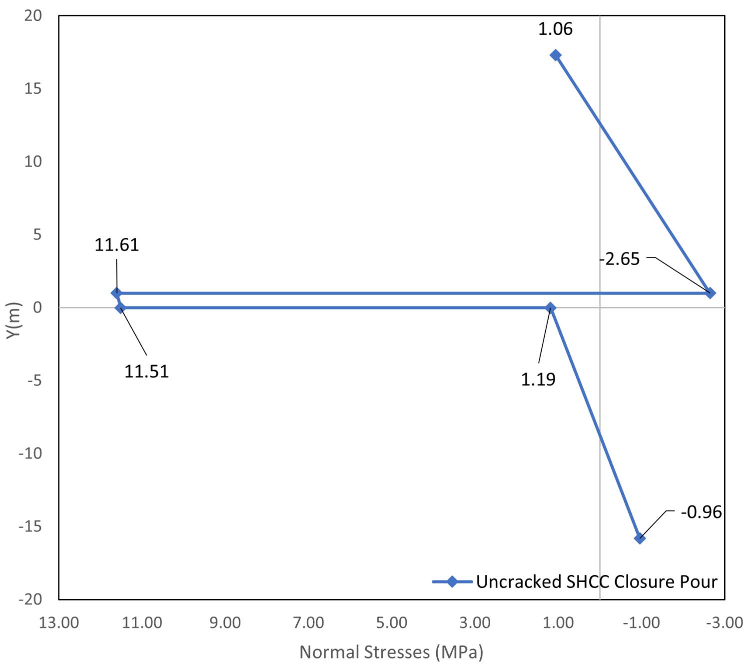

Figure G.7: Results of shrinking uncracked *SHCC* closure pour.

Based on the data presented in Table G.11 and Figure G.7, it can be concluded that the tensile stresses observed in the *SHCC* closure pour reach $11.61MPa$. This value is higher than the first cracking strength of Wang's SHCC, which is shown in Figure 2.7, and it is $2.950MPa$. As a result, *SHCC* cracking will occur. However, as mentioned at Section 3.1.2, that is not a concern. Thus, a modified elastic modulus of the material has to be calculated. This procedure is more complex than for concrete, so it is explained at Section D.1.

G.6.2 Including Crack

The final results of Section D.1 are that after cracking, *SHCC*'s elastic modulus was reduced to $3139MPa$ and its final maximum stress is $2.964MPa$ showed at Figure G.8.

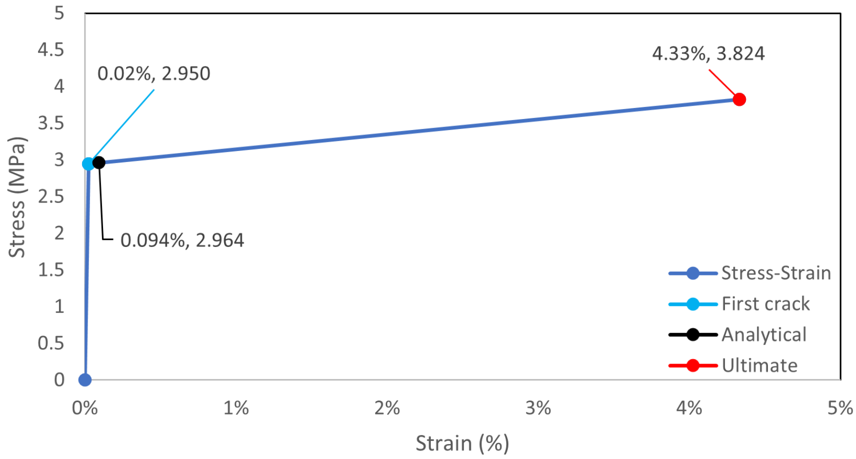

Figure G.8: Stress-strain curve of the cracked *SHCC*.

The data in Table G.12 was used to determine the values for the old bridge, *SHCC* closure pour, and new bridge during the shrinking process. The final results can be found in Table G.13 and Figure G.9.

Dimensions	Old Bridge	*SHCC CP*	New Bridge
Elastic Modulus (MPa)	30941	3139	18461
Shrinkage (ε)	-	9.85×10^{-4}	1.57×10^{-4}

Table G.12: Data for *SHCC* closure pour.

SHCC	Old top	Old bottom	CP top	CP bottom	New top	New bottom
item 1	0.00	0.00	3.09	3.09	2.90	2.90
item 2	-1.89	-1.89	-0.19	-0.19	-1.13	-1.13
item 3	1.37	1.37	0.05	0.05	-1.41	-1.41
item 4	1.79	-1.79	0.01	-0.01	1.03	-1.03
Total	1.26	-2.31	2.96	2.94	1.39	-0.67

Table G.13: Results of shrinking cracked *SHCC* closure pour.

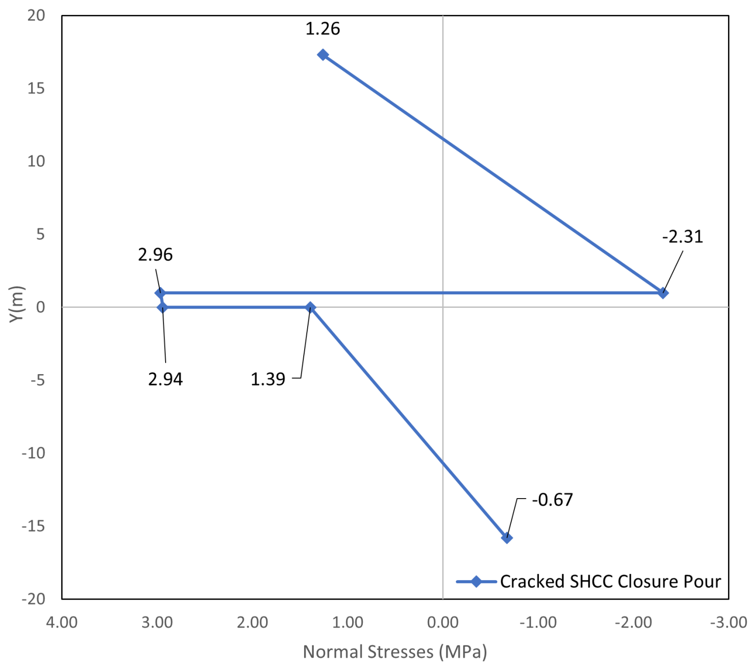

Figure G.9: Results of shrinking cracked *SHCC* closure pour.